

AUS DER LEHRSTUHL FÜR UNFALLCHIRURGIE
PROF. DR. DR. VOLKER ALT
DER FAKULTÄT FÜR MEDIZIN DER UNIVERSITÄT REGENSBURG

FUNCTIONAL ROLE OF TENOMODULIN IN THE DISTINCT
STAGES OF ACHILLES TENDON REPAIR



Dissertation
zur Erlangung des Doktorgrades
der Biomedizinischen Wissenschaften
(Dr. rer. physiol.)

der
Fakultät für Medizin
der Universität Regensburg

vorgelegt von
Manuel Delgado Cáceres
aus
Arequipa, Peru

im Jahr
2022

AUS DER LEHRSTUHL FÜR UNFALLCHIRURGIE
PROF. DR. DR. VOLKER ALT
DER FAKULTÄT FÜR MEDIZIN DER UNIVERSITÄT REGENSBURG

FUNCTIONAL ROLE OF TENOMODULIN IN THE DISTINCT
STAGES OF ACHILLES TENDON REPAIR



Dissertation
zur Erlangung des Doktorgrades
der Biomedizinischen Wissenschaften
(Dr. rer. physiol.)

der
Fakultät für Medizin
der Universität Regensburg

vorgelegt von
Manuel Delgado Cáceres
aus
Arequipa, Peru

im Jahr
2022

Dekan: Prof. Dr. med. Dirk Hellwig

Betreuerin: Prof. Dr. rer. nat. Denitsa Docheva

Tag der mündlichen Prüfung: 27. Februar 2023

Parts of this work have already been published in peer-reviewed journals in an open access format:

Delgado Caceres M, Angerpointner K, Galler M, Lin D, Michel PA, Brochhausen C, Lu X, Varadarajan AR, Warfsmann J, Stange R, Alt V, Pfeifer CG, Docheva D. Tenomodulin knockout mice exhibit worse late healing outcomes with augmented trauma-induced heterotopic ossification of Achilles tendon. *Cell Death & Disease* 12, 1049; 10.1038/s41419-021-04298-z (2021).

Delgado Caceres M, Pfeifer C.G, Docheva D. Understanding Tendons: Lessons from transgenic mouse models. *Stem Cells and Development* 27, 1161–1174; 10.1089/scd.2018.0121 (2018).

The text passages between quotation marks and in italics are exact text transcription from both publications.

ZUSAMMENFASSUNG

Die Achillessehne ist die dickste, größte und stärkste Sehne im menschlichen Körper. Die Hauptfunktion dieser Sehne besteht darin, den aus dem Gastrocnemius-Soleus-Muskelkomplex bestehenden Musculus triceps surae mit dem Fersenbein zu verbinden. Die durch die Kontraktion der Wadenmuskeln erzeugte Energie wird durch die Achillessehne übertragen und resultiert in einer Plantarflexion. Dadurch werden Bewegungen wie Gehen, Laufen oder Springen ermöglicht. Die Achillessehne kann beim Laufen Kräften standhalten, die 12-mal größer sind als das eigene Körpergewicht. In Kombination mit der von Natur aus schlechten Blutversorgung der Sehne ergibt sich daraus eine Prädisposition für Verletzungen. Eine mögliche Folge nach einer Sehnenverletzung ist die Bildung von ektopem Knochen im Sehnengewebe, was als heterotope Ossifikation (HO) bezeichnet wird. Bislang gibt es hierfür weder wirksame noch erfolgreiche klinische Behandlungsmethoden.

Tenomodulin (*Tnmd*), der bekannteste Marker für reife Zellen der Sehnenabstammung, hat wichtige Auswirkungen auf die Alterung und Funktion des Sehnengewebes. Wir haben bereits in vorherigen Publikationen berichtet, dass der Verlust von *Tnmd* zu einer minderwertigen frühen Sehnenreparatur führt und, dadurch fibrovaskuläre Narben gekennzeichnet ist. Daher stellten wir die Hypothese auf, dass das Fehlen von *Tnmd* auch in späteren Stadien zu einer mangelhaften Reparatur führt.

In dieser Studie wurden *Tnmd*-Knockout-Tiere (*Tnmd*^{-/-}) und Wildtyp-Tiere (WT) einer vollständigen chirurgischen Achilleshnendurchtrennung mit anschließender End-zu-End-Reparatur unterzogen. Lineage-Tracing-Analysen zeigten die Bildung eines fibrotischen Narbengewebes, das durch eine Verringerung der Zellen der Sehnenlinie (gekennzeichnet durch ScleraxisGFP-Expression) und eine signifikante Zunahme der Myofibroblasten mit Alpha Smooth Muscle Actin in *Tnmd*^{-/-}-Sehnenarben gekennzeichnet war.

Im proliferativen Stadium wurden keine signifikanten Unterschiede zwischen den beiden Genotypen hinsichtlich Innervation, Gefäßbildung, Kollagenfibrillenorientierung und Reifung festgestellt. Allerdings wurden in den verletzten Sehnen von *Tnmd*-defizienten Mäusen signifikant mehr pro-inflammatorische M1-Makrophagen und eine größere Kollagen-II-Knorpelanlage nachgewiesen. Darüber hinaus zeigte die qRT-PCR-Analyse eine deutliche Dysregulation klassischer sehnenbezogener Gene und Kollagenfibrillen-Regulatoren in den mutierten Sehnen,

was mit einer verzögerten Aktivierung der Tenogenese in der Narbe zusammenhängen könnte. Diese Ergebnisse stimmen mit unseren Transmissionselektronenmikroskopie (TEM)-Daten überein, bei denen signifikant dickere Kollagenfibrillen in nicht verletzten und verletzten AT von *Tnmd*^{-/-}-Sehnen gemessen wurden.

In der Umbauphase zeigte die histologische Auswertung eine geringere Reparaturqualität in den verletzten *Tnmd*^{-/-}-Sehnen, die mit einer höheren, mittels Mikro-CT quantifizierten HO einherging. Die biomechanischen Eigenschaften der Sehnen waren in beiden Gruppen nach der Verletzung beeinträchtigt. Allerdings stellten wir bei den nicht verletzten *Tnmd*^{-/-}-Sehnen eine abnormale Versteifung fest, die höhere statische und dynamische E-Moduli aufwies. Pathologisch dickere und abnormal geformte Kollagenfibrillen wurden mittels TEM in *Tnmd*^{-/-}-Sehnen beobachtet; und führten zusammen mit erhöhter HO zu einer verminderten Lauffähigkeit der *Tnmd*^{-/-}-Mäuse.

Diese neuen Erkenntnisse zeigen, dass *Tnmd* eine schützende Funktion bei traumabedingter endochondraler HO einnimmt. Dies könnte die Entwicklung neuer Therapeutika zur Beschleunigung der Reparatur anregen.

SUMMARY

The Achilles tendon (AT) is the thickest, largest, and strongest tendon in the human body. The main function of the AT is to connect the triceps surae muscle, composed of gastrocnemius-soleus muscle complex to the heel bone. The AT transmits the energy generated by the contraction of the calf muscles to induce plantar flexion allowing skeletal movements such as walking, running, or jumping. The AT can withstand forces 12 times greater than the bodyweight during running, which together with the natural poor blood supply in the AT predispose the tendon to injuries. One possible outcome after tendon injury is the formation of ectopic bone in the tendinous tissue, which is known as Heterotopic Ossification (HO). To date, neither effective nor successful treatments have been put in practice in the clinic.

“Tenomodulin (Tnmd), the best-known mature marker for tendon lineage cells, has important effects in tendon tissue aging and function. We have previously reported that loss of Tnmd leads to inferior early tendon repair characterized by fibrovascular scarring and therefore hypothesized that its absence will persistently cause deficient repair during later stages.

In this study, Tnmd knockout (Tnmd^{-/-}) and wild-type (WT) animals were subjected to complete AT surgical transection followed by end-to-end suture. Lineage tracing analyses revealed the formation of a fibrotic scar tissue, characterized by reduction in tendon-lineage cells (marked by ScleraxisGFP-expression), and the significant increase in the presence of alpha smooth muscle actin myofibroblasts in Tnmd^{-/-} tendon scars”.

At the proliferative stage, no significant differences were detected between both genotypes regarding innervation, vasculature formation, collagen fibril orientation and maturation. *“However, significantly more pro-inflammatory M1 macrophages and larger collagen II cartilaginous template were detected in the injured tendons of Tnmd-deficient mice. Furthermore, qRT-PCR analysis showed a clear dysregulation of classical tendon-related genes and collagen fibril regulators in mutant tendons, which might be associated to a delayed activation of tenogenesis in the scar”.* These results go in line with our TEM data, where significantly thicker collagen fibrils were measured in non-injured and injured AT of Tnmd^{-/-} tendons.

“At the remodeling stage, histological scoring revealed lower repair quality in the injured Tnmd-deficient tendons, which was coupled with higher HO quantified by micro-CT. Tendon biomechanical properties were compromised in both groups upon injury, however we identified an

abnormal stiffening on non-injured $Tnmd^{-/-}$ tendons, which possessed higher static and dynamic E-moduli. Pathologically thicker and abnormally shaped collagen fibrils were observed by TEM in $Tnmd^{-/-}$ tendons and this together with augmented HO resulted in diminished running capacity of $Tnmd^{-/-}$ mice. These novel findings demonstrate that $Tnmd$ plays a protecting role against trauma-induced endochondral HO and can inspire the generation of novel therapeutics to accelerate repair”.

Table of Contents

1. INTRODUCTION.....	1
1.1 CLINICAL RELEVANCE	1
1.2 TENDON DEVELOPMENT	2
1.3 TENDON FUNCTION, STRUCTURE AND COMPOSITION	4
1.4 CELL TYPES IN TENDON TISSUE	5
1.4.1 Tendon stem/progenitor cells, tenoblasts and tenocytes	5
1.4.2 Other cell types.....	7
1.5 TENDON REPAIR	8
1.5.1 Stages of tendon repair.....	8
1.5.2 Cells involved in the repair process	10
1.5.3 Heterotopic ossification in tendons: the erroneous reparative process upon injury.....	11
1.6 TENDON BIOMECHANICS	12
1.7 TENOMODULIN	15
1.7.1 Roles in vivo and in vitro	16
1.7.2 Challenging Tnmd and its role in early healing	16
1.8 AIM AND MILESTONES OF THE THESIS	18
2. MATERIALS AND METHODS	20
2.1 MATERIALS	20
2.1.1 Animals	20
2.1.2 Primary cells.....	20
2.1.3 Reagents and solutions	20
2.1.4 Kit-systems.....	22
2.1.5 Primers	22
2.1.6 Antibodies	23
2.1.7 Disposables.....	23
2.1.8 Devices	24
2.1.9 Software	25
2.2 METHODS.....	26
2.2.1 Animals	26
2.2.2 Histology & Histomorphometry.....	30
2.2.3 Transmission Electron Microscopy (TEM).....	37

2.2.4 Micro-Computed Tomography	38
2.2.5 Biomechanical testing	39
2.2.6 Voluntary Running Tests	41
2.2.7 Single cell RNA-Sequencing	42
2.2.8 RNA isolation and reverse transcription polymerase chain reaction	45
2.2.9 Statistics	46
3. RESULTS.....	47
3.1 Tnmd ^{-/-} scars contain significantly higher number of αSMA ⁺ cells and lower number of tendon-specific ScxGFP ⁺ cell during early and late healing.....	47
3.2 At day 21 post-injury Tnmd ^{-/-} scars are characterized by larger chondrogenic template	51
3.3 Tnmd-deficiency does not affect tendon innervation, vascularization, collagen maturation and presence of CD146 ⁺ progenitors at day 21 post-injury	53
3.4 At day 21 post-injury Tnmd ^{-/-} scars are characterized by lower number of BrdU ⁺ proliferative cells, and anti-inflammatory macrophages, but higher number of pro-inflammatory macrophages	57
3.5 Lack of Tnmd results in significant dysregulation of classical tendon-related gene markers during the healing process.....	60
3.6 The ECM of non-injured Tnmd ^{-/-} Achilles' tendons is characterized by persistently and significantly thicker collagen fibrils.....	61
3.7 The ECM of Tnmd ^{-/-} Achilles' tendons is distinguished by lower collagen fibril density concomitant with significantly thicker and atypically shaped collagen fibrils	63
3.8 Loss of Tnmd leads to significantly inferior tendon healing and remodeling during late repair.....	68
3.9 Lack of Tnmd results in significantly higher trauma-induced heterotopic ossification.....	70
3.10 Contralateral and non-injured Achilles tendon present marginal age-related HO	72
3.11 Tnmd ^{-/-} tendons are naturally stiffer and display significantly increased static and dynamic Elastic moduli; post injury, tendon viscoelastic properties are profoundly weakened in both genotypes.....	74
3.12 Tenomodulin-deficient mice run significantly less after injury	76

3.13 Pilot single cell RNA-Sequencing analysis reveals a significant transcriptomic shift between $Tnmd^{-/-}ScxGFP^{+}$ and WT $ScxGFP^{+}$ cells	77
3.13.1 Gene ontology analysis	85
3.13.2 Signaling pathway analysis suggest a $Tnmd$ involvement in Hippo and Wnt-signaling cascades	86
4. DISCUSSION	87
4.1 The interplay between extrinsic and intrinsic tissue repair in the context of $Tnmd$	88
4.2 $Tnmd$ role during the reparative proliferative stage of healing	89
4.3 Changes in Achilles tendon's ultrastructure, biomechanics and functionality upon injury and $Tnmd$ -deficiency	90
4.4 Transcriptomics shifts due to $Tnmd$ absence	92
5. CONCLUSIONS	94
6. OUTLOOK	96
7. BIBLIOGRAPHY	97
8. ATTACHMENT	114
8.1 List of abbreviations	114
8.2 Figures	115
8.3 Tables	117
ACKNOWLEDGMENTS	118
9. SELBSTSTÄNDIGKEITSERKLÄRUNG	119
CURRICULUM VITAE	120

1. INTRODUCTION

I would like to state clearly that parts of the introduction have already been published in Delgado Caceres M, Angerpointner K, Galler M, Lin D, Michel PA, Brochhausen C, Lu X, Varadarajan AR, Warfsmann J, Stange R, Alt V, Pfeifer CG, Docheva D. Tenomodulin knockout mice exhibit worse late healing outcomes with augmented trauma-induced heterotopic ossification of Achilles tendon. *Cell Death & Disease* (2021).

1.1 CLINICAL RELEVANCE

The Achilles tendon (AT) is the thickest, largest, and strongest tendon in the human body ^{1,2}. The main function of the AT is to connect the triceps surae muscle, composed of gastrocnemius-soleus muscle complex ³ to the heel bone (calcaneus) ² (Fig. 1). The anatomical region at which muscle and tendons intersect is called myotendinous junction (MTJ) ⁴⁻⁶, and the region at which tendons are inserted into bones is termed osteotendinous junction (OTJ) or enthesis ^{7,8} (Fig. 1). The AT transmits the energy generated by the contraction of the calf muscles to induce plantar flexion allowing skeletal movements such as walking, running or jumping ^{2,9}. The AT can withstand forces 12 times greater than the bodyweight during running (repetitive strain-overuse) ¹⁰, which together with the natural poor blood supply in the AT predispose the tendon to injuries ¹¹.

Concomitant to primary tendon disorders and degeneration (tendinopathies), Achilles tendon ruptures (ATRs) represent one of the most common injuries of the musculoskeletal apparatus ^{12,13}. The worldwide ATR incidence in the general population ¹⁴⁻¹⁸, as well as in athletes ¹⁹ is continuously increasing. In Germany alone, between 15.000 and 20.000 ATRs have been reported to occur every year, representing an incidence of approx. 20 cases per 100.000 inhabitants and year ²⁰. Plausible reasons for the increment of ATRs are the superior life expectancy and augmented activity in the population ²¹, whilst the ATR increment in athletes can be associated to cumulative tissue degeneration and excessive tendon mechanical loading (overuse, overload) ¹⁹. Lemme *et al.*, 2018 reported in a descriptive epidemiology study that the largest overall incidence of ATRs in male and females occurred at aged 20-39 and 40-59 years, respectively ¹⁸. Moreover, the majority of ATRs occur in male compared to female patients, with a distribution ratio of 5:1 ¹⁸. To date, there is still controversy regarding which strategies, either operative or conservative, should be pursued in order to support and accelerate tendon repair.

Therefore, with this body of work we underpin the necessity to further investigate biological targets to advance and develop tendon-specific drugs to augment tendon healing, resulting at the end, in the improvement of patients' quality of life.

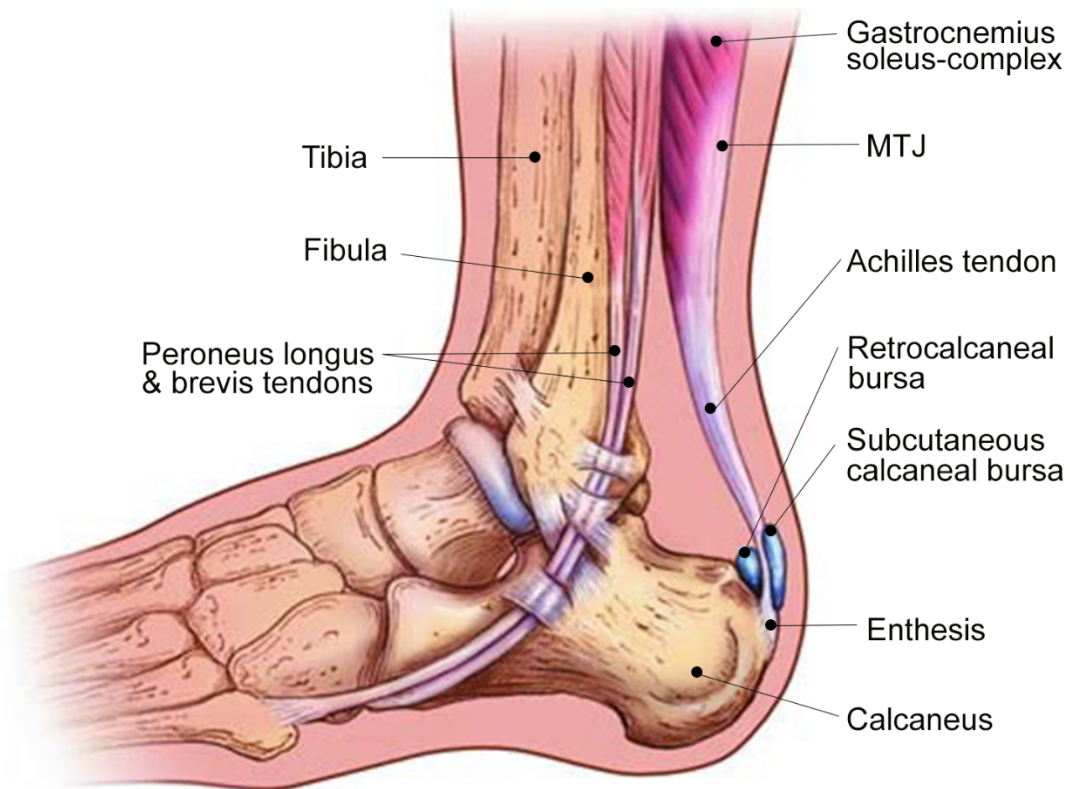


Fig. 1. Human AT anatomy. Figure derived from Mazzone and McCue, 2002 ¹¹, which has been published under the gold open access model. Annotations MTJ and Enthesis were added to the original figure.

1.2 TENDON DEVELOPMENT

“The establishment of a proper musculoskeletal system involves the finely orchestrated development of muscle, cartilage, and tendon lineages emerging from the somatic mesoderm ^{22,23}. During embryonic development, muscle and cartilage (systems that are better understood and studied than tendon) arise from the myotome and sclerotome respectively, in response to signals emitted from neighboring tissues. The tendon lineage is formed within the dorsolateral sclerotome, adjacent to and beneath the myotome, in a somite subdomain denominated as syndetome ²³. The ontogeny of the tenogenic lineage is not fully understood yet because of the absence of specific early tendon lineage markers. To our knowledge, there are two stages related to tendon

development. First, the emergence of precursor/progenitors based on their origin and localization and second, commitment and differentiation based on pivotal signaling cascades. With the identification of the beta helix-loop-helix transcription factor *Scleraxis* (*Scx*), an important and distinctive marker for early tendon development was found^{24,25}. Schweitzer et al. reported the usage of *Scx* expression as a method for the identification of a pool of tendon progenitors in the mesenchyme subjacent to the ectoderm²⁵. In mice, embryonic tendon and ligament development starts occurring between E9.5-E12.5²⁶.

The main function of the axial tendon is to bond the muscles that are located along the spinal column to the vertebrae and transfer the generated force to the axial skeleton, providing spinal stability and range of movement²⁶. Axial tendon progenitors, which per definition are *Scx*-expressing cells, originate during embryonic development from the ventral compartment of emerging somites, more precisely, from the syndetome, one of the four somatic sub compartments²⁷⁻³⁰. Fibroblast growth factors (FGF) play an important role in chick and mouse embryos during axial tendon development. In mice, FGF signaling starts from the upper myotome resulting in the activation of the mitogen-activated protein kinase pathways, E26 transformation-specific sequence (*Ets*) transcription factor, Phosphatidylinositol-4-phosphate 5-kinase (*Pea3*) and Ezrin/radixin/moesin (*Erm*). Last, *Scx* and transcription factor *Mohawk* (*Mkx*) promote final tendon lineage commitment and differentiation; this is characterized by the expression of collagen type I, type XIV, and Tenomodulin (*Tnmd*)^{23,31,32}; *Tnmd* is to date, the best-known mature marker for tendons³³⁻³⁵. On the other side, ventral midline sonic hedgehog expression can solely activate *Pax1*, which consequently has a negative effect on *Scx*, hindering its induction of *Sox5* and *Sox6*, which block *Scx* expression³².

Progenitors of the limb tendons develop differently to the cells that give rise to axial tendons because they are not localized within a specific subdomain in the somite but rather around the lateral plate mesoderm^{29,36}. Limb tendon progenitor cells are intermingled with migrating myoblasts in ventral and dorsal parts of the limb bud^{30,37}. During limb development, *Scx*-positive tendon progenitors are induced by ectodermal signals and constrained by bone morphogenetic protein³² in the limbs and position themselves between differentiating muscles and cartilage. Subsequently, they condense and finally differentiate to form distinct tendons³⁰. Not only FGF signaling has a pivotal role in regulating limb tendon differentiation, proteins from the TGF β superfamily have been reported to be inducers of limb bud tendons³⁸⁻⁴¹. It has been previously

described that the disruption of TGF β signal in double mutant Tgfb2^{-/-}/Tgfb3^{-/-} mouse embryos leads to the loss of most tendons and ligaments in the limbs, trunk, tail and head⁴². The close interaction between muscles and tendons during limb development^{29,37,43} suggests that transcription factors such as Six homeobox 1 and 2 (Six1/2) and transcriptional coactivator and phosphatase 1 and 2 (Eya1/2)⁴⁴ might play an indirect role in tendon formation. However Bonnin et al. showed using Six1-deficient mice that this gene is neither expressed in tendons nor essential for tendon development⁴⁵. Whole transcriptome expression profiling of mouse limb tendons using RNA-Seq. revealed no differential expression of Six1, while Six2 was found to be highly expressed in forming limb tendon cells at E13.5⁴⁶. As in axial tendon development, Scx and Mxk play a crucial role, giving the initial impulse for limb tendon formation. In a second step, Early growth response 1 and 2 (Egr1/2) act as molecular sensors for mechanical signals⁴⁷ guiding and regulating collagen maturation and leading to final tendon differentiation^{32,48-50}. The exact mechanisms triggering tenogenesis, which need to be finely orchestrated to guide progenitor cells to fully differentiated tendon cells, still remain elusive and worth further investigation since the whole process is dependent on various factors with different signaling cascades amongst the diverse cellular compartments²²”.

1.3 TENDON FUNCTION, STRUCTURE AND COMPOSITION

“Tendons appear to be simply organized tissues with the main function of connecting muscles with bones transmitting the muscle-generated force, thus allowing joint movement^{51,52}. Tendons, which could be compared to flexible strings, are primarily made of collagens and a minor fraction of elastin surrounded by a proteoglycan-rich matrix. Concerning the mechanical function, tendons can be classified as positional tendons, which are primarily loaded along their long axis permitting the interplay between muscles and bones^{51,53} and energy storing tendons that are more elastic and extensible and when loaded, release the accumulated energy to improve the efficiency of movement⁵⁴. The tendon extracellular matrix (ECM) consists mainly of collagens (60-85% of tissue’s dry weight)⁵⁵, with type I being the most prominent one (approx. 95%) and small amounts of type V, VI, XII, XIV and XV^{56,57}. The role of collagens within tendons has been well studied and characterized⁵⁸⁻⁶⁰ but the non-collagenous part of the matrix consisting of proteoglycans like fibromodulin, lumican, biglycan and decorin⁶¹⁻⁶³, requires more investigation as it is less defined.

Tendons are hierarchically organized structures with collagen fibrils as the smallest structural units; these are composed of parallel chains of collagen molecules bound together by covalent cross-links⁵². Fibrils aggregate gradually with other fibrils to form tube-like structures called fibers, which subsequently attach to other fibers and arrange themselves into bundles (collagen-rich fascicles). Collagen fascicles are aligned in the direction of force application⁶⁴ and are surrounded by thin layers of connective tissue known as endo- and epitenon (tendon sheaths), where nerves, blood vessels and tendon stem/progenitor cells are situated⁶³. Fully differentiated tendon cells (tenocytes) are localized between the collagen fibers⁶³”.

1.4 CELL TYPES IN TENDON TISSUE

1.4.1 Tendon stem/progenitor cells, tenoblasts and tenocytes

Bi *et al.* described in 2007 for the first time, a distinctive cell population termed tendon stem/progenitor cell (TSPC), which possessed the classical stem cell characteristics clonogenicity, self-renewal capacity and multipotency⁶⁵. Moreover, this Scx-expressing cell population with strong regenerative potential is influenced in its multipotency by biglycan (Bgn) and fibromodulin (Fmod)⁶⁵. Currently it is still debated where exactly these cells reside within tendons. According to Walia and Huang, 2019 and Huang *et al.*, 2021 three main TSPCs subpopulations were defined based on their location in the tissue: perivascular-derived, peritenon-derived and proper-derived TSPCs^{66,67} (Fig. 2).

The cells in the perivascular region are characterized by the expression of the local stem/progenitor and typical pericyte marker CD146⁶⁸, alongside with p75 neurotrophin receptor (P75)⁶⁹ and alpha smooth muscle actin (α SMA)⁷⁰ (Fig. 2). Peritenon-derived TSPCs were marked by the expression of osteocalcin (Ocn a.k.a Bglap)⁷¹ as well as Tubulin polymeration-promoting protein family member 3 (Tppp3)⁷² and platelet-derived growth factor receptor alpha (Pdgfra)⁷³. Lastly, proper-derived TSPCs are recognizable by the co-expression of Scx and Cathepsin K (Ctsk), the latter being a classical osteoclast marker that has been identified as contributor to heterotopic ossification (HO)⁷⁴. In all tendon tissue compartments the presence of Nestin⁺ Scx⁺ and Nestin⁻ Scx⁺ TSPCs was detected⁷⁵ (Fig. 2). Interestingly, Sakabe *et al.*, 2018 reported that Scx labels most, but not all tendon cells, underpinning the need for novel biomarkers to trace TSPCs subpopulations⁷⁶.

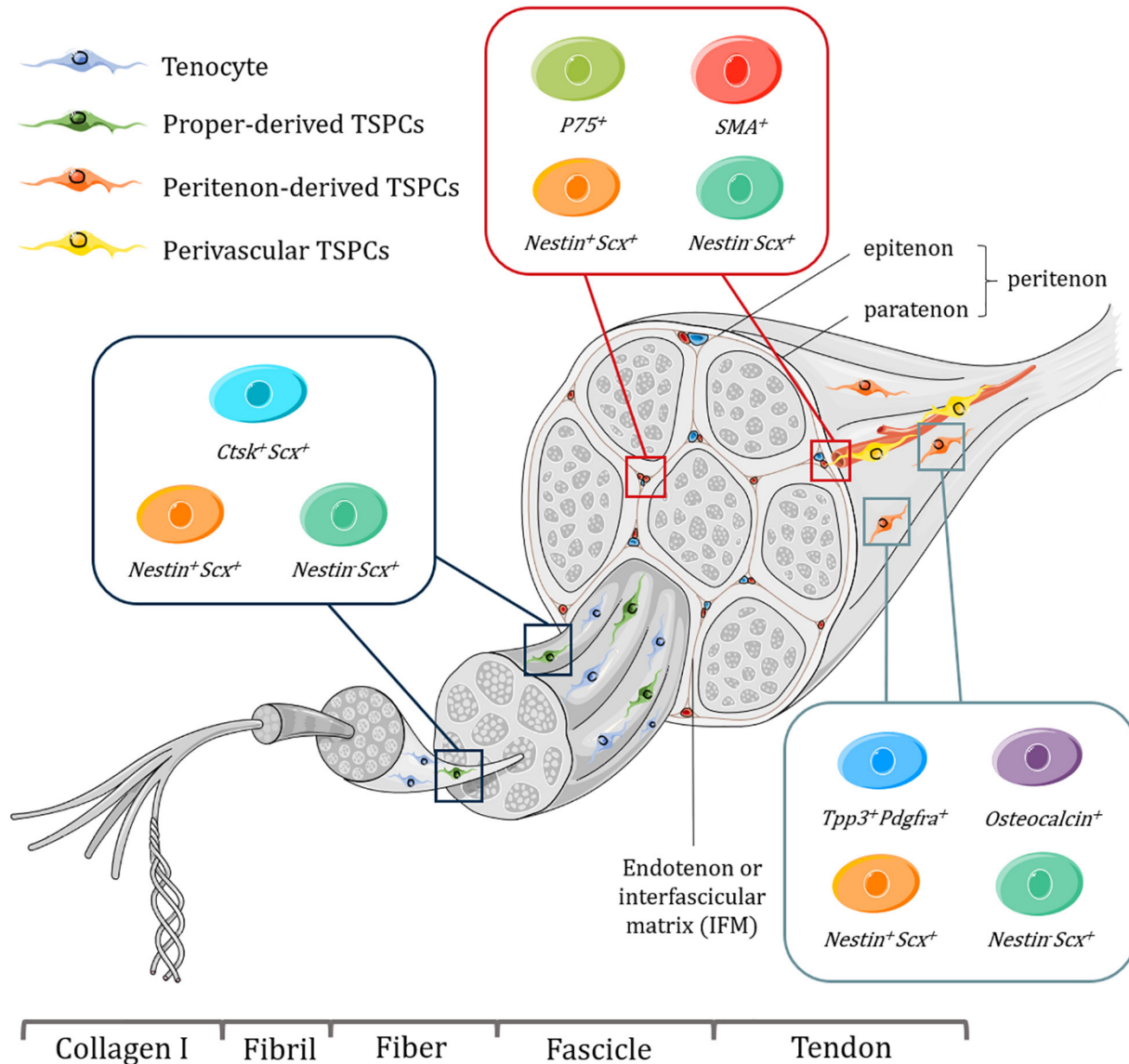


Fig. 2. Tendon hierarchical architecture and TSPCs subpopulation. Schematic illustration of the tendon unit conformed by collagen fibrils, fibers, fascicles surrounded by the tendon sheaths endotenon, epitenon and paratenon. Tenocytes are embedded within the fibers, and TSPCs are distributed in the tendon proper, peritenon and perivascular region. Figure derived from Huang *et al.*, 2021⁶⁷, which has been published under the gold open access model.

The current conception of the tenogenic differentiation cascade identifies tenoblasts and tenocytes as cell subsets with scarce to no plasticity, respectively and downstream from TSPCs. These cell populations are responsible for maintaining tendon homeostasis and conform 90%-95% of tendon tissue⁷⁷. Transcriptome analysis revealed that tenoblasts present a significant upregulation of aquaporin (*Aqp1*), HtrA serine peptidase 3 (*Htra3*), *Tnmd*, and several collagen genes⁴¹, whilst

tenocytes expressed *Tnmd*, *Mkx* and Thrombospondin-4 (*Thbs-4*)^{33,78–80}. Single-cell transcriptomic analysis conducted by De Micheli *et al.*, 2020 identified in total 11 cell subsets in murine ATs, among which, three groups of fibroblast referred to as tendon fibroblast 1 and 2 and junctional fibroblast were described for the first time⁸¹. The peculiarity of these three cell subsets was their classification based on the moderate-to-high expression of type I collagen (*Colla1*), and the additional expression of type XXII collagen (*Col22a1*), or co-expression of *Scx* and/or *Sox9*⁸¹. Moreover, the other eight cell subsets described, were referred to as: 1) Red blood cells; 2) Immune cells; 3) Nerve cells 1 and 2; 4) endothelial cells 1, 2 and 3; and 5) Pericytes⁸¹. The results reported by De Micheli *et al.*, 2020 reinforce the necessity for further efforts to discover the functions of each cell subset in tendons.

1.4.2 Other cell types

In addition to the cell subsets mentioned above, fibrochondrocytes have been identified in the fibrocartilaginous enthesis in tendons⁸². Moreover, Dyment *et al.*, 2015, Sugimoto *et al.*, 2013 and Ideo *et al.*, 2020 found GDF5⁺ and Scx⁺/Sox9⁺ progenitor cell populations to be directly involved in the formation, homeostasis and healing of the enthesis^{83–85}.

On the other hand, Lehrer *et al.* utilized in 2019 for the first time the term “Tenophage” to describe a macrophage-like tendon cell subpopulation, resident in the tendon core, which potentially executes surveillance functions⁸⁶. This cell population of tendon-origin (ScxGFP⁺) co-expressed CD68, as well as CD163 and exerted phagocytic activity *ex vivo*⁸⁶. Furthermore, single cell transcriptomics and proteomics analysis of healthy and diseased human tendon tissue permitted the identification of a SCX⁺ tendon cell population that expressed high levels of pro-inflammatory markers including Chemokine (C-X-C motif) ligand 1 (*CXCL1*), - ligand 6 (*CXCL6*), - ligand 8 (*CXCL8*), Podoplanin (*PDPN*) and Pentraxin-related protein PTX3 (*PTX3*)⁸⁷. Kendal *et al.*, 2020 described, beside of endothelial cells, T-cells, and monocytes, five tenocyte cell clusters with increased *COL1A1/2* expression⁸⁷. These five subsets consisted of 1) Cytokeratin *KRT7/SCX*⁺ cells expressing microfibril-related genes; 2) Pentraxin (*PTX3*⁺) cells co-expressing high levels of pro-inflammatory markers; 3) Apolipoprotein (*APOD*⁺) cells with a similar expression pattern to fibro-adipogenic progenitors (FAPs); 4) Tubulin Polymerization Promoting Protein Family Member 3/Proteoglycan 4 (*TPPP3/PRG4*⁺) chondrogenic cells and, 5) Integrin alpha 7 (*ITGA7*⁺) smooth

muscle-mesenchymal cells (SMMCs)⁸⁷. Hence, further research is required to disclose the specific role that each cell population plays, not only during tissue homeostasis, but also during healing.

1.5 TENDON REPAIR

The natural healing process of tendons, divided in early (inflammatory) and late (proliferative and remodelling) stages, is known to be inefficient, long-lasting and influenced by anatomic location and local mechanical environment^{88,89}. Dysregulated inflammatory response in tendon lesions can drive persistent fibrosis, misguided stem/progenitor cell differentiation and lead to heterotopic ossification (HO)^{90,91}. The discrete molecular mechanisms, as well as the origin, existence, and functions of different cell types throughout the long repair process are still not fully understood.

1.5.1 Stages of tendon repair

In every healing stage there are particular modifications occurring on molecular and cellular levels, as well as matrix organization. These changes have been summarized and described as graphical synopsis by Schneider *et al.*, 2018⁹² (Fig. 3). The first stage, the early inflammatory phase, is primarily characterized by the migration of immune cells (platelets/granulocytes, neutrophils, monocytes/macrophages, erythrocytes), circulatory-derived mesenchymal stem cells (MSC) and tendon-resident CD146⁺ stem/progenitor cells into the injury site and the formation of a scar tissue^{88,93–96}. During this stage, pro-inflammatory cytokines (i.e. Interleukin 6 (IL-6), -1β , IGF-1 and TGF- β 1 among others) are secreted and attract inflammatory cells into the injury site^{94,95}. Moreover, it has been reported that the initial hemorrhage and the secreted angiogenic factors Vascular endothelial growth factor (VEGF) and basic fibroblast growth factor (bFGF) initiate vasculature formation⁹⁷, are pivotal for the survival of the newly developing fibrous tissue, and have an impact on late tendon biomechanical properties by improving the collagen fibril orientation and resistance^{98,99}. Ackerman *et al.*, 2017 reported that the deletion of the Prostaglandin E₂ receptor 4 (EP₄) in S100 calcium binding protein a4-lineage cells in tendons has a positive effect in the reduction of scar tissue formation during the early, but not during the late stage of tendon healing. This indicates that targeting EP₄ might be a valid therapeutic approach to combat adhesion formation in tendon injuries¹⁰⁰. Furthermore, special attention has been set to macrophages and

their role regulating inflammation. While M1-polarized macrophages are pro-inflammatory cells expressing *IL-6*, *CD68*, and *CD80*¹⁰¹, M2-polarized macrophages are anti-inflammatory cells characterized by the expression of *IL-10*, *CD163* and *CD206*^{101,102}. A misbalance in the process of inducing and resolving inflammation has negative effects in overall tissue repair^{88,103,104}.

During the second stage of healing, the proliferative reparative stage, the more notable changes are the overall increment in cellularity and the production of the immature collagen type III, paralleled with the reduction of collagen type I and the expression of the growth/differentiation factor-5 (GDF-5), altogether leading to an isotropically arranged matrix in the scar tissue^{105,106}.

Finally, the third stage of healing (subdivided in consolidation and maturation) begins with a decrease in cellularity and collagen type III production, as well as with the expression of IGF-1 supporting and stimulating collagen type I synthesis¹⁰⁷. During this stage, collagen fibril cross-linking increases leading to the formation of a mature tendinous tissue. Nevertheless, it has been shown that injured tendons remain having overall inferior and impaired biomechanical properties¹⁰⁸.

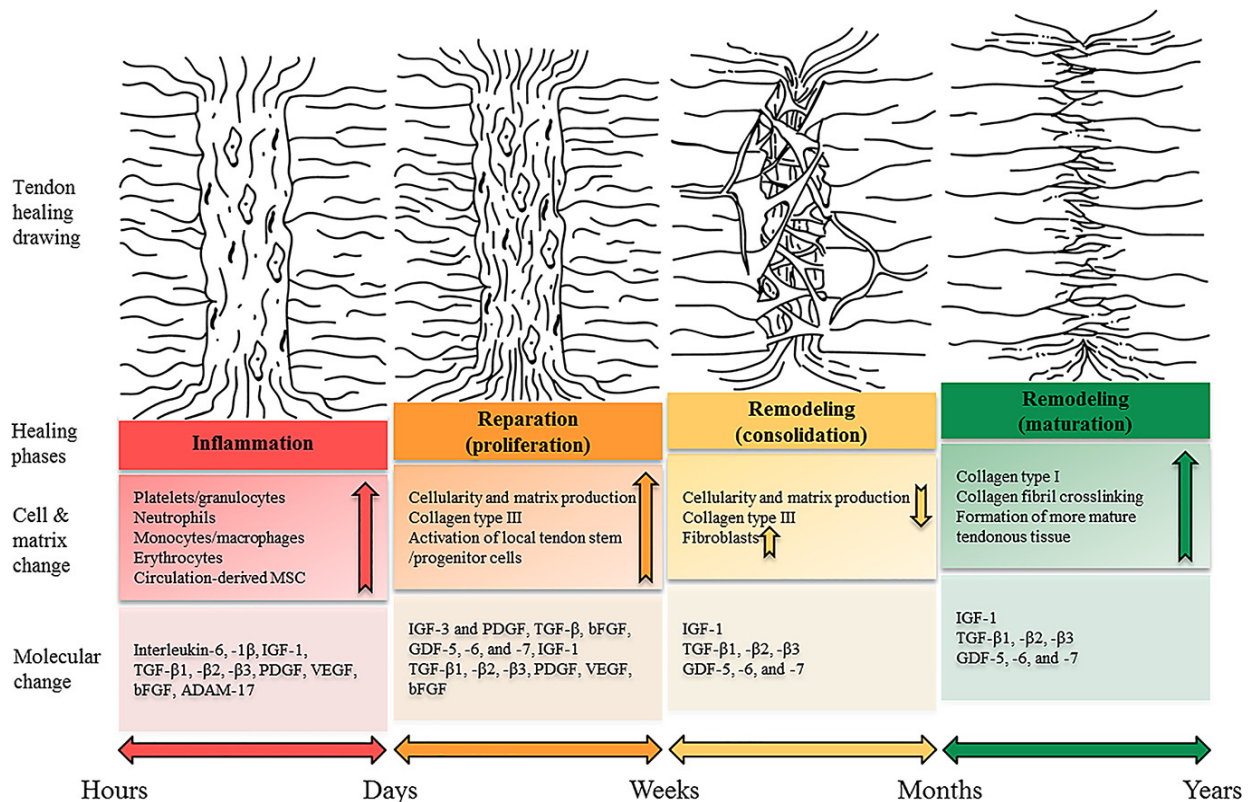


Fig. 3: Schematic illustration of the stages of tendon repair. The tendon healing process is divided in inflammation, repair and remodelling. At every stage, there are distinct modifications at a molecular and cellular levels, and matrix reorganization. Several cytokines, growth factors and cell types are involved in the repair process. Tendon repair is a process that may take years to conclude and results in impaired tendon functionality. Figure derived from Schneider *et al.*, 2018 ⁹², which has been published under the gold open access model.

1.5.2 Cells involved in the repair process

Tissue repair is a complex multifactorial physiological process that requires the highly orchestrated interaction between different cells and tissue compartments to overcome the damage produced by an injury ¹⁰⁹. To date, there is the notion that tendon repair is triggered by an interplay between “intrinsic and extrinsic tendon compartments” ^{110–112}. Whilst the intrinsic compartment comprises the fibrous collagen core with tenocytes embedded in collagen type I fibrils, the extrinsic compartment consist of a network that connects vasculature with innervation and the immune system ^{113–115} (Fig. 4). Tendon-resident cells are marked by the expression of Scleraxis (*Scx*) ³⁰ and their lineage can be tracked by using Scleraxis-GFP (*ScxGFP*) reporter mice ³⁹ and it has been crucial for the identification of cells triggering intrinsic tissue repair ^{70,116–118}. On the other hand, extrinsic epitenon/paratenon cells, expressing alpha smooth muscle actin (α SMA), as well as persistent pro- inflammatory M1 macrophages, have been shown to initiate pathologic scarring, chronic low-grade inflammation, poor tissue remodelling and HO ^{116,118,119}.

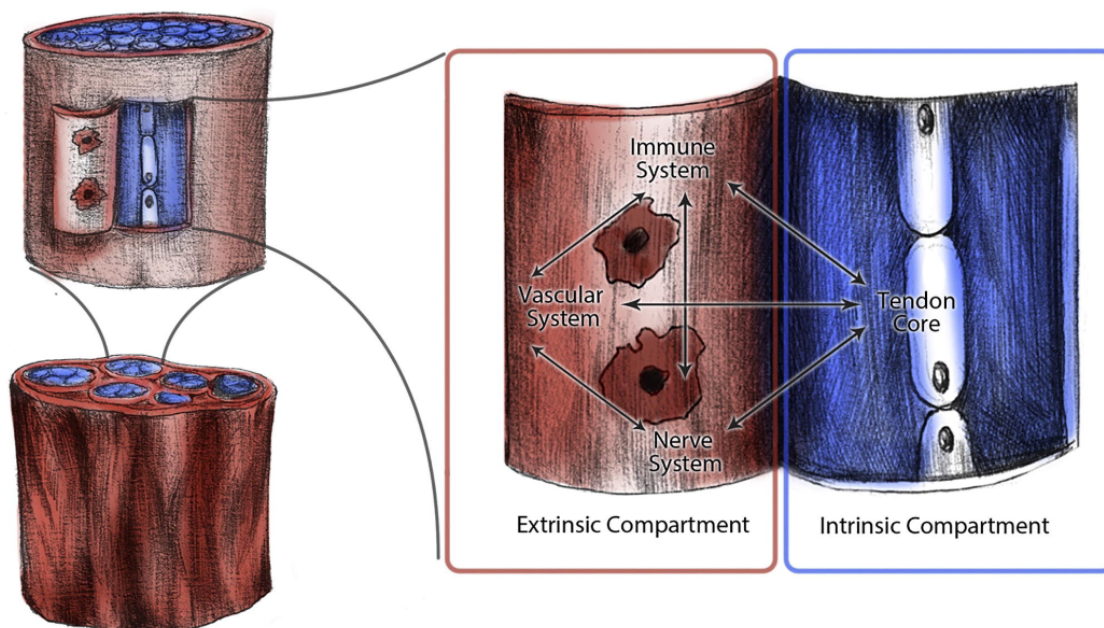


Fig. 4. Tendon's intrinsic and extrinsic compartments. The intrinsic compartment is composed of the tendon core with collagen type I fibrils and tendon cells. Tendon sheaths represent the extrinsic compartment, where the vascular, nerve and immune system is located. Figure derived from Snedecker *et al.*, 2017¹¹¹, which has been published under the gold open access model.

1.5.3 Heterotopic ossification in tendons: the erroneous reparative process upon injury

Heterotopic ossification (HO) is the process of pathological bone formation in soft tissues such as tendon and ligaments^{120–122}. HO is subclassified in non-cell-mediated and cell-mediated¹²³. Moreover, this pathology can be of genetic origin or acquired, i.e. as result of injury (trauma) or surgery¹²⁴. Whilst non-cell-mediated HO is distinguished primarily through calcium salts deposition in the soft tissue (i.e. dystrophic ossification, direct osseous metaplasia) without the intervention of osteoblast in the process; cell-mediated HO is activated by osteoblasts and leads to mature matrix mineralization and inevitably, bone formation¹²³.

When focused on the origin, the most severe form of genetically-induced HO is the rare autosomal dominant disorder called fibrodysplasia ossificans progressive (FOP), which originates from the gain-of-function mutation in the gene encoding activin A receptor type I (*ACVRI*)¹²⁵. On the other hand, trauma-induced HO has been reported in up to 28% of patients following open AT reconstructions^{126,127}. One suggested mechanism leading to trauma-induced HO is the formation of ectopic bone via endochondral ossification. In Fig. 5 is a schematic illustration from Shimono *et al.*, 2014 showing the different stages of HO formation, outgoing from soft-tissue damage until new bone formation¹²².

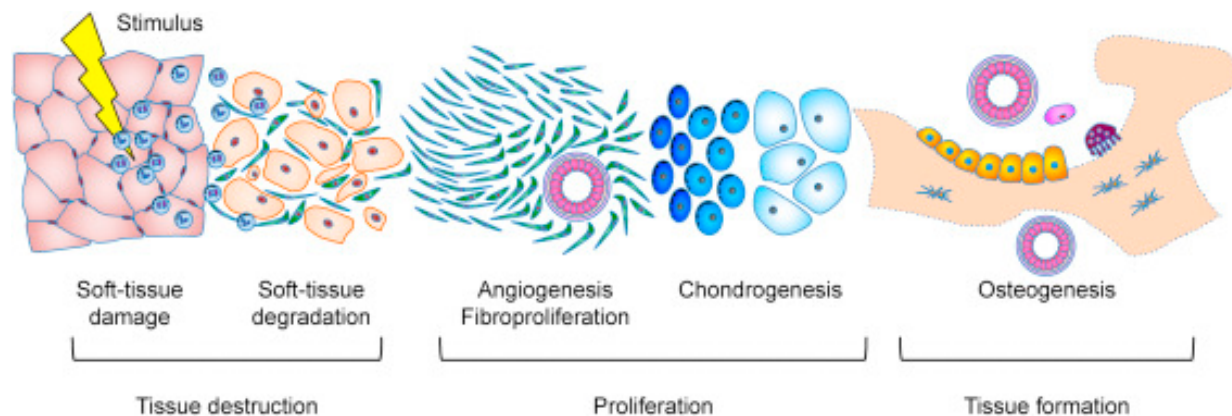


Fig. 5. HO formation process. HO formation process is divided in 3 major phases, first soft-tissue destruction (damage and degradation), followed by a proliferative stage characterized by angiogenesis and chondrogenesis and lastly, by new tissue formation and osteogenesis. Figure derived from Shimono *et al.*, 2014¹²², which has been published under the gold open access model.

Furthermore, Sorkin *et al.*, 2020 reported using a burn-tenotomy model that HO is regulated by transforming growth factor beta-1 (TGF β 1)-producing monocytes/macrophages at the injury site, which in turn induce erroneous resident mesenchymal stem cell differentiation towards osteochondrogenic cells¹¹⁹. More recently, Pagani *et al.*, 2021 and Pineault *et al.*, 2019 described, utilizing an inducible lineage-tracing mouse, that *Hoxa11*-lineage cells labels HO progenitors precisely in the zeugopod that are able to undergo adipogenesis, chondrogenesis and osteogenesis^{128,129}. Even though the exact molecular and cellular pathways leading to HO have not been fully unravel yet, there are three major conditions that have to be met in order for HO to occur: (1) presence of osteoinductive factors, (2) chondrocyte progenitor and osteoblast progenitor cells and lastly, (3) an environment permissive to osteogenesis^{122,130}. Once these conditions are fulfilled, mesenchymal stem/progenitor cells are recruited, proliferate and differentiate into chondrocytes and/or osteoblast resulting in the induction of ectopic bone¹³¹. The formation of ectopic bone in tendons significantly impacts tendon's viscoelastic properties because the tissue cannot store the muscle-generated energy^{93,132}. Moreover, HO has severe consequences for functional tendon outcomes¹³³ since there is an impairment in force transmission and movement, and most importantly, it leads to a serious decrease in patient's quality of life¹³⁴. To date, there is a scarce number of therapeutic targets under investigation to address and prevent, or to treat already-existing HO. In the review paper written by Zhang *et al.* 2020¹²³ the list of possible candidates included signaling pathway inhibitors of bone morphogenetic protein (BMP)^{135,136}, Hedgehog¹³⁷, Hypoxia-inducible factor 1 (HIF1)¹³⁸, and Retinoic acid receptor gamma (RAR γ) agonist^{139,140}.

1.6 TENDON BIOMECHANICS

As previously stated, the main function of tendons is to connect muscles to bones and to transfer the generated energy allowing skeletal movement^{51,52}. In the case of the human AT, there is a special feature since it arises from the triceps surae complex composed by the muscle gastrocnemius-soleus and is directly inserted into the calcaneal bone^{2,141}. Studies focusing on the

structure, function and involvement of the different muscle sub-units regarding force transmission in AT have been published elsewhere¹⁴²⁻¹⁴⁵. To properly execute their function, tendons must be capable to store and release energy efficiently. This task is performed primarily by collagen fibrils, fibers and fascicles, which experience dynamic uniaxial stress during the process of mechanical loading¹³² (Fig. 6A). Hence, alterations in tendon ECM ultrastructure caused by tissue degeneration (tendinosis), aging¹⁴⁶ and tendon injuries have negative effects in tendon functionality^{147,148}.

Important parameters that describe tendon mechanical properties are: strain (ϵ), stress (σ), stiffness (κ), elastic or Young's modulus (E), and ultimate load (load-to-failure). Strain or deformation describes tendon elongation (displacement) (ΔL) relative to the initial length (L_0) (Eq. [1])¹⁴⁹. Stress is the quotient of the applied force (F) per tendon area (cross-sectional area, CSA) (Eq. [2])¹⁴⁹. Moreover, the stiffness is the change in displacement (δ) in relation to the applied force (F) (Eq. [3])¹⁴⁹ and it is calculated from the linear region of the load/elongation curve and is represented by the slope (Fig. 6B). The elastic modulus (E-modulus) describes the resistance of a material to be elastically deformed and is quantified by the ratio of stress to strain in the linear region of the stress/strain curve (Eq. [4])¹⁴⁹ (Fig. 5C). Lastly, the ultimate load is the maximal force that a tendon can withstand before rupture¹⁴⁹ (Fig. 6B).

Strain
$$\epsilon = \frac{\Delta L}{L_0} \quad (1)$$

Strain (ϵ); difference in length (ΔL); initial length (L_0)

Stress
$$\sigma = \frac{F}{A} \quad (2)$$

Stress (σ); force (F); tendon area (cross-sectional area, CSA)

Stiffness
$$\kappa = \frac{F}{\delta} \quad (3)$$

Stiffness (κ); force (F); displacement (δ)

$$\text{Elastic modulus} \quad E^* = \frac{\sigma}{\varepsilon} \quad (4)$$

Young's modulus (E); stress (σ), strain (ε)

Moreover, tendons experience a variety of multiscale changes when forces are applied. In the first region of the stress/strain curve, the toe region ($\varepsilon \leq 2\%$), collagen fibrils become more aligned and less crimped^{150,151} (Fig. 6C). In the second region, collagen fibers react linearly to uniaxial load ($\varepsilon \leq 4\%$) (Fig. 6C). At this level, the deformation is elastic since the tissue is able to return to its original length once unloaded. At strain values between 4-8% the first microscale lesions might occur and finally, at strain values above 8-10% macroscale tendon failure follows^{152,153}.

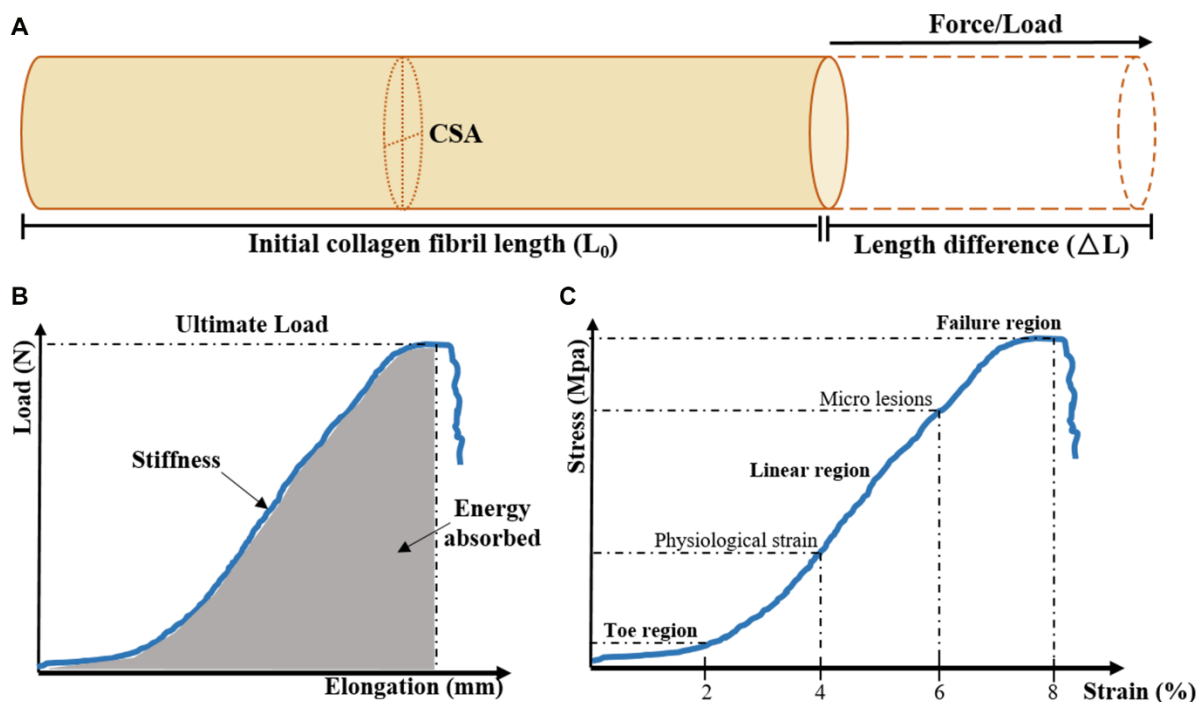


Fig. 6. Schematic representation of tensile load applied on collagen fibril, load/elongation, and stress/strain curves. (A) Illustration of a collagen fibril experiencing a change in length caused by uniaxial loading. (B) Load/elongation curve for stiffness calculation (linear region). Grey-marked region below represent the energy absorbed by the tendon. (C) Stress/strain curve is divided in Toe, linear and failure regions. E-modulus is calculated from the slope in the linear region of stress/strain curve. Figures B and C were derived from Woo *et al.*, 2000¹⁵².

1.7 TENOMODULIN

The gene Tenomodulin (*TNMD*) was independently discovered by two research groups, namely by Brandau *et al.* and Shukunami *et al.* in 2001^{154,155}. *Tnmd*, predominantly expressed in tendons and ligaments, encodes a type II transmembrane glycoprotein with a cleavable C-terminal cysteine-rich domain, that is subsequently deposited in the extracellular matrix (ECM) proximal to type I collagen fibrils^{80,89,154,155}. The gene comprises of seven exons localized on the X chromosome, accounting for a 1.4 kb transcript and an expected protein consisting of 317 amino acids^{154,155} (Fig. 7A, B). Moreover, the C-terminal hydrophobic tail has been reported to exert a dual role, namely stimulating proliferation of tendon cells³³, while inhibiting vascular cell migration^{156,157}.

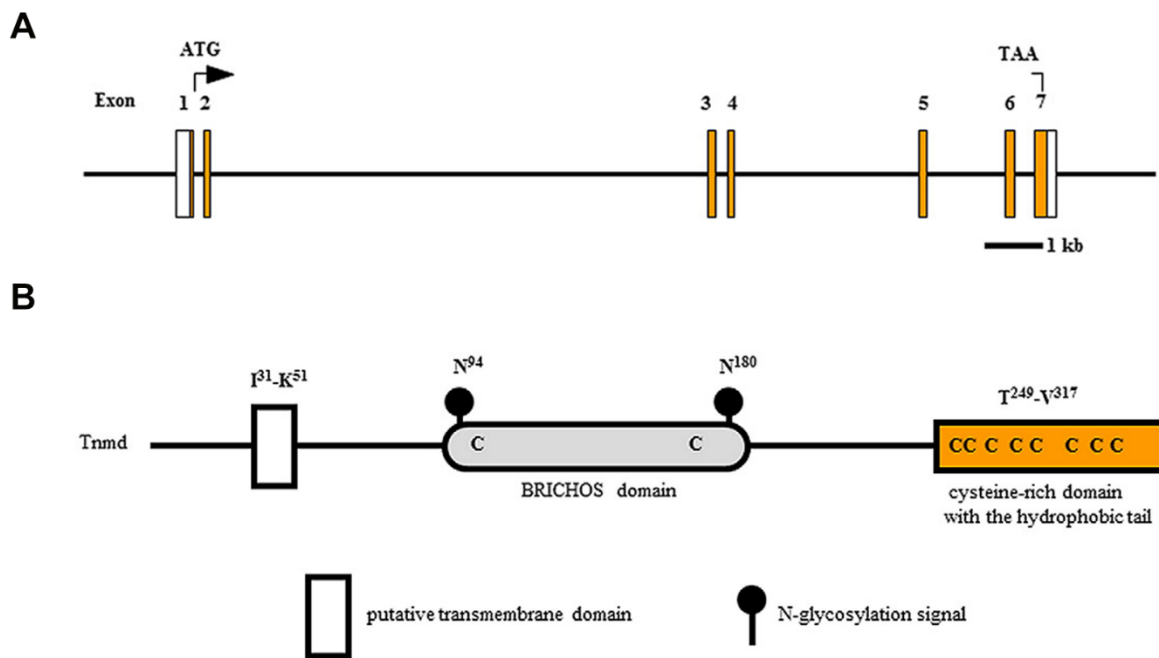


Fig. 7. Tenomodulin gene and protein structure. (A) Graphical exemplification of the gene *TNMD* (human) with 5' and 3' UTR sites (white boxes) and 7 exons (orange boxes). Start and stop codon (ATG, TAA, respectively); kb, kilo base. (B) Human TNMD protein contains a type II transmembrane domain at the N-terminus, a BRICHOS domain (flanked by two N-glycosylation sites) and a cysteine-rich C-terminal domain. Figure derived from Dex *et al.*, 2016⁸⁰, which has been published under the gold open access model.

1.7.1 Roles *in vivo* and *in vitro*

The functions attributed to *Tnmd* using *in vivo* and *in vitro* models are very briefly summarized in Table 1. For a far more comprehensive and focused review on Tenomodulin, I would like to refer to Dex *et al.*, 2016 article entitled “TENOgenic MODULating INside factor: systematic assessment on the functions of tenomodulin gene”⁸⁰.

Table 1: Summary of *Tnmd* functions.

<i>In vivo</i>	References
<i>Tnmd</i> is strongly expressed in tendons, but it is also found in other tissues (diaphragm, brain, skeletal muscle, eye, skin, chordae tendineae cordis and intervertebral disc’s outer anulus fibrosus).	33,154,155,158–160,
<i>Tnmd</i> supports tendon maturation, is needed for tenocyte proliferation, and is involved in collagen fibril thickening.	33
<i>Tnmd</i> 1) regulates collagen I fibril biomechanical and structural properties, 2) localizes in close proximity to collagen I and, 3) is required for optimal running performance in mice.	35
<i>In vitro</i>	References
Loss of <i>Tnmd</i> results in TSPC’s increased senescence and apoptosis, reduced proliferative and metabolic capacity.	34,161
Lack of <i>Tnmd</i> leads to decreased periodontal ligament fibroblasts cell adhesion capacity	162
<i>Tnmd</i> ^{-/-} TSPC exhibited a reduction of adhesion to collagen type I, impairment to contract 3D collagen matrix and abnormal gene expression profile.	161
<i>Tnmd</i> absence results in significantly lesser tendon stem/progenitor cell migratory capacities coupled with accelerated adipogenic differentiation rate.	160
<i>Tnmd</i> has an anti-angiogenic effect. It suppresses capillary-like morphogenesis of retina vascular endothelial cells, hinders tube formation and reduces HUVEC’s migration capacities.	156,159,163

1.7.2 Challenging *Tnmd* and its role in early healing

Docheva *et al.* reported in 2005 that the gene targeted *Tnmd*-deficient mice did not present any developmental, but rather a mild phenotype characterized by reduced cell density and proliferation, and the pathological thickening of collagen fibrils³³. Moreover, *Tnmd*-deficient mice were viable, had a normal life span and reproduction was not affected³³. In a follow-up study, Lin *et al.*, 2017 challenged *Tnmd* role and subjected skeletally mature *Tnmd*^{-/-} and WT mice to surgically induced full thickness ATR^{160,164}. The major findings regarding early tendon healing are shown as graphical synopsis in Fig. 8. At day 8 post-injury *Tnmd*^{-/-} mice displayed inferior scar tissue

characterized by lower histological healing scores, significantly reduced cell density and proliferation paralleled with increased blood vessel and adipocytes infiltration ¹⁶⁰. Moreover, senescence and apoptosis occurrence were significantly increased, whilst the total number of local CD146⁺ stem/progenitor cells was reduced ¹⁶⁰. Furthermore, erroneous deposition of ECM proteins biglycan, Cartilage oligomeric matrix protein (Comp) and fibronectin, as well as the accumulation of CD68⁺/CD80⁺ M1 polarized pro-inflammatory and the significant reduction of CD163⁺ M2 anti-inflammatory macrophages was detected in *Tnmd*^{-/-} scars ¹⁶⁰.

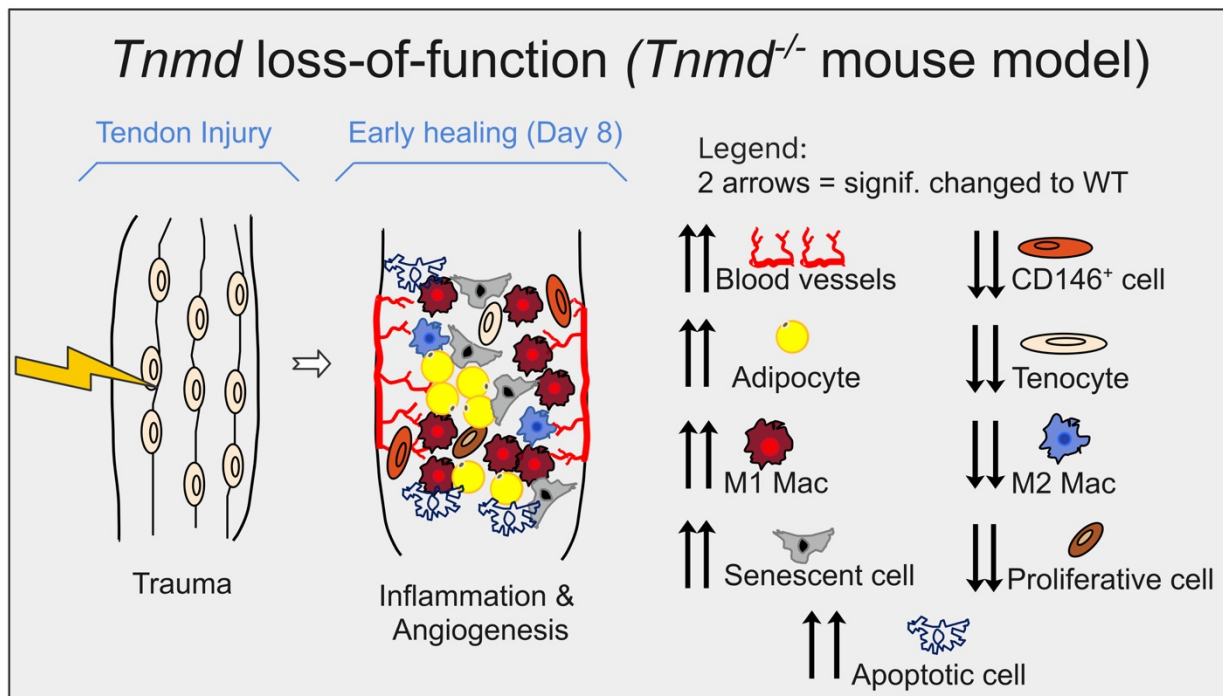


Fig. 8. Roles of Tenomodulin in early healing. Graphical synopsis is based on Lin *et al.*, 2017 ¹⁶⁰.

1.8 AIM AND MILESTONES OF THE THESIS

The main aim of this study was to compare and to identify the differences in the tendon healing process between *Tnmd*^{-/-} and wild type (WT) mice at three time points, namely, at day 8, day 21 and day 100 after a tenotomy. Grounded on the outcomes acquired from our study of the early stage of tendon repair¹⁶⁰, we implemented the established surgical model and carried out with *Tnmd*^{-/-} and WT animals a longitudinal in-depth characterization of the healing process up to day 100 post-injury. Our main hypothesis is that the lack of *Tnmd* will cause deficient and inferior repair during the later proliferative and remodeling stages and will lead to a significant endochondral heterotopic ossification of AT. In order to deliver evidence and prove of that, the following milestones were defined:

1. Detection, localization, and quantification of tendon-specific Scleraxis-expressing, and α SMA⁺ myofibroblastic cells during the healing process in injured *Tnmd*^{-/-} and WT ATs.
2. Assessment of *Tnmd*^{-/-} and WT ATs cellular and ECM composition at day 21 and 100 post-injury based on histological scoring and immuno-histomorphometry.
3. Analysis of gene expression profiles in *Tnmd*^{-/-} and WT ATs upon injury (at day 21 and 100) using custom-designed qRT-PCR plates.
4. Investigation of collagen fibril ultrastructural arrangement, conformation and morphology in non-injured controls, and injured *Tnmd*^{-/-} and WT ATs using Transmission Electron Microscopy (TEM).
5. Potential age-related HO formation in the AT of non-injured 6- and 9-month-old *Tnmd*^{-/-} and WT mice. Analysis of trauma-induced HO formation during late healing and respective quantification of bone surface and volume using micro-computed tomography (μ CT).
6. Assessment of AT viscoelastic properties, such as stiffness, dynamic and static elastic modulus by carrying out biomechanical testing protocols with injured and non-injured control *Tnmd*^{-/-} and

WT ATs. Evaluation of tendon functionality based on the recording of distance that *Tnmd*^{-/-} and WT mice voluntarily run 100 days post-injury.

7. Detection of transcriptional differences in cells isolated from non-injured *Tnmd*^{-/-} and WT ScxGFP⁺ ATs using single cell RNA-sequencing.

2. MATERIALS AND METHODS

2.1 MATERIALS

2.1.1 Animals

Table 2: List of transgenic mice.

Mouse strain name	Target Gene	Reference
Tenomodulin WT/Heterozygous	<i>Tnmd</i>	33
Tenomodulin-Knockout	<i>Tnmd</i>	33
Scleraxis-GFP	<i>ScxGFP</i>	33,34,39

2.1.2 Primary cells

Table 3: List of used cells.

Cell type	Donor	Cell origin	Reference
TSPCs	6-months old mice <i>Tnmd</i> ^{-/-} <i>ScxGFP</i> ⁺	ATs	33,34,39
TSPCs	6-months old mice WT <i>ScxGFP</i> ⁺	ATs	33,34,39

2.1.3 Reagents and solutions

Table 4: List of media and supplements.

Media and supplements	Catalog Nr.	Manufacturer
DMEM/Ham's F-12 1:1 medium with stable glutamine	A2612	Biochrom, Berlin, Germany
Dulbecco's Phosphate Buffered Saline	D8537	Sigma-Aldrich, St. Louis, Missouri, USA
Fetal Bovine Serum (FBS) Premium	P30-3302	PAN Biotech, Aidenbach, Germany
L-ascorbic acid-2-phosphate	A8960	Sigma-Aldrich, Munich, Germany
Minimal Essential Medium Amino Acids Solution (50x)	#11130-036	Gibco by life sciences, Darmstadt, Germany
Penicillin-Streptomycin	P0781	Sigma-Aldrich, St. Louis, Missouri, USA

Table 5: List of chemicals.

Chemicals	Catalog Nr.	Manufacturer
Acetic acid	#33209M	Sigma-Aldrich, St. Louis, Missouri, USA
Albumin Fraction V, $\geq 98\%$ (BSA)		Carl Roth, Karlsruhe, Germany
Biozym LE Agarose	#840004	Biozym Scientific, Oldendorf, Germany
4',6-Diamidin-2-phenylindol (DAPI)		Sigma-Aldrich, St. Louis, Missouri, USA
D(+)-Sucrose $\geq 99.5\%$	#4621.2	Carl Roth, Karlsruhe, Germany
Diethylpyrocarbonat (DEPC)	W4502	Merck, Darmstadt, Germany
Direct Red 80 solution, Dye content 25%	#365548-5G	Sigma-Aldrich, St. Louis, Missouri, USA
Ethanol Rotipurano $\geq 99.8\%$	#9065.4	Carl Roth, Karlsruhe, Germany
Ethylenediaminetetraacetic acid disodium salt dihydrate (EDTA)	X986.3	Carl Roth, Karlsruhe, Germany
Eosin Y disodium salt	E4382	Merck, Darmstadt, Germany
Isopropanol (2-Propanol)	#109634	Merck, Darmstadt, Germany
Hematoxylin solution, Gill NO. 3	GHS332	Sigma-Aldrich, St. Louis, Missouri, USA
Methanol	#106009	Merck, Darmstadt, Germany
Mowiol 4-88		Carl Roth, Karlsruhe, Germany
Orange G loading dye	#0318.1	Carl Roth, Karlsruhe, Germany
Paraformaldehyde (PFA)	#0964.3	Carl Roth, Karlsruhe, Germany
Proteinase K, recombinant, PCR grade (20mg/ml)	#E00491	ThermoFischer Scientific, Waltham, Massachusetts, USA
Roti®-GelStain	#3865.1	Carl Roth, Karlsruhe, Germany
TrackIt™ 1 kb Plus DNA ladder	#10488085	Invitrogen, Carlsbad, California, USA
Trizma base	T1503	Sigma-Aldrich, St. Louis, Missouri, USA
Tween 20	P1379	Sigma-Aldrich, St. Louis, Missouri, USA
Xylol	#108298	Merck, Darmstadt, Germany

Table 6: List of buffers.

Stock solution / buffer	Components	Concentration	Volume/Mass
Phosphate-buffered saline (PBS)		10x	
	KCl	26 mM	2 g
	KH ₂ PO ₄	10.5 mM	2 g
	NaCl	1.36 M	80 g
	Na ₂ HPO ₄ *7H ₂ O	81 mM	25.6 g
	dH ₂ O	Ad 1000 ml	
Tris-acetate-EDTA (TAE) Buffer		50x	
	EDTA	0.5 M	100 ml
	Glacial acetic acid	1 M	57.1 ml
	Tris Base	2 M	242 g
	dH ₂ O	Ad 1000 ml	

2.1.4 Kit-systems

Table 7: List of used kits.

Kit	Catalog Nr.	Manufacturer
Custom-designed PCR plates Analyzed genes (Table 15)	#10025218	BioRad Laboratories, Hercules, California, USA
2x SsoAdvanced Universal SYBR Green Supermix	#1725271	BioRad Laboratories, Hercules, California, USA
Herovici's collagen differentiation staining kit	#18432.00500	Morphisto GmbH, Frankfurt am Main, Germany
Qiagen RNeasy Mini kit	#74104	Qiagen, Hilden, Germany
Taq DNA Polymerase (1000 U)	#201205	Qiagen, Hilden, Germany
Transcriptor First Strand cDNA Synthesis kit	#04379012001	Roche, Mannheim, Germany

2.1.5 Primers

Table 8: List of primers used.

Target gene	Primers	Annealing temperature	Cycle number	Product size	Reference
Tnmd genomic PCR					
5' UTR-f2	F 5'-catctggtagccgactcactt-3'	47°C	35	WT: 136 bp	161
XTG PGK PA-f3	F 5'-ttaagggccagctcattcctc-3'			KO: 332 bp	
INT 1-r2	R 5'-agaatgtgacagccctcacag-3'				

GFP genomic PCR					
Forward	5'-caagctgaccctgaagttcatctgc-3'	59°C	35	GFP: 409 bp	165
Reverse	5'-cacgctgccgtcctcgatgttggtg-3'				

2.1.6 Antibodies

Table 9: Primary and secondary antibodies used.

Primary antibodies				
Target protein	Source / host species	Catalog # (clone)	Company	Dilution IHC (in 3% BSA/PBS)
anti-Aggrecan	Rabbit polyclonal	ab216965	Abcam	1:50
anti- α SMA	Rabbit polyclonal	ab5694	Abcam	1:50
anti-BrdU-POD	Rabbit polyclonal	11585860001	Sigma-Aldrich	1:30
anti-CD68	Rabbit polyclonal	ab125212	Abcam	1:50
anti-CD146	Rabbit polyclonal	ab75769	Abcam	1:50
anti-CD163	Rabbit polyclonal	ab182422	Abcam	1:50
anti-Col II	Rabbit polyclonal	ab34712	Abcam	1:50
anti-Col IV	Rabbit polyclonal	ab6586	Abcam	1:50
anti-NEFH	Rabbit polyclonal	ab8135	Abcam	1:50

Secondary antibodies				
Target species	Host	Catalog # (clone)	Company	Dilution IHC (in 3% BSA/PBS)
anti-rabbit HRP	goat	111-065-045	Jackson ImmunoResearch, Pennsylvania, USA	1:500
anti-rabbit Cy TM 3-conjugated	goat	111-165-144	Jackson ImmunoResearch, Pennsylvania, USA	1:200

2.1.7 Disposables

Table 10: List of disposables.

Utensil	Manufacturer
PCR mini cooler with transparent lid	Merck, Darmstadt, Germany
Costar Stripette 5-to-50 ml	Corning, NY, USA
Cover slide 24x60 mm	Carl Roth, Karlsruhe, Germany
Falcon 15- and 50 ml high-clarity Polypropylene conical tube	Corning, NY, USA
Filter tips (10 μ l – 1000 μ l)	Nerbeplus, Winsen/Luhe, Germany
PCR-foil Ultra clear RT-PCR G060/UC-RT	Kisker Biotech, Steinfurt, Germany
PCR Strips (0.2 ml 8-Tube) with corresponding optical, ultraclear Caps	Bio-Rad Laboratories GmbH, Munich, Germany
Safe-lock Tubes 1.5- and 2.0 ml	Eppendorf, Hamburg, Germany

SuperFrost® Plus glass slides	Menzel GmbH & Co, Braunschweig, Germany
-------------------------------	---

2.1.8 Devices

Table 11: List of used instruments.

Instrument	Model	Manufacturer
Axial test-bench for biomechanical testing	LM1	TA Instruments, New Castle, USA
Cryotome	Leica CM1950	Leica Biosystems Nussloch GmbH, Nußloch, Germany
Electron microscope	LEO912AB	Carl Zeiss, Oberkochen, Germany
Electrophoresis chamber	WideMini-Sub Cell GT	Bio-Rad Laboratories GmbH, Munich, Germany
Electronic pipetting aid	Easypet 3	Eppendorf, Hamburg, Germany
Electrophoresis power supply	PowerPac™ Basic Power Supply #1645050	Bio-Rad Laboratories GmbH, Munich, Germany
Gel Doc imaging system	EZ Imager #1708270	Bio-Rad Laboratories GmbH, Munich, Germany
Micro-CT system	Phoenix v tome x s 240/180	GE Sensing & Inspection Technologies, Frankfurt am Main, Germany
Microwave	8022 L	Privileg, Benton Harbor, Michigan, USA
Microtome	Reichert Ultracut-S	Leica, Bensheim, Germany
NanoDrop™ Spectrophotometer	NanoDrop™ 2000	ThermoFischer Scientific, Waltham, Massachusetts, USA
Polarized light microscope	OLYMPUS BX52 microscope	OLYMPUS, Shinjuku, Tokyo, Japan
Precision balance	Kern 770	Kern & Sohn GmbH, Balingen, Germany
Real time q-PCR detection system	CFX96	Bio-Rad Laboratories GmbH, Munich, Germany
Single channel pipette 1-1000 µl	Research plus	Eppendorf, Hamburg, Germany
Water purification system	Milli-Q	Merck Millipore, Burlington, Massachusetts, USA
Zeiss inversed microscope	Axio Observer	Carl Zeiss, Oberkochen, Germany

2.1.9 Software

Table 12: List of software used.

Software	Provider
Adobe Photoshop CC 2020 21.2.3	Adobe Inc., San Jose, California, USA
Bio-Rad CFX manager 3.1	Bio-Rad Laboratories GmbH, Munich, Germany
GraphPad Prism 8.0	GraphPad, La Jolla, California, USA
Image Lab	Bio-Rad Laboratories GmbH, Munich, Germany
ImageJ 1.53a	National Institutes of Health, Bethesda, Maryland, USA
iTEM software	Olympus, Tokyo, Japan
Microsoft Office (Excel, Word, PowerPoint)	Microsoft, Redmond, Washington, USA
NIKON D3-L3 software	Nikon, Chiyoda, Tokyo, Japan
Volume Graphics VG Studio Max 2.2.3	Volume Graphics, Heidelberg, Germany
Zen 3.0 (blue edition)	Carl Zeiss, Oberkochen, Germany

2.2 METHODS

I would like to state clearly that parts of the methods have already been published in Delgado Caceres M, Angerpointner K, Galler M, Lin D, Michel PA, Brochhausen C, Lu X, Varadarajan AR, Warfsmann J, Stange R, Alt V, Pfeifer CG, Docheva D. Tenomodulin knockout mice exhibit worse late healing outcomes with augmented trauma-induced heterotopic ossification of Achilles tendon. *Cell Death & Disease* (2021) ⁸⁹.

2.2.1 Animals

2.2.1.1 Housing and breeding

Transgenic mice described in chapter 2.1.1 were housed under specific-pathogen-free (SPF) conditions with controlled temperature and ventilation, under a 12:12 h light/dark cycle and fed *ad libitum* in the central animal laboratory facilities at the Regensburg University Medical Centre. Mice were backcrossed at least 6 times to C57BL/6J background. The breeding strategy applied in this study is summarized in Fig. 9. To follow the 3R-principle (Replacement, Reduction and Refinement), we designed a breeding scheme, which regardless of sex, would allow us to include all generated animals in our study. One *Tnmd*^{+/-} male mouse (Tnmd X⁻Y) was placed with a maximum of two heterozygous females (X⁺X⁻) in the same breeding cage. This scheme applies also to the *ScxGFP* animals used for lineage tracing experiments. With this approach we were able to obtain 25%/25% -hemizygous/knockout male, and 25%/25%-heterozygous/homozygous female mutant mice. For the matter of simplicity, the term WT will be used hereafter to refer heterozygous mice too.

♀ +	♂	X ⁻	Y
X ⁺		X ⁺ X ⁻	X ⁺ Y
X ⁻		X ⁻ X ⁻	X ⁻ Y

Fig. 9. Breeding scheme shows Mendelian ratio of genotypes. With this strategy, all generated animals can be included in the study. Breeding results in 50% of WT vs. 50% knockout mice (male or female).

2.2.1.2 Genotyping

First, genomic DNA (gDNA) was isolated from ear clip biopsies, which were enzymatically digested overnight at 56°C in 0.2 ml lysis buffer composed of 1x PCR Buffer (Taq Polymerase Kit, Qiagen, Hilden, Germany) supplemented with proteinase K (ThermoFischer Scientific, Waltham, Massachusetts, USA) to a final concentration of 0.2 mg/ml. Next, after total tissue lysis, proteinase K was heat-inactivated at 95°C for 10 min, samples were centrifuged at 12000 rpm for 5 min, and supernatant containing genomic DNA was harvested in a new Eppendorf reaction tube and stored at 4°C until use. Genotyping was performed by genomic PCR in a CFX96 Real time q-PCR detection system (Bio-Rad Laboratories GmbH, Munich, Germany) using the mix of forward primers in the 5'-untranslated region (5'-UTR) of the *Tnmd* gene and the PGK poly(A) signal sequence of the neomycin cassette, and a reverse primer in exon 2 (Table 8). The *ScxGFP* transgenic mice was genotyped using specific primers for the *GFP* gene (Table 8). The composition of the PCR reaction mix and program is shown in Table 13.

Table 13. PCR reaction mix and program for *Tnmd* and GFP genotyping.

PCR reaction mix	Volume [20 µl in total]	PCR program
10x PCR buffer	2	95°C → 10 min 95°C → 30 sec 49°C → 30 sec 34x 72°C → 1 min 72°C → 10 min 4°C → forever
dNTPs	0.4	
5'-UTR-f2	0.5	
XTG PGK PA-f3	0.5	
INT 1-r2	1	
Taq polymerase	0.2	
H ₂ O (PCR grade)	13.9	
gDNA template	1.5	
PCR reaction mix	Volume [20 µl in total]	PCR program
10x PCR buffer	2	95°C → 10 min 95°C → 30 sec 49°C → 30 sec 34x 72°C → 1 min 72°C → 10 min 4°C → forever
dNTPs	0.4	
GFP-Forward primer	0.5	
GFP-Reverse primer	0.5	
Taq polymerase	0.2	
H ₂ O (PCR grade)	14.9	
gDNA template	1.5	

Lastly, 1x Orange G loading dye (Carl Roth, Karlsruhe, Germany) was added to the PCR-amplified products and subjected to gel electrophoresis. For DNA visualization, Roti GelStain (Carl Roth,

Karlsruhe, Germany) was supplemented to a 2% agarose gel made with 1x TAE buffer. For *Tnmd* gene, wild type allele was detectable by one band of 136 bp (between 5'-UTR and exon 2). The *Tnmd*-knockout allele gives a band of 332 bp (between PGK promotor of the neomycin cassette and exon 2). Heterozygous mice showed both bands (Fig. 10A). For *GFP* gene, a single DNA fragment was detectable by one band of 409 bp (Fig. 10B).

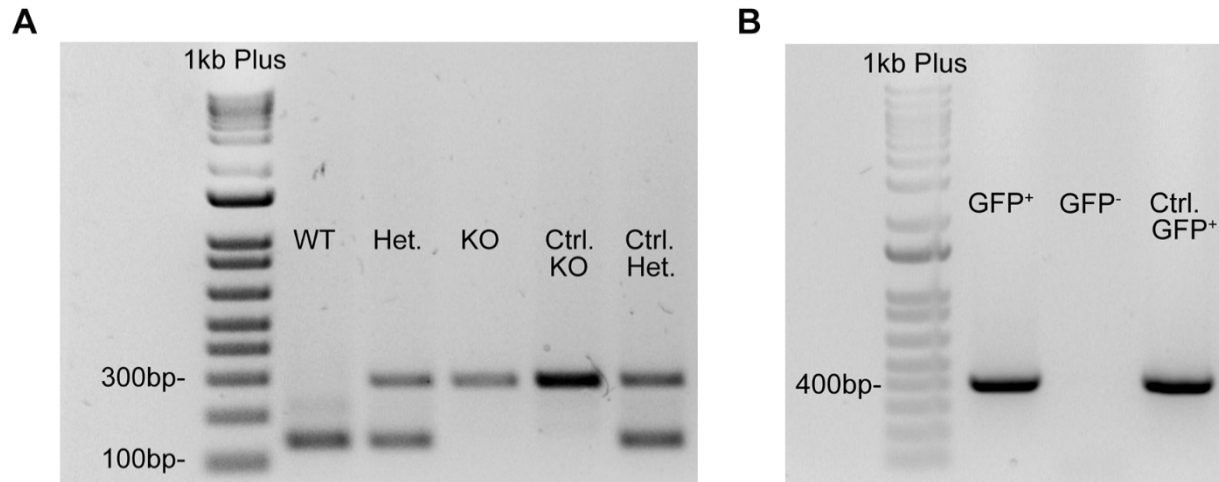


Fig. 10. Gel electrophoresis showing genotyping results. (A) Representative gel images showing the PCR-amplified DNA product of different sizes after reaction with specific primers for *Tnmd* and (B) *GFP*. Ctrl=control DNA from previously genotyped animals.

2.2.1.3 Experimental design

To deliver a comprehensible scheme and display the experimental group and size's distribution, a tree diagram was created (Fig. 11). "*Tnmd* gene is located on the X-Chromosome, therefore the WT group comprised hemizygous male, homozygous-, and heterozygous female mice. In total, 4 experimental groups were generated, and 3 time points were carefully chosen for in-depth characterization of the healing process.

Bio-statistical design of the group sizes was based on the values of $\alpha=0.05$ and $\beta=0.2$ for the power and type one error, respectively".

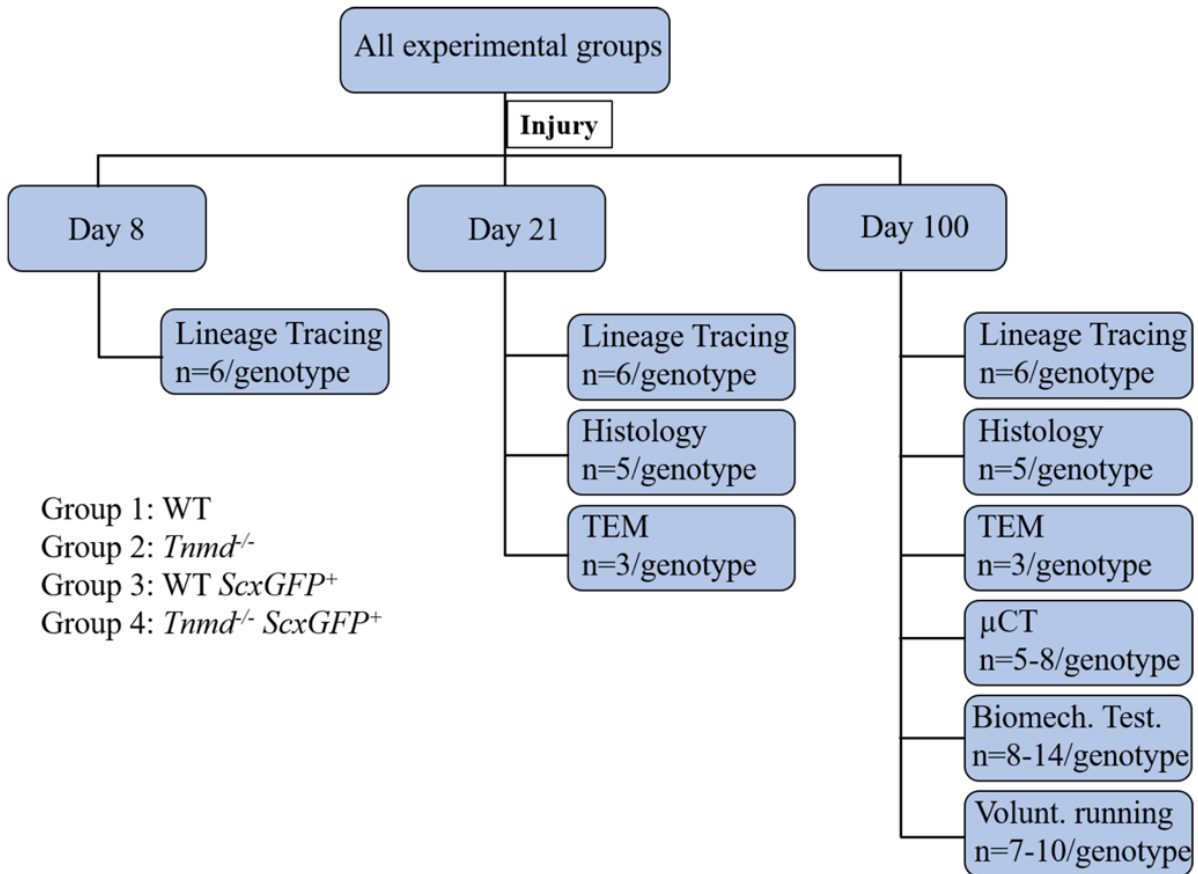


Fig. 11. Experimental design. Schematic representation of the experimental group design and size distribution. Figure derived from Suppl. Fig. 1A, Delgado Caceres *et al.*, 2021⁸⁹, which has been published under the gold open access model.

2.2.1.4 Surgical procedure

This work was performed in collaboration with Dr. med. Katharina Angerpointner, Dr. med. Michael Galler and Prof. Dr. med. Christian G. Pfeifer from the Clinic and Policlinic for Trauma Surgery, University Regensburg Medical Centre, Regensburg, Germany. All procedures were approved by the Animal Care and Use Committee of the Lower Franconia Government (Grant Nr. 55.2-2532-2-466).

*“Skeletally mature animals (6-month old) were selected because skeletal growth plateau was reached at this stage¹⁶⁶ and more important, it corresponds to approx. 40-year old humans, which belong to the risk group for ATR¹⁸. Mice were operated according to Lin *et al.*, 2017¹⁶⁰. In brief, after anaesthesia and skin incision, the left AT was fully resected 5 mm proximal of the calcaneus,*

followed by end-to-end reconstruction by Kirchmayr-Kessler suture technique (8-0 Ethilon) (Fig. 12). To circumvent suture failure, the range of movement of the talocrural joint was limited by a cerclage that was inserted through the tibiofibular fork and secured between the calcaneus and the plantar aponeurosis (6-0 Prolene). This guarantees a limited degree of extension (~30%) but permitting tensile load transmission. Experimental groups were allocated randomly, and the surgical team was blinded to the experimental group distribution”.

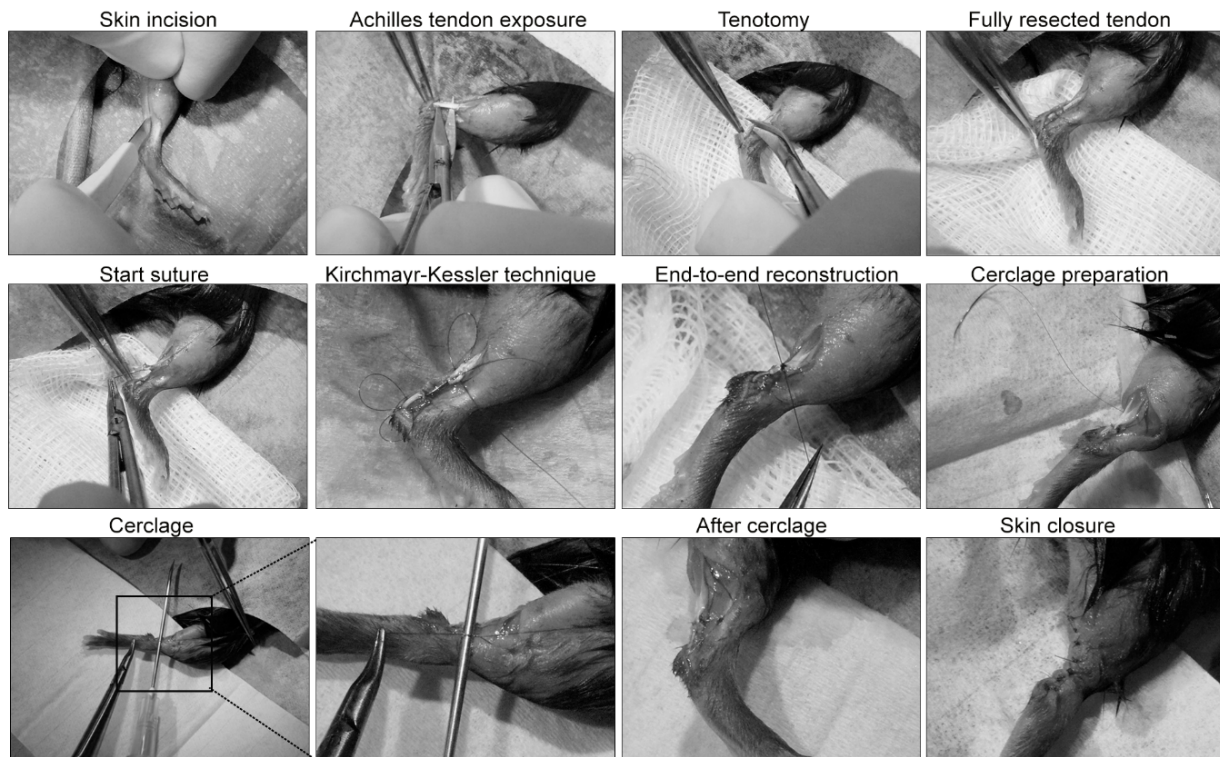


Fig. 12. Surgical procedure. Representative images of the surgical procedure. Figure was derived from Suppl. Fig. 1B, Delgado Caceres *et al.*, 2021⁸⁹ which has been published under the gold open access model.

2.2.2 Histology & Histomorphometry

2.2.2.1 Achilles tendon tissue processing

Upon sacrifice, mice hindlimbs were de-skinned and excised 0.5 cm inferiorly to the knee joint. The complex composed of gastrocnemius muscle-AT-calcaneus was used to obtain an overview of the whole AT anatomy, namely, from the MTJ until the enthesis. Next, mouse hindlimbs were rinsed with PBS and fixed overnight (4°C) under gentle shaking either in fresh, ice-cold 4%

paraformaldehyde (PFA, Merck, Darmstadt, Germany) in phosphate-buffered saline (PBS; pH 7.4) or in 95% ethanol- 5% glacial acetic acid (Saint Marie-SM fixation solution). On the next day, specimens fixed with PFA were rinsed 3x15 min in PBS at room temperature, whilst SM-fixed specimens were rehydrated in a descending ethanol row: 90%-, 80%-, 70% ethanol/dH₂O for 2 h at 4°C and lastly in 50% ethanol/PBS ON at 4°C. Next day, SM-fixed specimens were rinsed 3x15 min in PBS. Specimens were subsequently decalcified in 10% ethylen diamine tetraacetic acid (EDTA)/phosphate buffered saline (PBS) pH 8.0 (Sigma-Aldrich, Munich, Germany) for 4 weeks. Solution was changed every third day.

After an internal control for proper decalcification (needle-test), specimens were rinsed 3x15 min in PBS and subsequently cryoprotected in an ascending solution of sucrose/PBS: 10% for 4 h, and 20% ON at 4°C. The next day, specimens went to a 30% sucrose/PBS for 4 h and into a 1:1 solution of 30% sucrose/Tissue-Tek O.C.T (Sakura Finetek Europe B.V., Alphen aan den Rijn, The Netherlands) ON at 4°C. Finally, specimens were placed in a plastic disposable mold, fixed with forceps to form a 90° angle between the AT and calcaneus and positioned on a copper plate onto dry ice. Once specimens were fully frozen, were wrapped in Parafilm M (Bemis, Neenah, Wisconsin, USA) and stored at -80°C until use.

After embedding, cryosectioning was performed with a Leica CM1950 cryotome (Leica Biosystems Nussloch GmbH, Nußloch, Germany). Tissue sections with a thickness of 10µm were prepared, collected onto SuperFrost plus glass slides (Menzel GmbH & Co, Braunschweig, Germany) and stored at -20°C until use.

2.2.2.2 Hematoxylin and eosin (H&E) staining

This histological staining technique allows an overall screening of the tissue morphology. Hematoxylin is a basic dye, and therefore it stains negative-charged molecules purple (DNA, cell nuclei). Eosin in contrast, is an anionic dye and stains most proteins in the cytoplasm and ECM in varying degrees of pink¹⁶⁷.

Every 10th slide was stained with Hematoxylin-Eosin following standard protocol. In brief, tissue sections were taken from the -20°C freezer and maintained at RT for 45 min. Next, tissue sections were rinsed 1x for 5 min in dH₂O, submerged for 5 min in a glass-jar containing Hematoxylin solution (Gill Nr. III) and followed by rinsing with running tap water for 5 min. Then, the sections were submerged for 2 sec in a 0.1% aqueous HCl solution. For differentiation, tissue sections were

placed for 5 min in running tap water and subsequently placed for 3 min in a 0.5% aqueous Eosin Y solution. After a brief rinsing in tap water, tissue sections were dehydrated in an ascending ethanol row (70-, 80-, 90-, 96- and 100%). Finally, sections were cleared by 2 steps in Xylol for 5 min each and mounted with DePeX mounting media (Serva, Heidelberg, Germany). Images were taken on an inverted Zeiss microscope (Axio Observer) implemented with monochromatic and color Axiocam cameras (Carl Zeiss, Jena, Germany).

2.2.2.3 Herovici staining

To assess collagen maturation, Herovici staining was performed with Herovici's collagen differentiation staining kit, (Morphisto GmbH, Frankfurt am Main, Germany) according to the manufacture's protocol. The Tissue sections were selected based on equivalent regional planes between the genotypes. In brief, sections were taken from the -20°C freezer and maintained at RT for 45 min. Sections were rehydrated in a descending ethanol row: 96%-, 80%-, 70%-, and 60% ethanol/dH₂O for 5 min each and subsequently rinsed in dH₂O for 30 sec. After a 5 min immersion in Coelestine blue–Iron-Alum solution and subsequent rinsing step for 1 min in tap water, the tissue sections were immersed in Aluminum iron hematoxylin solution for 5 min and rinsed again for 15 min in running tap water. Next, the sections were placed for 2 min in 2% Metanil yellow solution, for 4 min in 1% acetic acid and rinsed for 30 sec in dH₂O. After a 2 min immersion in 0.05% Lithium carbonate solution and 2 min immersion in Hansen's Picric Fuchsine, tissue sections were kept for 2 min in 1% acetic acid. Tissue sections were dehydrated by 2 steps in 99% ethanol, 2 min each and immersed for 5 min in Isopropanol. Last, tissue sections were cleared by 2 steps in Xylol for 5 min each and mounted with DePeX mounting media (Serva, Heidelberg, Germany). The result of the staining can be interpreted as follows: the blue dye stains immature collagen III and the red dye, the mature, organized collagen type I ¹⁶⁸. Herovici staining was performed with specimens obtained at day 21 post-injury. In total 6 animals/genotype were selected for staining. Each animal was represented by 3 tissue sections. Images were taken on an inverted Zeiss microscope (Axio Observer) implemented with monochromatic and color Axiocam cameras.

2.2.2.4 Picrosirius red staining

Picrosirius red staining was performed to evaluate collagen fibril alignment in *Tnmd*^{-/-} and WT ATs at day 21 post-injury with n=4 animals/genotype. Each animal was represented by 3 tissue sections. The tissue sections were selected based on equivalent regional planes between the genotypes. Staining was performed using Direct Red 80 solution (Sigma-Aldrich) following standard protocol. In brief, sections were taken from the -20°C freezer and maintained at RT for 45 min. Next, sections were hydrated for 10 min in dH₂O, immersed in Weigert's hematoxylin solution for 8 min and then rinsed for 10 min in running tap water. Subsequently, the tissue sections were immersed in Picrosirius red solution for 1 h and rinsed by 2 steps in acidified water (5 ml acetic acid to 1 L dH₂O) for 1 min each. Tissue sections were dehydrated by 3 steps in 100% ethanol for 3 min each and cleared by 2 steps in Xylol for 5 min each. Finally, tissue sections were mounted with DePeX mounting media (Serva, Heidelberg, Germany).

Polarized light microscopy was performed with the OLYMPUS BX51 microscope (OLYMPUS, Shinjuku, Tokyo, Japan) equipped with a polarized filter was used. Four animals/genotype (n=4) at day 21 post-injury were used for staining. Each animal was represented by 3 tissue sections. Each tissue section was analyzed using the identical analyzer-polarizer settings allowing direct comparison between the specimens. NIKON digital camera DS-Fi2 and NIKON D3-L3 software (Nikon, Chiyoda, Tokyo, Japan) were used for image acquisition. In order to cover the entire tendon area, consecutive images were taken manually and digitally stitched as mosaic with Adobe Photoshop version: 22.5.1 (Adobe System, CA, USA). The bright yellow to orange/red color specifies bigger and better aligned fibrils, whilst green color indicates thin and poorly aligned fibrils.

2.2.2.5 Immunohistochemistry

For immunohistochemistry, tissue sections were treated with 10% H₂O₂ in methanol for 30 min, 1 mg/ml Pepsin (Sigma-Aldrich) for 15 min and blocked with 10% goat serum (Sigma-Aldrich) for 90 min (all at RT). Primary antibody against collagen type II (ab34712) and neurofilament-heavy chain (ab8135) (Abcam, Cambridge, UK) were diluted 1:50 in blocking solution and applied overnight at 4°C. Next day, corresponding goat anti rabbit biotinylated secondary antibody (Jackson ImmunoResearch, Pennsylvania, USA) was diluted 1:500 in blocking solution and

applied for 1 hour at RT. Sections were treated with ABC-Kit (Vector Laboratories, Burlingame, USA) for 90 min, then with chromogen 3,3-diaminobenzidine tetrahydrochloride (DAB) and a nickel enhancer (Sigma-Aldrich), incubated for a maximum of 4 min and lastly mounted with DePeX (Serva, Heidelberg, Germany). For collagen type II staining, 8 animals/genotype were selected, and each animal was represented by 3 tissue sections. In the case of the neurofilament-heavy chain staining, 4 animals/genotype were selected, and each animal was represented by 3 tissue sections.

To detect proliferative cells, 90 min. prior to euthanasia, operated mice received an intraperitoneal injection with BrdU (50 µg/g body weight, Catalog Nr. 550891, BD Pharmingen). BrdU detection in tissue sections was performed according to the manufacturer's instructions. In brief, sections were treated with 4N HCl for 20 min. at room temperature to denature the DNA and rinsed 2 times for 5 min. each with PBS. Next, 10% H₂O₂ in methanol was used to quench endogenous peroxidase activity for 30 min following an enzymatic digestion step with 1 mg/ml Pepsin (Sigma-Aldrich) for 15 min. To avoid non-specific binding, tissue sections were blocked with 0.5% BSA/0.1% Tween 20/PBS (Sigma-Aldrich) for 60 min. BrdU-POD antibody (REF11585860001, Sigma-Aldrich) was diluted 1:40 in blocking solution, added to tissue sections and incubated at 4°C overnight. Next day, sections were treated with chromogen 3,3-diaminobenzidine tetrahydrochloride (DAB) and a nickel enhancer (Sigma-Aldrich) until proper signal was visible (without exceeding 4 min), rinsed with distilled H₂O (dH₂O) for 5 min, incubated in Hematoxylin solution for 5 min. and mounted with DePeX (Serva, Heidelberg, Germany). For this staining, 3 animals/genotype were selected, each animal was represented by 3 tissue sections.

2.2.2.6 Immunofluorescence

For immunofluorescence, tissue sections (exact n-numbers are shown in the respective figure legends) were treated with 2mg/ml hyaluronidase (Sigma-Aldrich) for 30 min at 37°C and subsequently blocked with 3% BSA bovine serum albumin (BSA)/PBS (Sigma-Aldrich) for 90 min. Primary antibodies against αSMA (ab5694), CD68 (ab125212), collagen IV (ab6586), CD146 (ab75769), CD163 (ab182422) and OPN (ab8448) (all Abcam) (Table 9) were applied overnight at 4°C, followed by goat anti-rabbit CyTM3-conjugated secondary antibody (Jackson ImmunoResearch) for 1 hour at RT. Last, sections were counter-stained with 4',6-diamidino-2-phenylindole (DAPI) for 10 min and finally mounted.

2.2.2.7 Scoring system

Tissue sections prepared from injured *Tnmd*^{-/-}, WT, *Tnmd*^{-/-} *ScxGFP*⁺ and WT *ScxGFP*⁺ ATs were selected for detailed investigation based on equivalent regional planes between the genotypes. If not otherwise stated, H&E-stained sections were used for histological scoring of the samples from day 21 and day 100 post-injury. For day 21, in total n=10 animals/genotype were selected, and each animal was represented by one tissue section. For the day 100 specimens, in total n=11 animals/genotype were selected, and each animal was represented by one tissue section.

For the assessment of cartilage formation and in addition to H&E staining, 3 tissue sections from n=8 animals/genotype were stained against COL II and 1 section/animal/genotype was scored. For the evaluation of inflammation, 3 tissue sections from n=6 animals/genotype were stained against CD68 and CD163 and 1 section/animal/genotype was scored. For vascularization and innervation, 3 tissue sections from n=4 animals/genotype were stained against COL IV and NEFH, respectively and 1 tissue section/animal/genotype was scored. Lastly, for the analysis of bone formation and in addition to H&E staining, 3 tissue sections from n=3/genotype were stained against OPN and 1 section/animal/genotype was scored.

Histological scoring was carried out by two independent observers according to Lin *et al.*, 2017 and Stoll *et al.*, 2011^{160,169} (Table 14).

Table 14. Histological scoring system, 21- and 100-days post-injury.

Evaluated parameters	Points
<i>Extracellular matrix (ECM) organization of the whole tendon</i>	
Wavy, compact and parallel arranged collagen fibers	2
In part compact, in part loose or not orderly	1
Loosely composed, not orderly (“granulation” tissue)	0
<i>Cellularity/cell-matrix-ratio</i>	
Physiological	2
Locally increased cell density	1
Increased cell density or decreased ECM content	0
<i>Cell alignment</i>	
Uniaxial	2
Areas of irregularly arranged cells (10-50%)	1
More than 50% of cells with no uniaxial alignment	0
<i>Cell distribution</i>	
Homogeneous, physiological	1
Focal areas of elevated cell density (cell clustering)	0

<i>Cell nucleus morphology</i>	
Predominantly elongated, heterochromatic cell nuclei (tenocytes)	2
10-30% of the cells possess large, oval, euchromatic or polymorph heterochromatic nuclei	1
Predominantly larger, oval, euchromatic or polymorph, heterochromatic nuclei	0
<i>Organization of repair tissue of the tendon callus</i>	
Homogeneous (whole tissue with similar composition)	2
Locally heterogeneous tissue composition	1
Whole tissue composition completely changed	0
<i>Transition from defect to normal tissue</i>	
Scaffold integrated, no gaps at the margin visible	2
Recognizable transition	1
Abrupt transition, splitting/gaps detectable, callus tissue	0
<i>Configuration of callus</i>	
Normal, only in the defect area, locally confined	1
Strong, change of whole tendon, thickened	0
<i>Cartilage formation (COL II staining)</i>	
Non existing	2
Focally increased	1
Assembly of cartilage (more than 25% of the tendon)	0
<i>Degenerative changes/tissue metaplasia</i>	
Non existing	2
Moderate formation of oedema	1
Intense oedema with inclusion of fat, cell and/or fibers destruction, fibrin deposition, gaps, adhesions	0
<i>Inflammation (CD68/CD163 staining)</i>	
No inflammatory cell infiltrates	1
Infiltrating inflammatory cells (macrophages)	0
<i>Vascularization in the defect area (COL IV staining)</i>	
Hypo-vascularized, like surrounding tendon (small capillaries)	1
Hyper-vascularized (increased numbers of small or larger capillaries)	0
<i>Nerves (NEFH-staining)</i>	
Non existing	2
Focally increased (less than 25% of the entire tendon length)	1
Distributed through/along the entire tendon (more than 25%)	0
<i>Bone formation (OPN staining) → Analyzed only 100 days post-injury</i>	
Non existing	2
Focally increased (less than 25% of the tendon length)	1
Distributed through/along the entire tendon (more than 25%)	0

Table was derived from Suppl. Table 1 Delgado Caceres *et al.*, 2021⁸⁹, which has been published under the gold open access model. Additional references^{160,169}

2.2.2.8 Algorithm for automated quantification

To quantify positively labeled cells (ScxGFP, α SMA, CD146, CD68, and CD163), an automated quantitative image analysis was performed using ImageJ, software version 1.8.0_112 (National Institutes of Health, Bethesda, MD, USA). For automated quantification, 1 stained tissue section per animal/genotype and time point was used (depending on the staining performed, n=3-6 animals/genotype/time point).

The following algorithm was applied: (1) region of interest (ROI) (entire tendon) was manually selected and mosaic images from the antibody-stained tissue sections were generated using the inverted Zeiss microscope (Axio Observer). Next, using the “freehand selection” tool the ROI was designated; (2) RGB image was converted to 8-bit gray scale and inverted; (3) threshold for black and white colors was accustomed and fixed; (4) “Image-based Tool for Counting (ITCN)” was adjusted based on standard values for pixel width and minimum distance, as well as a threshold to ensure the quantification of single cells; (5) using the “analyze tool” the particles were automatically counted; (6) the procedure was applied first to quantify the total number of DAPI⁺ nuclei, and afterwards with the green (quantification of only ScxGFP⁺ cells) and red (quantification of only α SMA⁺, CD146⁺, CD68⁺, and CD163⁺ cells, respectively) fluorescence channels; (7) the data was expressed in % to total number of DAPI⁺ cells.

2.2.3 Transmission Electron Microscopy (TEM)

This work was performed by Prof. Dr. med. Christoph Brochhausen-Delius from the Institute of Pathology, University of Regensburg, Regensburg, Germany. Manuel Delgado Cáceres explanted the specimens for assessment and afterwards performed the quantitative analysis.

Injured and contralateral ATs were explanted at day 21 and 100 post-injury (n=3/genotype/time point), fixed in Karnovsky (0.1 M cacodylate-buffer with 2.5% glutaraldehyde and 2% paraformaldehyde), enclosed in 4% low melting agarose, post-fixed in 1% osmium tetroxide (pH 7.3), dehydrated in graded ethanol, and embedded in the EMbed-812 epoxy resin (all reagents Science Services, Munich, Germany). After 48 h heat polymerization at 60 °C, semi-thin sections (0.8 μ m) were prepared and stained with 1% toluidine blue and basic fuchsin to choose representative areas for further analysis. Ultrathin sections (0.08 μ m) were collected using a Reichert Ultracut-S microtome (Leica, Bensheim, Germany), mounted on copper-grids, and

stained with aqueous 2% uranyl acetate and lead citrate solutions (10 min each). The ultrathin sections for further analysis came from the injury region and from mid-portion in contralateral tendons, and were analyzed in a LEO912AB electron microscope (Zeiss, Oberkochen, Germany) operating at 100 kV. Findings were documented with a side-mounted 2 k x 2 k-CCD-camera (TRS, Moorenweis, Germany). The iTEM software (Olympus, Tokyo, Japan) was used to measure collagen fibril diameter. Five images (40000x magnification)/tendon (n=2/genotype/time point) were used for quantification, resulting in average of 2800 fibrils/group/time point being analyzed.

2.2.4 Micro-Computed Tomography

This work was performed under paid contract by Dr. Birgit Striegl from the Regensburg Centre of Biomedical Engineering, Regensburg, Germany. Manuel Delgado Cáceres excised, collected and prepared the specimens for analysis.

The specimens consisting of Muscle-Achilles tendon-calcaneus complex were collected 100 days post-injury (contralateral and non-injured ATs too) (n=4-8 animals/genotype), fixed as described above and scans were performed with the μ CT system Phoenix v|tome|x s 240/180 (GE Sensing & Inspection Technologies, Frankfurt am Main, Germany). The scanning parameters for *Tnmd*^{-/-} and WT hindlimbs were as follows: 50 kV voltage, 620 μ A current, 500 ms time, 2000 images, voxel size 10 μ m. Reconstructed volumes were processed using the manufacturer's software phoenix datos|x 2 reconstruction 2.4.0. The threshold value defining the material and background was set to 0.12 absorption coefficient. The 3D images, the surface area and volume parameters were obtained with the software Volume Graphics VG Studio Max 2.2.3 (Volume Graphics, Heidelberg, Germany). The ROIs were defined as follows: ROI 1 (red) start was set above the calcaneus (section plane at tibia base) and extended proximally 2.50 mm; ROI 2 (green) began at the final plane of ROI 1 and extended in proximal direction until the end (Fig. 13).

Moreover, to exclude that *Tnmd* might affect bone mass of skeletal system, the tibiofibular bone surface and volume in injured and non-injured hindlimbs was measured. The calcaneal bone surface and volume was measured in control, non-injured hindlimbs. The calcaneal-ROI started 0.60 \pm 0.05 mm from the end of the calcaneus and encompassed 0.60 \pm 0.05 mm region towards the

ankle joint; tibiofibular-ROI started 3.50 ± 0.05 mm above the calcaneus and covered 1.00 ± 0.05 mm region towards the knee joint.

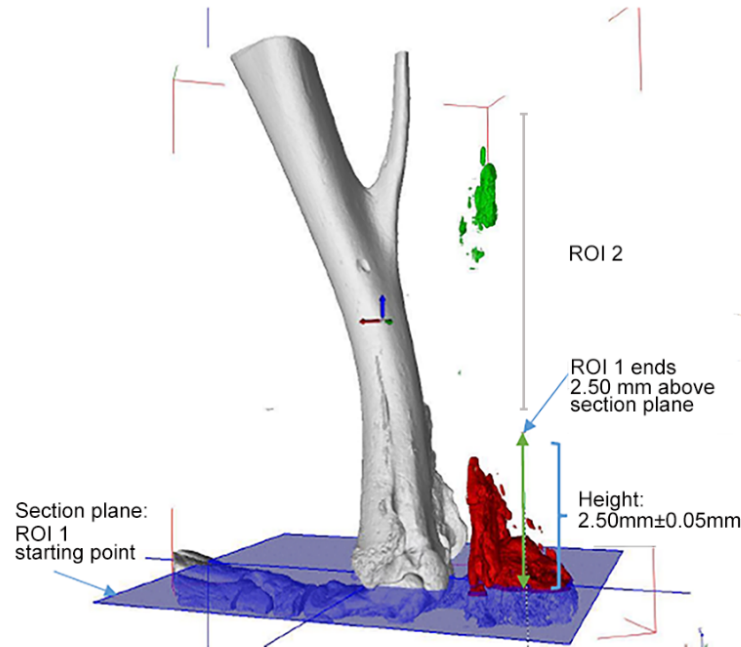


Fig. 13. Region of interest (ROI) used for μ CT quantification.

2.2.5 Biomechanical testing

This work was performed with the supervision of Dr. med. Philipp A. Michel and Prof. Dr. med. Richard Stange from the Department of Trauma-, Hand-, and Reconstructive Surgery, University Hospital Münster, Münster, Germany and the Department of Regenerative Musculoskeletal Medicine, University Hospital Muenster, Westfälische Wilhelms-University, Muenster, Germany.

2.2.5.1 Testing apparatus

After euthanasia with CO_2 , animal hindlimbs ($n=8-14/\text{genotype}$) were explanted, wrapped in a gauze soaked in PBS and stored at -20°C until testing. On testing day, hindlimbs were thawed for 30 minutes at RT and the suture material used for the cerclage (6-0 prolene) was carefully removed. The suture material used for the end-to-end reconstruction (8-0 ethilon) remained in order to avoid AT tissue damage. The viscoelastic biomechanical tests were performed with day 100 specimens

(non-injured, contralateral and injured) using LM1 machine (TA Instruments, New Castle, USA) and custom-made clamps securing the calcaneal and myotendinous junction ends (Fig. 14, left panel). All tests were performed in PBS-bath at room temperature. Biomechanical testing at day 21 was not carried out, because the scar tissue is dominated by cells and literature has previously reported that viscoelastic properties of rodent ATs are greatly compromised in first weeks after injury^{108,170}.

2.2.5.2 Viscoelastic testing protocol

The testing protocol was based on Dourte *et al.*, 2012¹⁷¹ and Hochstrat *et al.*, 2019¹⁷². In brief, tendon length (Fig. 14, panel in the middle) and width were measured with two digital microscope cameras (Dino-Lite Digital Microscope, Hsinchu, Taiwan) positioned in a 90° angle from each other. Prior to testing, a tendon-specific pretensioning force was applied. This force was calculated as follows: the cross-sectional area of each tendon was multiplied by a pre-defined standardized stress of 0.5 Mpa resulting in values oscillating between 0.18-1.96 N. In addition, the specimens were pre-conditioned with cyclic loading between 0.5% and 1.5% strain at 0.25Hz (10 cycles) and allowed to relax at 0% for 300 s. Next, specimens were subjected to a sinusoidal testing at different strain-levels (4, 6 and 8%) and frequencies (0.01; 0,1; 1; 5 and 10Hz) as a stress-relaxation test was performed at the start of every strain-level for 10 min. The frequency of 1Hz was used for reporting the dynamic E-modulus. After the last strain-level, tendons were returned to the pretension force and a load-to-failure ramp was applied (Fig. 14, right panel). The analysis of the data was carried out with a custom-written Matlab software protocol (MathWorks, Natick, Massachusetts, USA). The parameters cross-sectional area (mm²), static and dynamic E-Modulus (N/mm²) stiffness (N/mm) and load-to-failure (N) were evaluated. Specimens, which did not complete the entire testing protocol described above, either technical issue or because tendons ruptured during the testing process, were excluded from the analyses.

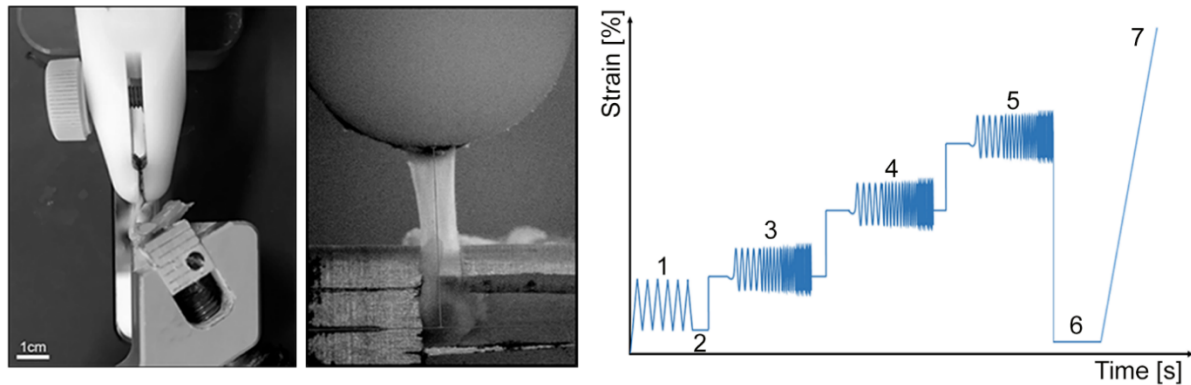


Fig. 14. Testing apparatus and viscoelastic testing protocol. Left panel, specimens fixed with custom-made clamps. Panel in the middle, tendon length and width measurement prior pretensioning force calculation. Right panel, schematic representation of the viscoelastic testing protocol. Figure derived from Suppl. Fig. 6A-B, Delgado Caceres *et al.*, 2021⁸⁹, which has been published under the gold open access model.

2.2.6 Voluntary Running Tests

For voluntary running tests, $n=7-10$ mice/genotype were allowed to voluntarily run at day 100 post-injury. Mice were acclimatized for 3 days to the experimental cage, containing a standard free-spinning mouse running wheel (12cm diameter) equipped with wired bike computer BC 5.16 (Sigma Sport, Neustadt, Germany). The magnet (M) was installed and connected to the mouse running wheel, whilst the detector (D) sends the signal to the sensor (S) placed outside the experimental cage (Fig. 15, left panel). At day 4, mice were placed individually in the experimental cage, left overnight (12 hours) to voluntarily use the wheel and the running distance was recorded (Fig. 15, right panel).

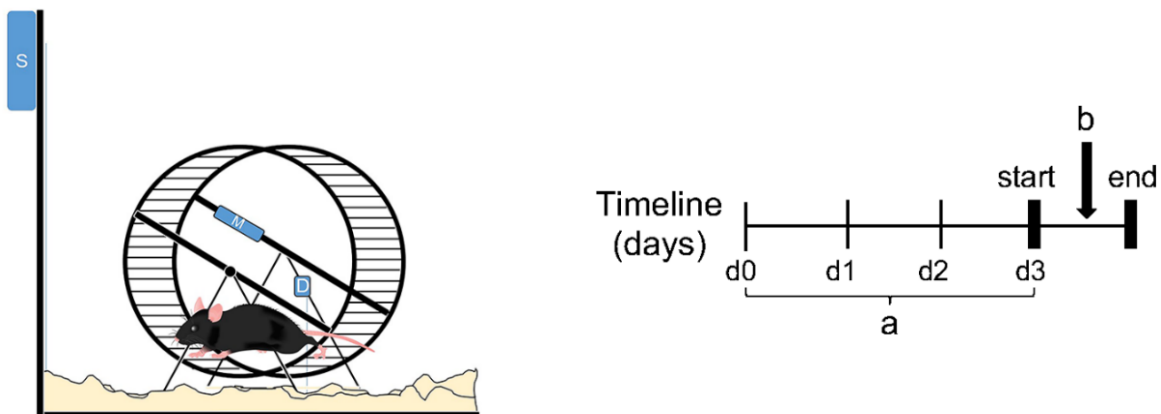


Fig. 15. Voluntary running test. Test setup (left panel) and timeline (right panel) for voluntary running tests. Figure derived from Fig. 6E. Delgado Cáceres *et al.*, 2021⁸⁹, which has been published under the gold open access model.

2.2.7 Single cell RNA-Sequencing

This work was performed under paid contract by Dr. Sarah Hücker and Dr. Stephan Kirsch from the Division of Personalized Tumor Therapy at the Fraunhofer Institute for Toxicology and Experimental Medicine (ITEM), Regensburg, Germany.

2.2.7.1 Cell isolation and whole transcriptome amplification and library preparation

Control, non-injured *Tnmd*^{-/-} *ScxGFP*⁺ and WT *ScxGFP*⁺ ATs (n=2/genotype) were explanted, cells were isolated by Manuel Delgado Cáceres as previously described by Alberton *et al.*, 2015³⁴ and subsequently delivered to Dr. Sarah Hücker. After lysis, centrifugation and filtration, cells were resuspended in Dulbecco's phosphate-buffered saline (DPBS) (Thermo Fisher Scientific, Waltham, Massachusetts, USA) and placed on AdcellTM diagnostic slides (Thermo Fisher Scientific), 20 *ScxGFP*⁺ cells/genotype) were isolated in 1 µl PBS each using a micromanipulator (Patchman NP2) with pump (CellTram, both Eppendorf, Hamburg, Germany) and subsequently stored in lysis buffer at -80°C.

The whole transcriptome amplification (WTA) and Illumina Nextera XT library preparation (Illumina, San Diego, California, USA) were performed as described by Picelli *et al.*, 2014¹⁷³. The protocol is divided in the following steps: single-cell lysis, reverse transcription, PCR preamplification, PCR purification, quality check of the cDNA library, tagmentation, amplification of adapter-ligated fragments, 2nd. PCR purification step, and a 2nd. quality check of final cDNA library. Finally, the libraries were quantified using the KAPA Library Quantification Kit (Roche Diagnostics, Mannheim, Germany), pooled in equimolar amount and sequenced paired-end with read length 2x150 bp and yield of 30 million reads per library on Illumina HiSeq. In total, six *ScxGFP*⁺ cells/genotype were subjected to scRNA-Seq. analysis.

2.2.7.2 Bioinformatics analysis

This work was performed in collaboration by Dr. Xin Lu, Dr. Adithi R. Varadarajan and Dr. Jens Warfsmann from the Division of Personalized Tumor Therapy at the Fraunhofer Institute for Toxicology and Experimental Medicine (ITEM), Regensburg, Germany.

*“The bioinformatics analysis started, after demultiplexing, with raw FASTQ files, which were submitted to an in-house single cell mRNA analysis pipeline 0.9.5.7. The raw sequence data from six ScxGFP⁺ cells/genotype (n=6) were trimmed with BBDuk 38.84¹⁷⁴, removing remaining adapter sequences and poor-quality bases at the end of each read. Read decontamination was performed using BioBloom Tolls 2.0.13¹⁷⁵ with filters for the genomes of *Mus musculus* (mm38), *Homo sapiens* (hg38), *Escherichia coli* (BL21), *Mycoplasma pneumonia* (M129), *Sphingobium* sp. (SYK-6), *Bradyrhizobium japonicum* (USDA 110), *Pichia pastoris* (GS115), *Malassezia globosa* (CBS 7966), *Aspergillus fumigatus* (AF293), and a set of viral genomes (RefSeq, 5k+ genomes). All reads that did not map exclusively to mm38 (Ensembl version 96, GRCm38 DNA primary assembly) were defined as likely contaminations and discarded from downstream processing. Sequence quality per sample was evaluated before as well as after trimming and decontamination using FastQC 0.11.9¹⁷⁶ and, in addition, all samples were analyzed as a collective with MultiQC 1.9¹⁷⁷. Next, the cleaned sample reads were aligned to the reference genome mm38 with STAR 2.5.1b¹⁷⁸. Reads mapping uniquely in exonic regions were counted per gene and per sample using feature counts from Subread 2.0.0¹⁷⁹. Further quality characteristics such as library complexity, using Preseq 2.0.3¹⁸⁰, and the genomic origin of the reads and the 5’-3’-bias, both with QualiMap 2.2.2d¹⁸¹, were assessed. The final counts table of the 12 samples (6 cells/genotype) were used further for differential gene expression analysis. The top 500 most variable genes were clustered using principal component analysis (PCA) and t-distributed stochastic neighbor embedding (t-SNE) with the Bioconductor package scater 1.14.6¹⁸². Raw counts were normalized and scaled into logCPM values before proceeding to batch correction. The bias introduced by degradation were corrected using cells with better quality as reference by Combat¹⁸³ function in the Bioconductor package sva 3.34.0¹⁸⁴. Differential expression analysis was performed between *Tnmd*^{-/-} ScxGFP⁺ and WT ScxGFP⁺ cells with the Bioconductor package edgeR 3.28.1¹⁸⁵ and DESeq2 1.26.0¹⁸⁶. Functional classification of differentially expressed genes (DEGs) into Gene Ontology (GO)¹⁸⁷ and Kyoto Encyclopedia of Genes and Genomes (KEGG)¹⁸⁸ categories were*

performed in R programming language 4.0.2 ¹⁸⁹ using Bioconductor 1.30.10 packages. GO enrichment annotates DEGs into three categories including Biological Process (BP), Molecular Function (MF) and Cellular Component (CC) whereas KEGG annotates DEGs into pathways. Intersection genes identified as differentially expressed in both DESeq2 and EdgeR were processed for enrichment analysis and log Fold change (logFc), p-value and adjusted p-value for the intersection genes were extracted from the DESeq2 method. Furthermore, this final list of 1430 DEGs were filtered for adjusted p-value <0.05 and |logFc|> 1. Goseq 1.42.0 ¹⁹⁰ with Wallenius noncentral hypergeometric distribution method used for GO enrichment analysis. This method uses a Probability Weighting Function (PWF) to correct for bias in gene length before performing an enrichment on DEGs. ClusterProfiler 3.18.1 ¹⁹¹ was used to perform Gene Set Enrichment analysis (GSEA) on KEGG terms and org.Mm.eg.db 312.0 was imported to map the gene symbols to Entrez gene identifiers in the mice database. For Gene Set Enrichment Analysis (GSEA), filtered genes were ranked according to their log Fold Change values. All figures were plotted using ggplot2 3.3.3 ¹⁹². ScRNA-Seq datasets used for the analysis have been deposited at Gene Expression Omnibus database at the National Center for Biotechnology Information and are part of Delgado Caceres et al., 2021 ⁸⁹, and can be found under the Accession number GSE179454”.

2.2.8 RNA isolation and reverse transcription polymerase chain reaction

Total RNA was isolated from *Tnmd*^{-/-} and WT ATs at day 21 and day 100 post-injury (pool of n=3 per genotype/time point) using the Qiagen RNeasy Mini kit (Qiagen, Hilden, Germany). Concentration and RNA purity were measured with the NanoDrop™ 2000 Spectrophotometer (ThermoFischer Scientific, Waltham, Massachusetts, USA). A260/A280 ratio higher than 2.0 was considered pure. Next, 1 µg total RNA was used for cDNA synthesis using Transcriptor First-Strand cDNA Synthesis kit (Roche, Mannheim, Germany) and following manufacturer's instructions. Custom-designed PCR plates containing primers for transcription factors, growth factor, extracellular matrix genes and collagen fibril regulator genes (Bio-Rad Laboratories GmbH, Munich, Germany, Cat. Nr. 10025218) were employed (Table 15). In brief, a master mix containing 10µl 2x SsoAdvanced Universal SYBR Green Supermix, 9µl PCR grade water and 1µl undiluted cDNA template was prepared (on ice) and carefully pipetted into each well. Next, the custom-designed PCR plate was placed into the CFX96 real time qPCR detection system and the following protocol was started: 2 min activation at 95°C, followed by 40 cycles of denaturation steps for 5 s at 95°C and annealing/elongation steps for 30 s at 60°C each. Finally, melt curve analysis was performed starting at 60°C for 1 min and increasing the temperature in 0.3°C steps for 15 s each 95°C were reached. Gene expression was analyzed with the $\Delta\Delta$ CT method and presented as fold change of *Tnmd*^{-/-} to WT. Three independent PCR experiments per genotype were carried out.

Table 15. List of genes analyzed by quantitative PCR using custom-designed PCR plates.

Target gene	Abbreviation	Category
Early growth response 1	<i>Egr1</i>	Transcription factors
Early growth response 2	<i>Egr2</i>	
Mohawk homeobox	<i>Mkx</i>	
Scleraxis homolog A	<i>Scx</i>	
Transforming growth factor beta 1	<i>Tgf-β1</i>	Growth factor
Collagen type I alpha 1	<i>Coll1a1</i>	Extracellular matrix
Collagen type III alpha 1	<i>Col3a1</i>	
Tenomodulin	<i>Tnmd</i>	
Biglycan	<i>Bgn</i>	Collagen fibril regulators
Decorin	<i>Dcn</i>	
Fibromodulin	<i>Fmod</i>	
Lumican	<i>Lum</i>	
Lysyl oxidase	<i>Lox</i>	
Transglutaminase 2	<i>Tgm2</i>	

2.2.9 Statistics

The row data was processed with Microsoft Excel 2016 (Microsoft Corporation, Redmond, Washington, USA). Statistical calculations were performed with GraphPad Prism 7 (San Diego, CA, USA). The results are presented as box plots with median and interquartile range (IQR), which is the difference between the 75th and 25th percentile; as well as whiskers that show minimum and maximum values. After normality Shapiro-Wilk check, two-group analyses were performed, if not otherwise stated, with 2-tailed parametric unpaired Student's t-test. Multi-group comparisons were evaluated by one-way ANOVA with Bonferroni post-hoc test for multiple comparisons (biomechanics). Differences were considered statistically significant according to values of * $p < 0.05$, ** $p < 0.01$, *** $p < 0.001$ and **** $p < 0.0001$.

3. RESULTS

I would like to state clearly that these results have already been published in Delgado Caceres M, Angerpointner K, Galler M, Lin D, Michel PA, Brochhausen C, Lu X, Varadarajan AR, Warfsmann J, Stange R, Alt V, Pfeifer CG, Docheva D. Tenomodulin knockout mice exhibit worse late healing outcomes with augmented trauma-induced heterotopic ossification of Achilles tendon. *Cell Death & Disease* (2021) ⁸⁹.

3.1 *Tnmd*^{-/-} scars contain significantly higher number of α SMA⁺ cells and lower number of tendon-specific ScxGFP⁺ cell during early and late healing

To identify the presence of the two cell populations involved in tendon healing we performed lineage tracing analysis using *Tnmd*^{-/-} ScxGFP⁺ and WT ScxGFP⁺ mice, and immunofluorescence stainings for α SMA at day 8, 21 and 100 post-injury. Interestingly, at the earliest time point ScxGFP⁺ cells were predominantly distributed at both tendon stumps, at the enthesis and at the MTJ, and only a very scarce number of ScxGFP⁺ cells was present directly at the injury site (Fig. 16A-B1).

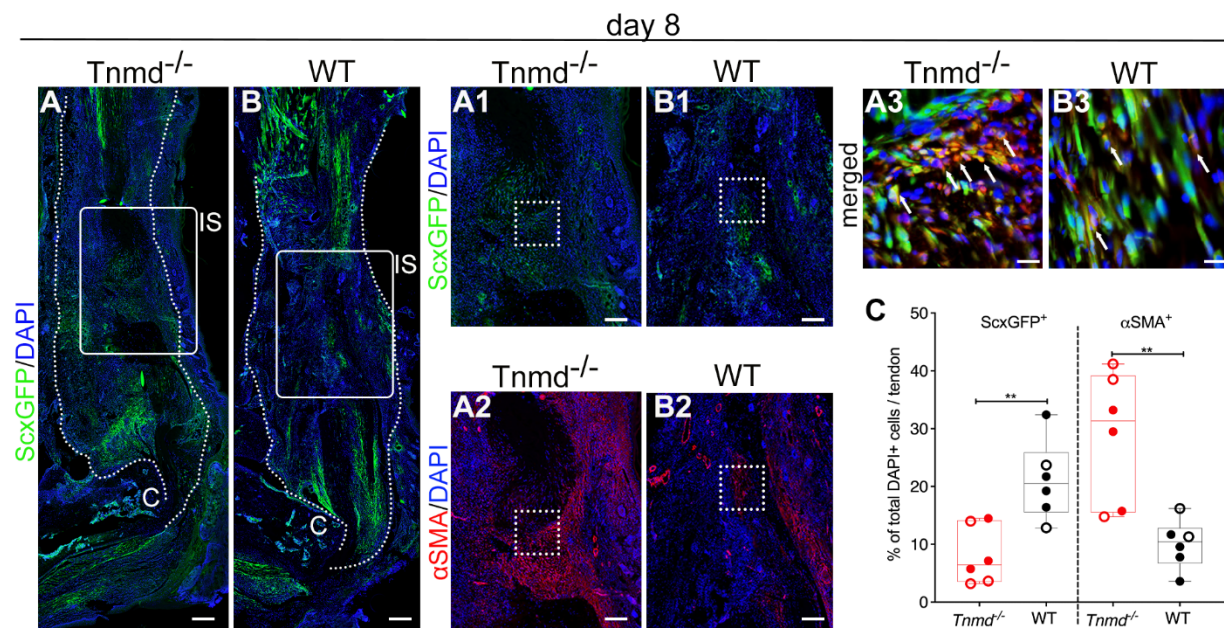


Fig. 16. Incidence of ScxGFP⁺ and α SMA⁺ cell populations during tendon healing at day 8 post-injury. (A-B) Representative mosaic images of injured *Tnmd*^{-/-} ScxGFP and WT ScxGFP ATs 8 days post-injury. (A1-B3) ScxGFP⁺ cell occurrence with corresponding immunofluorescence images of α SMA⁺ staining from the injury site, and (C) quantitative analysis of ScxGFP⁺ and α SMA⁺ cells as percentage of total number of DAPI⁺ cells within AT scars.

Results

White dotted lines frame ATs; white arrows mark double positive ScxGFP⁺/αSMA⁺ cells. C= calcaneus, IS=injury site. Scale bar: 200μm (panels A-B); 100μm (panels A1-B2); 20μm (panel A3, B3). ScxGFP imaging, αSMA staining and quantification were performed with n=6 animals/genotype; each animal represented by three tissue sections. Box plots show median ± interquartile range (IQR), statistical significance was assessed with 2-tailed unpaired parametric Student's t-test, *p<0.05, **p<0.01. Empty dot represents female mouse; filled dot represents male mouse. Figure was derived from Fig. 1A-D, Delgado Caceres *et al.*, 2021⁸⁹, which has been published under the gold open access model.

The corresponding quantitative analysis revealed significantly less tendon-specific ScxGFP⁺ cells in injured *Tnmd*^{-/-} tendons, in comparison to WT (6.5% vs. 20.5%, respectively) (Fig. 16C). In contrast, approx. one third (31.3%) of DAPI⁺ cells were positively stained for αSMA in *Tnmd*^{-/-} scars (Fig. 16A2-B2, C). Interestingly, single cells were double positive for ScxGFP and αSMA (Fig. 16A3, B3).

Next, the second stage of healing (reparative, proliferative phase) was assessed. At day 21 post-injury ScxGFP⁺ cell numbers were strongly increased in both groups (26% vs. 32.5%) and bridged entirely the defect between the sutured AT ends (Fig. 17A-B1, C). On the other hand, a clear decline in αSMA⁺ cells was detected in the injured *Tnmd*^{-/-} ATs (9.3%) compared to day 8, however the changes were not significant between the genotypes (Fig. 17A2-B2, C). Furthermore, at this stage yet again single cells were double positive for ScxGFP and αSMA (Fig. 17A3, B3).

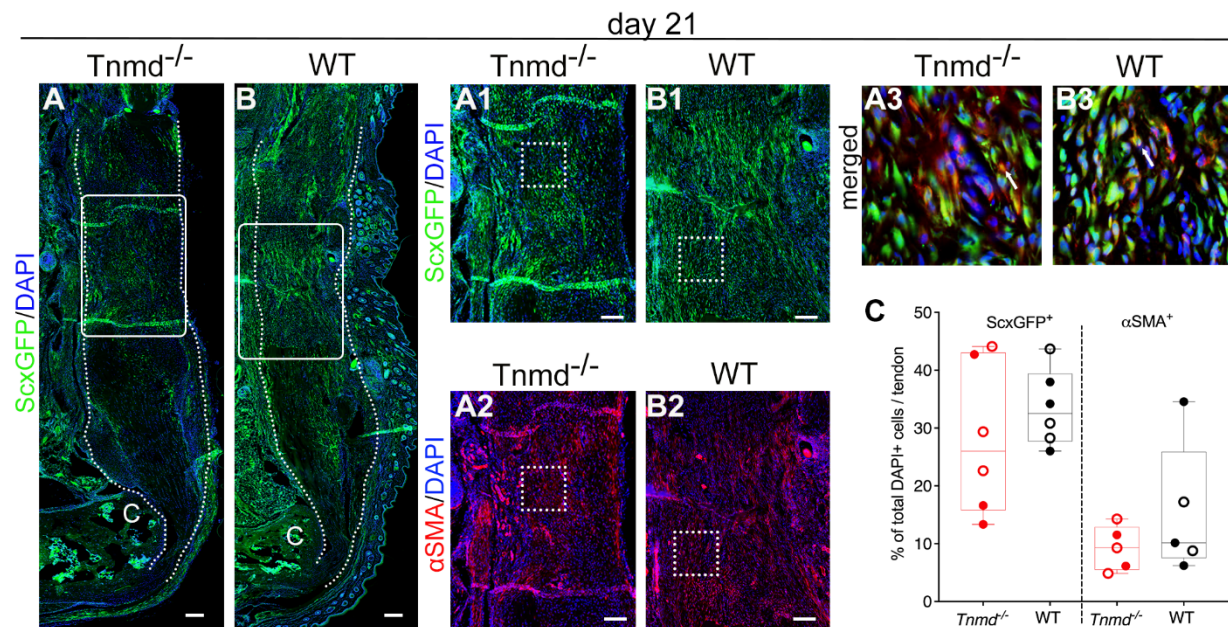


Fig. 17. Incidence of ScxGFP⁺ and αSMA⁺ cell populations during tendon healing at day 21. (A-B) Representative mosaic images of injured *Tnmd*^{-/-} ScxGFP and WT ScxGFP ATs at day 21 post-injury. (A1-B3) ScxGFP⁺ cell

Results

occurrence, corresponding immunofluorescence images of α SMA⁺ staining and (C) quantification of ScxGFP⁺ and α SMA⁺ cells as percentage of total number of DAPI⁺ cells within AT scars. White dotted lines frame ATs; white arrows mark double positive ScxGFP⁺/ α SMA⁺ cells. C= calcaneus. Scale bar: 200 μ m (panels A-B); 100 μ m (panels A1-B2); 20 μ m (panel A3, B3). ScxGFP imaging, α SMA staining and quantification were performed with n=5-6 animals/genotype; each animal represented by three tissue sections. Box plots show median \pm interquartile range (IQR), statistical significance was assessed with 2-tailed unpaired parametric Student's t-test, *p<0.05, **p<0.01. Empty dot represents female mouse; filled dot represents male mouse. Figure was derived from Fig. 1C-F3, Delgado Caceres *et al.*, 2021⁸⁹, which has been published under the gold open access model.

Finally, at day 100 post-injury (remodeling stage of healing) ScxGFP⁺ and α SMA⁺ cells were primarily, but not exclusively located in the scar regions that appeared to be ossified (Fig. 18A-B3). The percentage of ScxGFP⁺ cells was yet again significantly lower in injured *Tnmd*^{-/-} tendons compared to WT (8.8% vs. 22.9%, respectively) (Fig. 18C), whilst the very low abundant α SMA⁺ cells were comparable between the groups (Fig. 18C).

“Altogether, these results put in evidence that loss of Tnmd results in myofibroblast-enriched early scar tissue and significantly lower content of tendon lineage ScxGFP⁺ cells during early and late healing stages”.

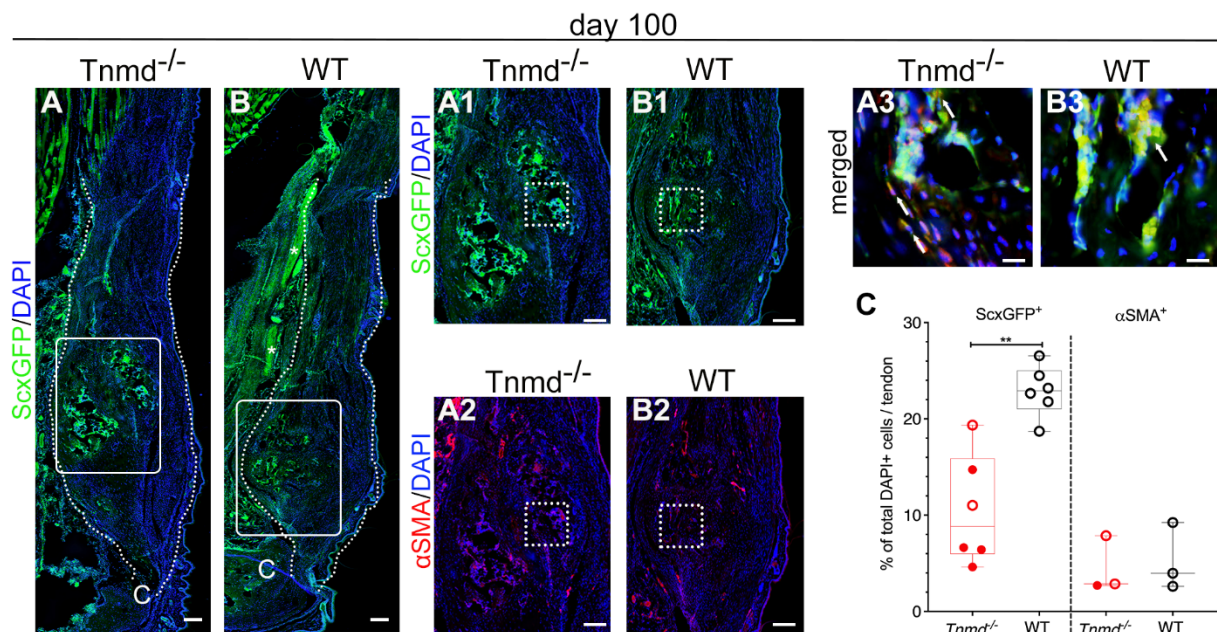


Fig. 18. Incidence of ScxGFP⁺ and α SMA⁺ cell populations during tendon healing at day 100. (A-B) Representative mosaic images of injured *Tnmd*^{-/-} ScxGFP and WT ScxGFP ATs at day 100 post-injury. (A1-B3) ScxGFP⁺ cell occurrence, corresponding immunofluorescence images of α SMA⁺ stainings, and (C) quantitative

Results

analysis of ScxGFP⁺ and α SMA⁺ cells as percentage of total number of DAPI⁺ cells within AT scars. White dotted lines frame ATs; white arrows mark double positive ScxGFP⁺/ α SMA⁺ cells. C= calcaneus. Scale bar: 200 μ m (panels A-B); 100 μ m (panels A1-B2); 20 μ m (panel A3, B3). ScxGFP imaging, α SMA staining and quantification were performed with n=3-6 animals/genotype; each animal represented by three tissue sections. Box plots show median \pm interquartile range (IQR), statistical significance was assessed with 2-tailed unpaired parametric Student's t-test, *p<0.05, **p<0.01. Empty dot represents female mouse; filled dot represents male mouse. Figure was derived from Fig. 1C, D, G-H3, Delgado Caceres *et al.*, 2021⁸⁹, which has been published under the gold open access model.

3.2 At day 21 post-injury *Tnmd*^{-/-} scars are characterized by larger chondrogenic template

With the intention to further characterize the cellular and ECM composition of the scar tissue, we first performed haematoxylin-eosin (H&E) staining at day 21 post-injury. The gross appearance analysis revealed the presence of a cartilage-like nodule adjacent to the enthesis in the ATs of both genotypes, as well as large blood vessels and nerve fibers running in the peritendinous space of the injured tendons (Fig. 19A-B). Moreover, the injured *Tnmd*^{-/-} tendon scars appeared to be broader and more dilated than in the WT. In addition, a clear increment in cellularity at the injury site, as well as throughout the entire tendon was detectable in both genotypes. High magnification images exposed the occurrence of chondrocytic cells (Fig. 19A1-B1), and histological scoring¹⁶⁹ (Table 14) suggested inferior total scores for mutant compared to WT ATs (4.8 and 6.1 points, respectively) (Fig. 19C).

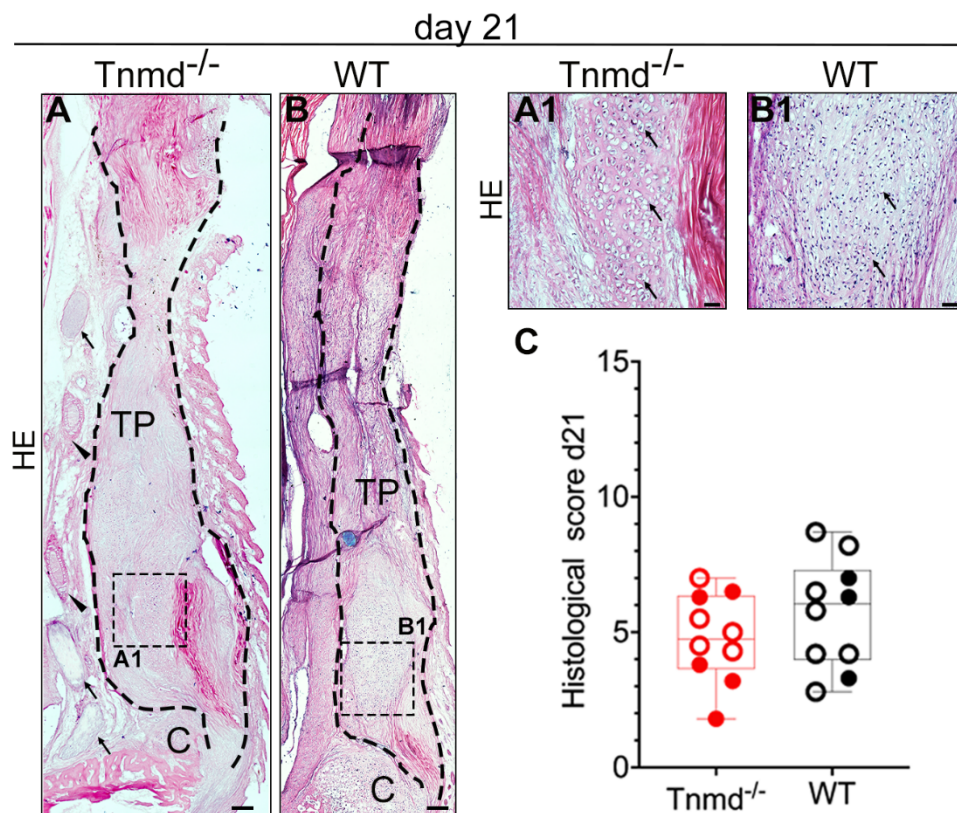


Fig. 19. Comparison of AT repair between *Tnmd*^{-/-} and WT mice at day 21 post-injury. (A-B) Representative mosaic H&E, (A1-B1) higher magnification images of injured *Tnmd*^{-/-} and WT ATs, and (C) histological scoring at day 21. Black dotted lines frame ATs; vessels and nerves in the peritendinous space are marked with black arrowheads and arrows, respectively; blue bright spot in (B): cerclage 6-0 prolene suture material. C=calcaneus, TP=tendon proper.

Results

Scale bar: 200 μ m (panels A-B); 50 μ m (panels A1-B1). (C) Histological scoring, n=10 animals/genotype. Box plots show median \pm IQR. Empty dot represents female mouse; filled dot represents male mouse. Figure was derived from Fig. 2A-B1 and Suppl. Fig. 2G, Delgado Caceres *et al.*, 2021⁸⁹, which has been published under the gold open access model.

To confirm the presence of chondrocytic cells, immunohistochemical staining against type II collagen (COLII) was performed. The staining revealed the clear COLII-deposition in the territorial ECM (Fig. 20A-B1), and the corresponding quantitative analysis of the COLII⁺-area per injured tendon revealed a strong tendency (p=0.0641) of larger cartilage template in the *Tnmd*^{-/-} group (Fig. 20C).

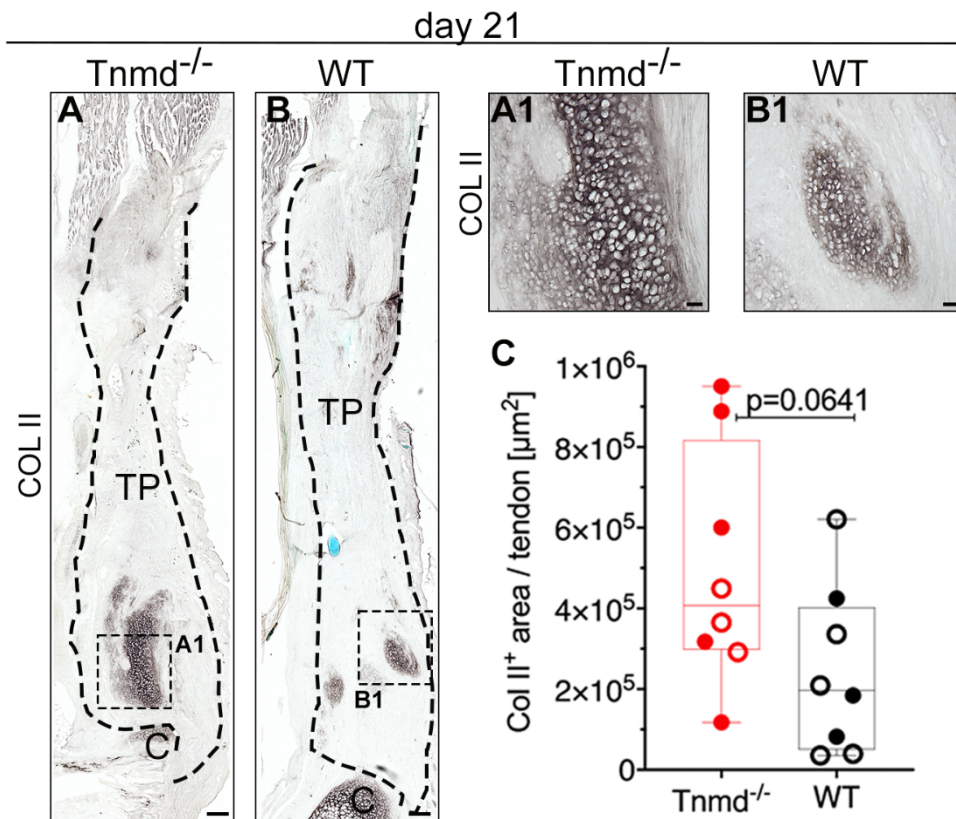


Fig. 20. Comparison of cartilage-like tissue formation and COLII deposition in *Tnmd*^{-/-} and WT ATs at day 21 post-injury. (A-B) Representative mosaic, (A1-B1) higher magnification DAB images of type II collagen (COLII) staining and (C) quantitative analysis of COLII⁺ area/tendon. Black dotted lines frame ATs; blue bright spot in (B): cerclage 6-0 prolene suture material. C=calcaneus, TP=tendon proper. Scale bar: 200 μ m (panels A-B); 50 μ m (panels A1-B1). Staining and quantification was performed with n=8 animals/genotype; each animal represented by three mosaic tissue sections. Box plots show median \pm IQR; statistical significance was assessed with 2-tailed unpaired

parametric Student's t-test. Empty dot represents female mouse; filled dot represents male mouse. Figure was derived from Fig. 2C-E, Delgado Caceres *et al.*, 2021⁸⁹, which has been published under the gold open access model.

3.3 *Tnmd*-deficiency does not affect tendon innervation, vascularization, collagen maturation and presence of CD146⁺ progenitors at day 21 post-injury

Next, innervation was validated and quantified by neurofilament protein-heavy chain (NEFH) staining at day 21 post-injury (Fig. 21A-B1). The NEFH⁺-areas were localized mainly in the peritendinous space of injured *Tnmd*^{-/-} and WT AT. The matching quantitative analysis did not reveal any significant genotypic differences (Fig. 21C).

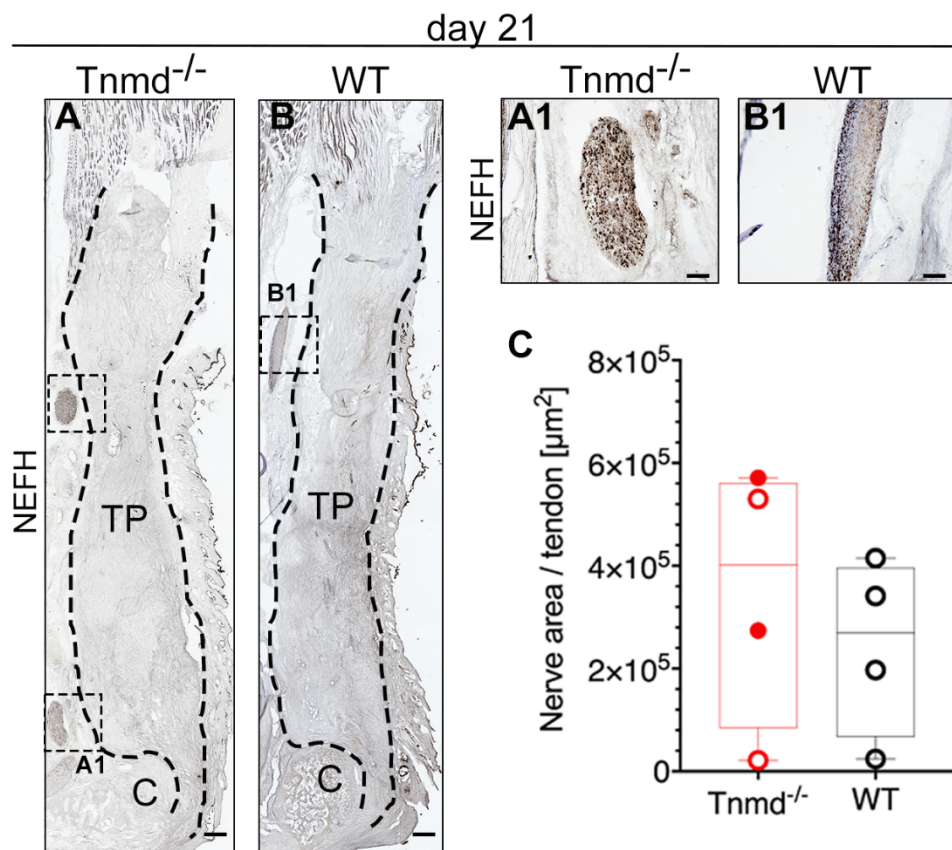


Fig. 21. Detection of nerves in *Tnmd*^{-/-} and WT ATs at day 21 post-injury. (A-B) Representative mosaic images, (A1-B1) higher magnification DAB images of Neurofilament heavy polypeptide (NEFH) staining of injured *Tnmd*^{-/-} and WT ATs, and (C) quantification of NEFH⁺ area/tendon. Black dotted lines frame ATs. C=calcaneus, TP=tendon proper. Scale bar: 200µm (panels A-B); 50µm (panels A1-B1). Staining and quantification was performed with n=4 animals/ genotype; each animal represented by three mosaic tissue sections. Box plots show median ± IQR; statistical significance was assessed with 2-tailed unpaired parametric Student's t-test. Empty dot represents female mouse; filled

Results

dot represents male mouse. Figure was derived from Suppl. Fig. 2A-C, Delgado Caceres *et al.*, 2021⁸⁹, which has been published under the gold open access model.

Then, in order to follow up the hint delivered by the results of early healing regarding vasculature¹⁶⁰, and to distinguish the progression of neo-vascularization, as well as to quantify the collagen IV-labeled blood vessels/tendon, immunofluorescence staining against collagen type IV (COLIV) was performed in *Tnmd*^{-/-} and WT AT 21 days post-injury (Fig. 22A-B1). The quantitative analysis revealed comparable results in both injured ATs (514 in mutant vs. 535 in WT tendons) (Fig. 22C).

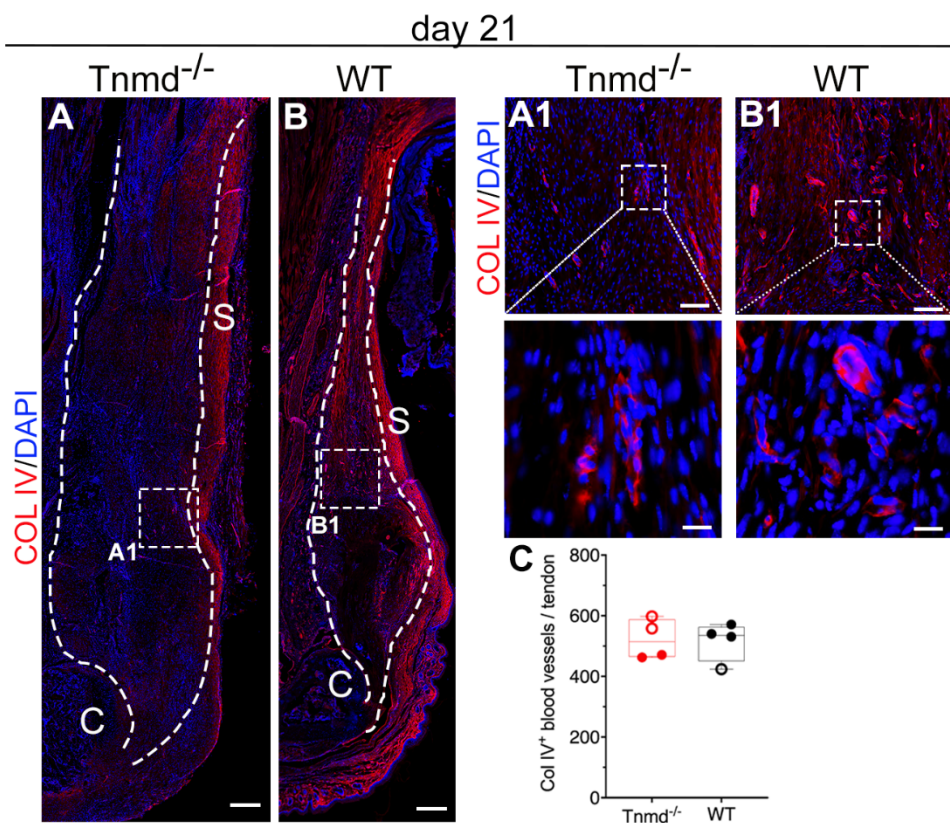


Fig. 22. Analysis of blood vessels in *Tnmd*^{-/-} and WT ATs at day 21 post-injury. (A-B) Representative mosaic, (A1, B1) higher magnification fluorescent images of type IV collagen (COLIV) staining, and (C) quantitative analysis of COLIV⁺ blood vessels/tendon. White dotted lines frame ATs. C=calcaneus, S=skin. Scale bar: 200 μ m (panels A-B); 50 μ m (panels A1-B1); 20 μ m (zoom-in regions). Staining and quantification was performed with n=4 animals/genotype; each animal represented by three mosaic tissue sections. Box plots show median \pm IQR; statistical significance was assessed with 2-tailed unpaired parametric Student's t-test. Empty dot represents female mouse; filled dot represents male mouse. Figure was derived from Suppl. Fig. 2D-F, Delgado Caceres *et al.*, 2021⁸⁹, which has been published under the gold open access model.

Due to the observed peritendinous neo-vascularization, we also evaluated the incidence of pericyte, multipotent progenitors by immunofluorescent staining for CD146, but no significant differences were detected between the genotypes at this time point (14.1% vs. 24.4% in WT) (Fig. 23A-C).

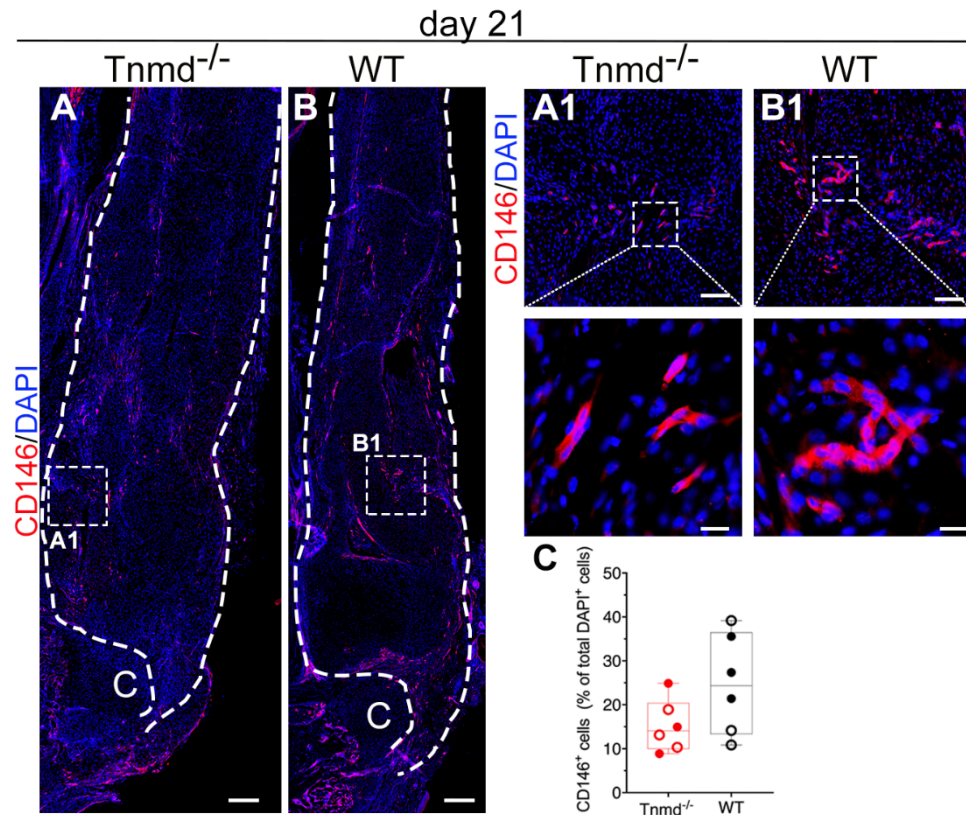


Fig. 23. Detection of pericytes at day 21 post-injury. (A-B) Representative mosaic, (A1-B1) higher magnification fluorescent images for CD146 staining and (C) quantification of CD146⁺ cells/injured *Tnmd*^{-/-} and WT AT. White dotted lines frame ATs. C=calcaneus. Scale bar: 200µm (panels A-B); 50µm (panels A1-B1); 20µm (zoom-in regions). Staining and quantification was performed with n=6 animals/genotype; each animal represented by three mosaic tissue sections. Box plots show median ± IQR; statistical significance was assessed with 2-tailed unpaired parametric Student's t-test. Empty dot represents female mouse; filled dot represents male mouse. Figure was derived from Suppl. Fig. 2H-J, Delgado Caceres *et al.*, 2021⁸⁹, which has been published under the gold open access model.

Lastly, we assessed collagen fibres maturation and alignment by Herovici and Picrosirius red staining, respectively (Fig. 24A-D). Regardless of genotype, Herovici staining showed predominantly blue colour at the injury site, indicating principally younger, immature collagen III (COLIII) production (Fig. 24A1, B1). Moreover, these regions were characterized by an isotropic ECM organization and poor collagen fibril alignment (Fig. 24C1, D1). Conversely, mature

Results

collagen type I fibers (red dye) were still parallel aligned and localized mainly at the tendons ends, at the MTJ and at the entheses.

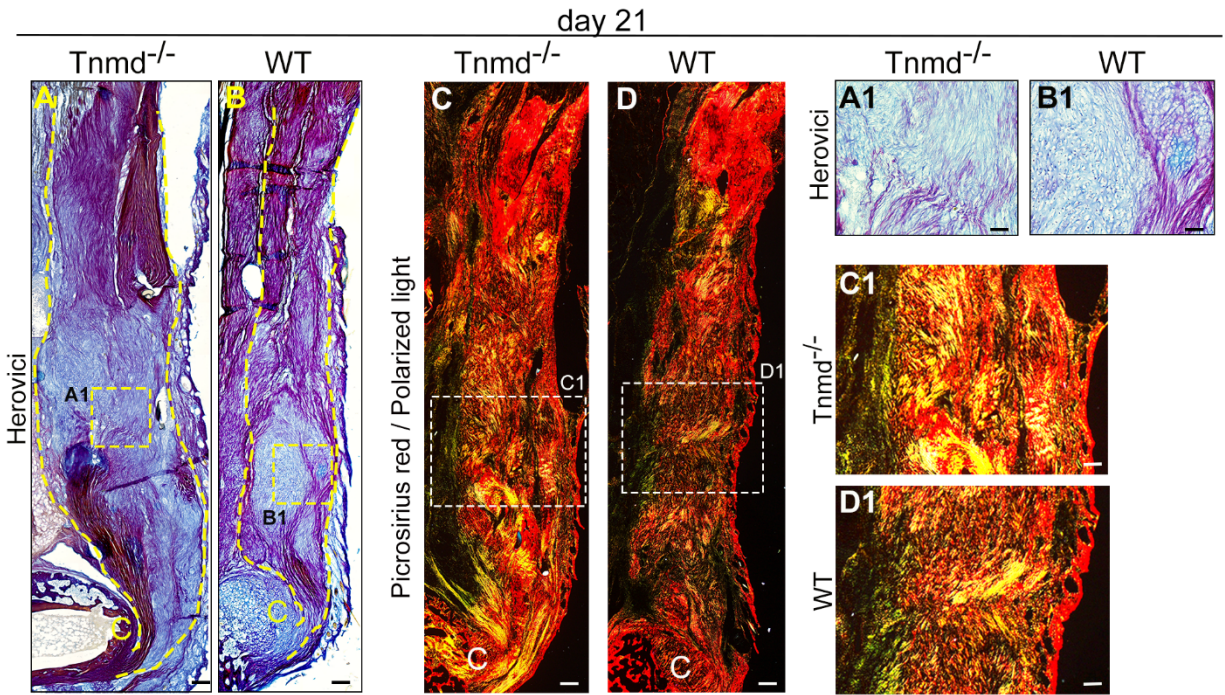


Fig. 24. Collagen maturation and fibril alignment in *Tnmd*^{-/-} and WT ATs at day 21 post-injury. (A, B) Representative and (A1, B1) higher magnification images of Herovici staining. (C, D) Representative mosaic, (C1, D1) higher magnification images of Picrosirius red staining. Yellow dotted lines frame ATs. C=calcaneus. Scale bar: 200 μ m (panels A-D); 50 μ m (panels A1-D1). Stainings was performed with n=4-6 animals/genotype, each animal represented by three tissue sections. Figure was derived from Suppl. Fig. 3A-D1, Delgado Caceres *et al.*, 2021⁸⁹, which has been published under the gold open access model.

Altogether, our data reveals that despite the larger collagen II cartilaginous anlage detected in injured *Tnmd*-deficient scars at day 21 post-injury, *Tnmd* absence did not affect tendon innervation, vascularization, and percentage of CD146⁺ cells nor collagen maturation and alignment during the proliferative stage of healing.

3.4 At day 21 post-injury *Tnmd*^{-/-} scars are characterized by lower number of BrdU⁺ proliferative cells, and anti-inflammatory macrophages, but higher number of pro-inflammatory macrophages

The limited healing response in tendons is associated, among other factors, to hypocellularity¹⁹³ and their less active metabolism¹⁹⁴. Therefore, we focused next on the detection of proliferative cells in mutant and WT tendons 21 days post-injury. Interestingly, similar to day 8¹⁶⁰, at day 21 *Tnmd*^{-/-} scars contained significantly less proliferative BrdU⁺ cells than WT scars (80 vs. 132 BrdU⁺ cells) (Fig. 25A, B).

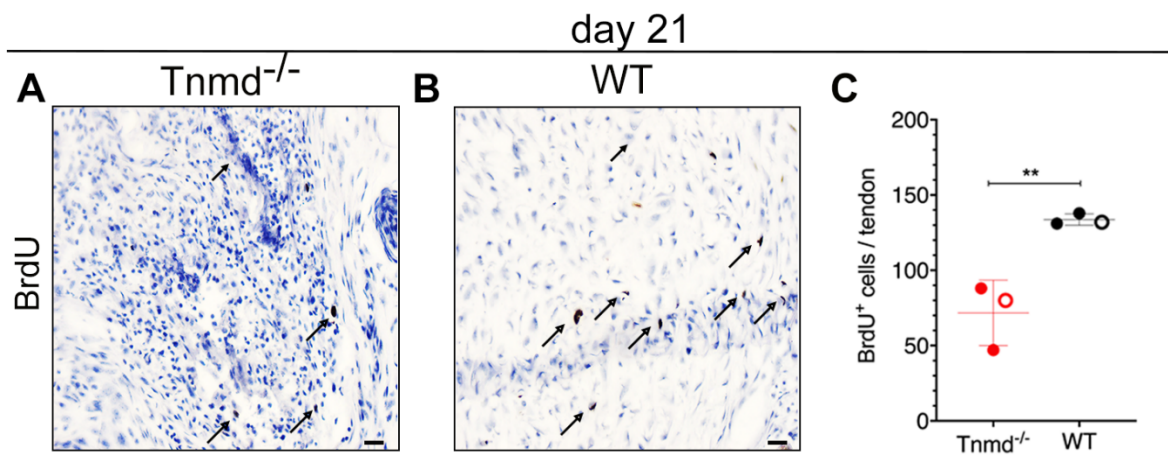


Fig. 25. Detection and quantification of BrdU⁺ cells in *Tnmd*^{-/-} and WT ATs at day 21 post-injury. (A) Representative higher magnification images for BrdU staining and (B) quantitative analysis of BrdU⁺ cells/injured *Tnmd*^{-/-} and WT AT. Black arrows in (A) mark BrdU⁺ cells. C=calcaneus. Scale bar: 20 μ m. Stainings and quantifications were performed with n=3 animals/genotype; each animal represented by three mosaic tissue sections; statistical significance was assessed with 2-tailed unpaired parametric Student's t-test, *p<0.05, **p<0.01. Empty dots represent female mouse; filled dot represent male mouse. Figure was derived from Fig. 2F-G, Delgado Caceres *et al.*, 2021⁸⁹, which has been published under the gold open access model.

Then, we analyzed the presence of pro-inflammatory M1 polarized macrophages in tendons 21 days post-injury. In the injured ATs, CD68⁺ cells were distributed throughout the entire tissue, including the tendon core and midsubstance but also on tendon's lateral region, near to the skin (Fig. 26A-B1). “Similarly to the phenotype described by Lin *et al.*, 2017 during early healing¹⁶⁰, we too detected significantly higher numbers of pro-inflammatory M1 CD68⁺ macrophages (11.7% mutant vs. 6.2% WT group) in contrast to the WT scars (Fig. 26C)”.

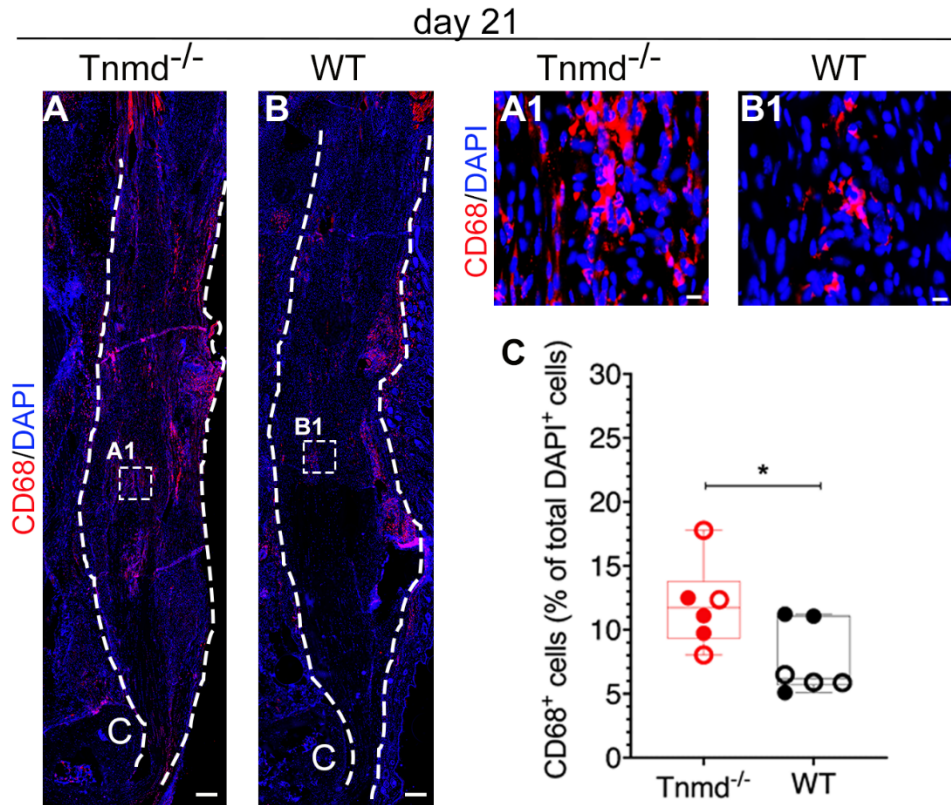


Fig. 26. Analysis of M1 macrophages in *Tnmd*^{-/-} and WT ATs at day 21 post-injury. (A-B) Representative mosaic, (A1-B1) higher magnification fluorescent images for CD68 staining and (C) quantitative analysis of CD68⁺ cells/injured *Tnmd*^{-/-} and WT AT. White dotted lines frame ATs. C=calcaneus. Scale bar: 200 μ m (panels A-B); 20 μ m (panels A1-B1). Staining and quantification was performed with n=6 animals/genotype; each animal represented by three mosaic tissue sections. Box plots show median \pm IQR; statistical significance was assessed with 2-tailed unpaired parametric Student's t-test. Empty dot represents female mouse; filled dot represents male mouse. Figure was derived from Fig. 2H-J, Delgado Caceres *et al.*, 2021⁸⁹, which has been published under the gold open access model.

Next, we detected the presence and quantified total number of anti-inflammatory M2 polarized macrophages in relation to total number of DAPI⁺ cells (Fig. 27A, B1) by immunofluorescence staining of injured AT tissue sections against CD163. Conversely to the situation observed with M1 macrophages, the WT scars were majorly dominated by CD163⁺ macrophages and the values were significantly higher than in *Tnmd*^{-/-} tendons (5.2% mutant vs. 16.8% WT group, Fig. 27C).

*“Taken together, the above data revealed that the absence of *Tnmd* leads to abnormal, rather pro-inflammatory macrophage profile and reduced cell proliferation in the reparative stage of the tendon healing process suggesting overall soft tissue destruction favouring ectopic chondrogenesis”.*

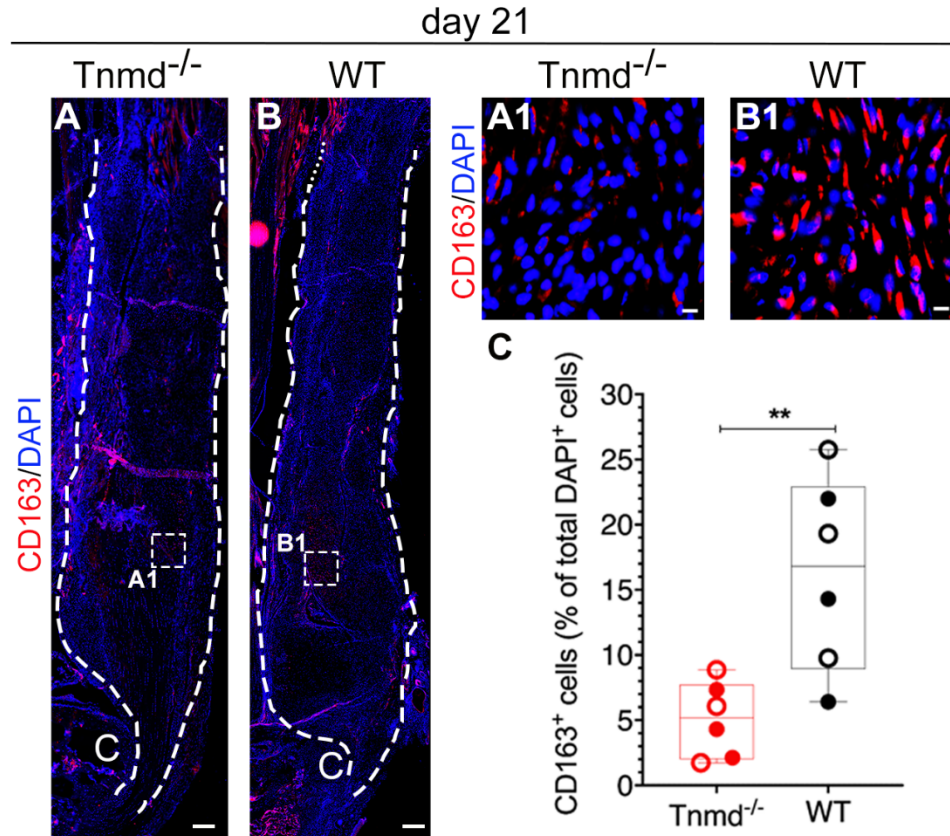


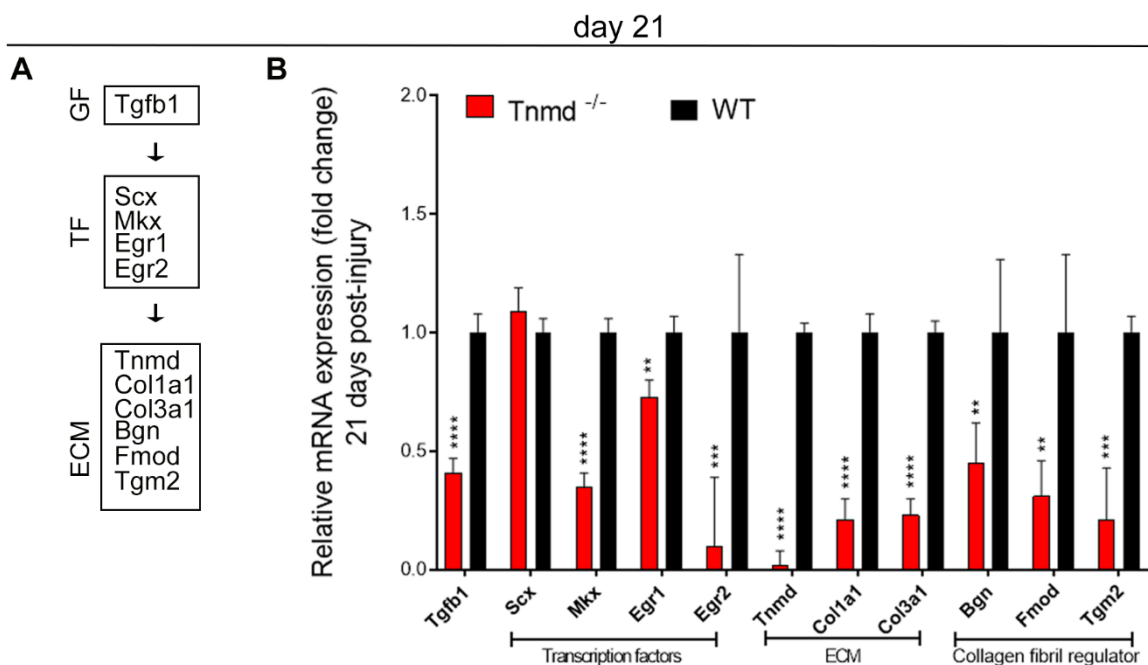
Fig. 27. Analysis of M2 macrophages in *Tnmd*^{-/-} and WT ATs at day 21 post-injury. (A-B) Representative mosaic, (A1-B1) higher magnification fluorescent images for CD163 and (C) quantification of CD163⁺ cells/tendon in injured *Tnmd*^{-/-} and WT ATs. White dotted lines frame ATs. C=calcaneus. Scale bar: 200 μ m (panels A-B); 20 μ m (panels A1-B1). Staining and quantification was performed with n=6 animals/genotype; each animal represented by three mosaic tissue sections. Box plots show median \pm IQR; statistical significance was assessed with 2-tailed unpaired parametric Student's t-test. Empty dot represents female mouse; filled dot represents male mouse. Figure was derived from Fig. 2K-M, Delgado Caceres *et al.*, 2021⁸⁹, which has been published under the gold open access model.

3.5 Lack of *Tnmd* results in significant dysregulation of classical tendon-related gene markers during the healing process

In order to assess the modifications at mRNA-messenger level occurring during the healing process in both, injured *Tnmd*^{-/-} and WT ATs, we evaluated the expression of tendon-related gene markers (Fig. 28A, C) by qRT-PCR at day 21 and day 100 post-injury.

The analysis at day 21 revealed the significant downregulation of Transforming growth factor beta 1 (*Tgf-β1*), the transcription factors Mohawk (*Mkx*) and early growth response protein-1 and 2 (*Egr1*, *Egr2*); as well as the ECM genes alpha-1 type I and alpha-1 type III collagen (*Col1a1*, *Col3a1*) in the *Tnmd*^{-/-} group (Fig. 28B). Moreover, the expression of the small leucine-rich proteoglycans biglycan (*Bgn*) and fibromodulin (*Fmod*), and transglutaminase 2 (*Tgm2*) were significantly downregulated in the mutant tendons, which might be indicative of delayed activation of tenogenesis in the scar (Fig. 28B)⁸⁹.

Furthermore, qRT-PCR analysis at day 100 revealed significantly higher mRNA levels of most assessed genes in *Tnmd*^{-/-} tendons (Fig. 28D) including decorin (*Dcn*), lumican (*Lum*) and lysyl-oxidase (*Lox*), which might be indicative of still ongoing tenogenesis⁸⁹. In sum, our qRT-PCR data revealed that the lack of *Tnmd* affects the gene expression of tendon-related and collagen fibril regulator genes during the reparative proliferative, and remodeling stages of tendon healing.



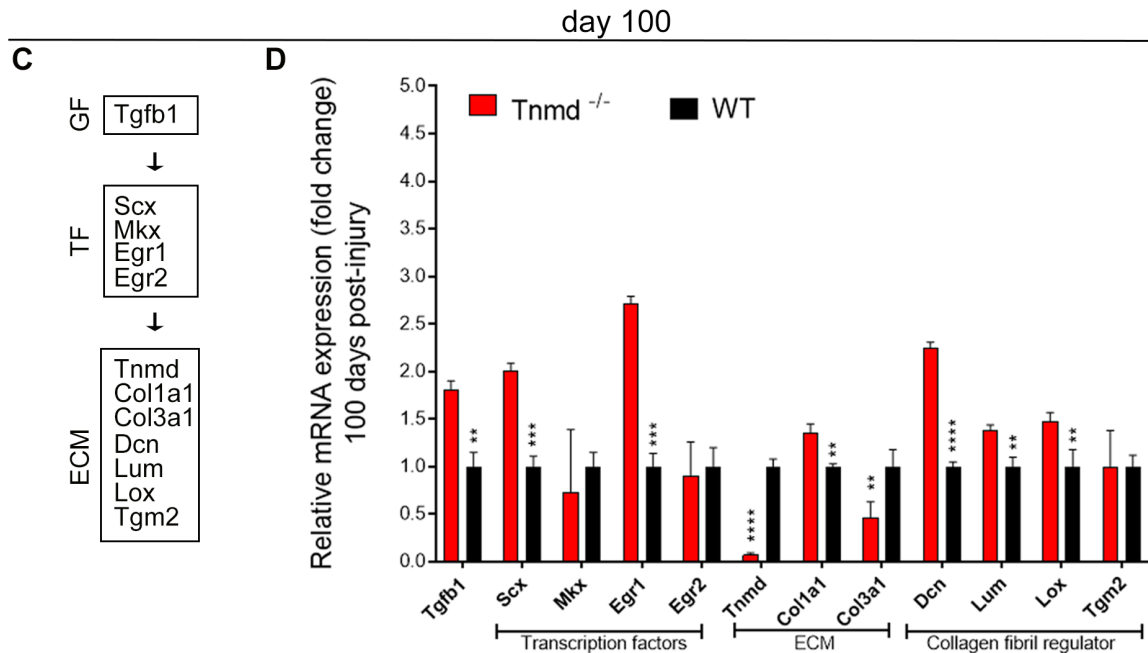


Fig. 28. Gene expression analyses at day 21 and 100 post-injury. (A) List of well-known tendon-related markers involved in proliferative and (C) late healing. GF=Growth factor, TF=Transcription factor, ECM=Extracellular matrix. (B) qRT-PCR analysis at day 21 and (D) at day 100 post-injury. Pool of n=3 injured ATs/genotype/time point, 3 independent experiments. Statistical significance was calculated using two-tailed, unpaired parametric Student's t-test. **p<0.01, ***p<0.001, ****p>0.0001. Figure was derived from Suppl. Fig. 3E-G, Delgado Caceres *et al.*, 2021⁸⁹, which has been published under the gold open access model.

3.6 The ECM of non-injured *Tnmd*^{-/-} Achilles' tendons is characterized by persistently and significantly thicker collagen fibrils

We utilized Transmission Electron Microscopy (TEM) to determine tendon matrix ultrastructure, organization, and to analyze collagen fibril diameter distribution. We concentrated first on the tendon mid-substance in non-injured, contralateral tendons. The representative TEM and high magnification images showed tenocytes with respective protrusions embedded in-between collagen fibrils, which were dense and tightly arranged (Fig. 29A-B1). The pattern firstly described by Docheva *et al.*, 2005³³ towards significantly large sizes in collagen fibril diameters in *Tnmd*^{-/-} tendons was consistent in the non-injured, contralateral setting from day 21 (6 month-old) (Fig. 29A2, B2). The mean value for collagen fibril diameter was 148.33 ± 41.67 nm in the mutant and 122.4 ± 41.36 nm in WT tendons. The smallest and largest fibril diameter detected in tendons were 33 nm and 277 nm in *Tnmd*^{-/-}, and 12 nm and 230 nm in the WT, respectively (Table 16).

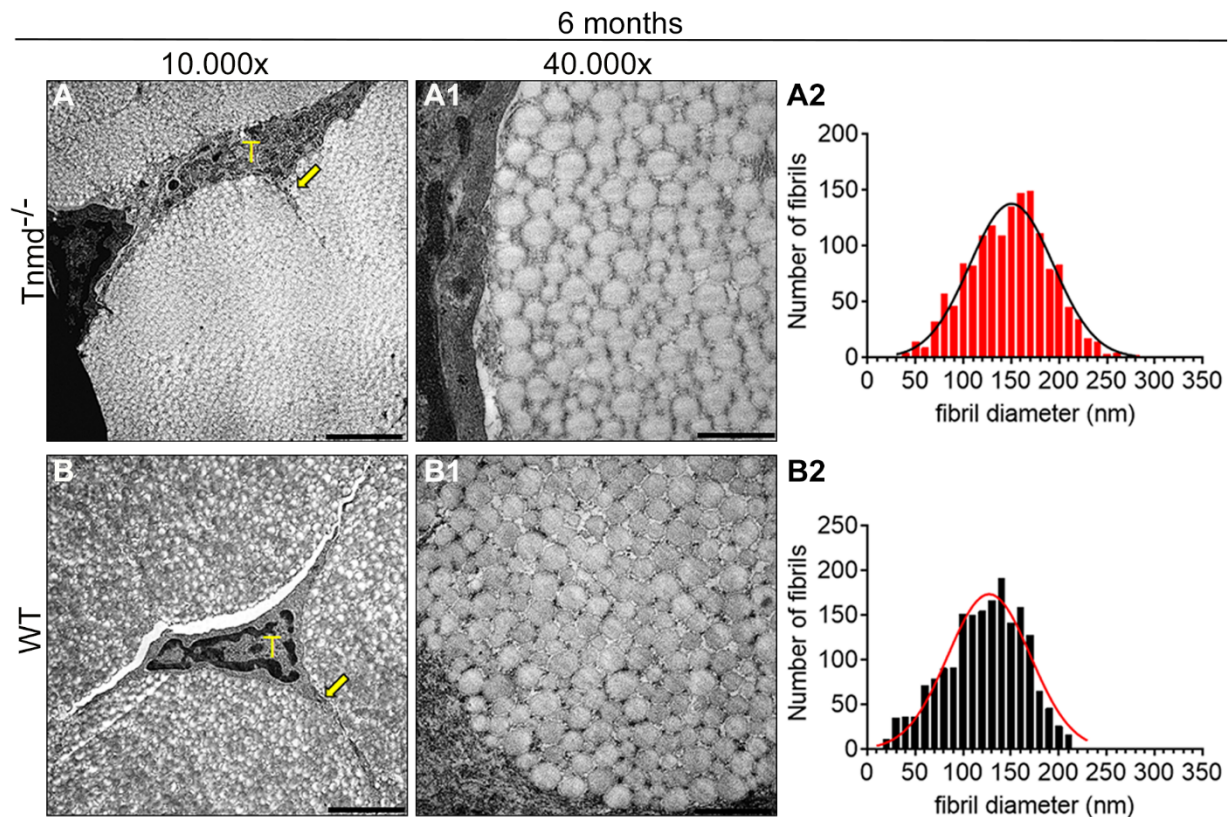


Fig. 29. TEM and collagen fibril diameter analysis of contralateral ATs in 6-month-old mice. (A-B) Representative 10000x and (A1-B1) 40000x magnification images of contralateral *Tnmd*^{-/-} and WT ATs. T=Tenocyte; yellow arrow=cell protrusions. Scale bars: 2 μ m (panels A-B); 500nm (panels A1-B1). (A2-B2) Histograms showing incidence of collagen fibril size. Figure was taken from Suppl. Fig. 4A-B2, Delgado Caceres *et al.*, 2021⁸⁹, which has been published under the gold open access model.

In the 9-month-old non-injured ATs, the tenocytes and collagen fibrils were similarly distributed in both genotypes (Fig. 30A-B1) and the effect concerning fibril diameter towards significantly large sizes in *Tnmd*^{-/-} tendons remained constant (Fig. 30A2, B2). The mean value for collagen fibril diameter was 145.83 ± 52.96 nm in the mutant and 109.9 ± 42.37 nm in WT tendons. The smallest and largest fibril diameter detected in *Tnmd*^{-/-} tendons were 35.05 nm and 293.85 nm, and 5.18 nm and 246.46 nm in the WT. Moreover, no signs of ECM mineral deposition were detected.

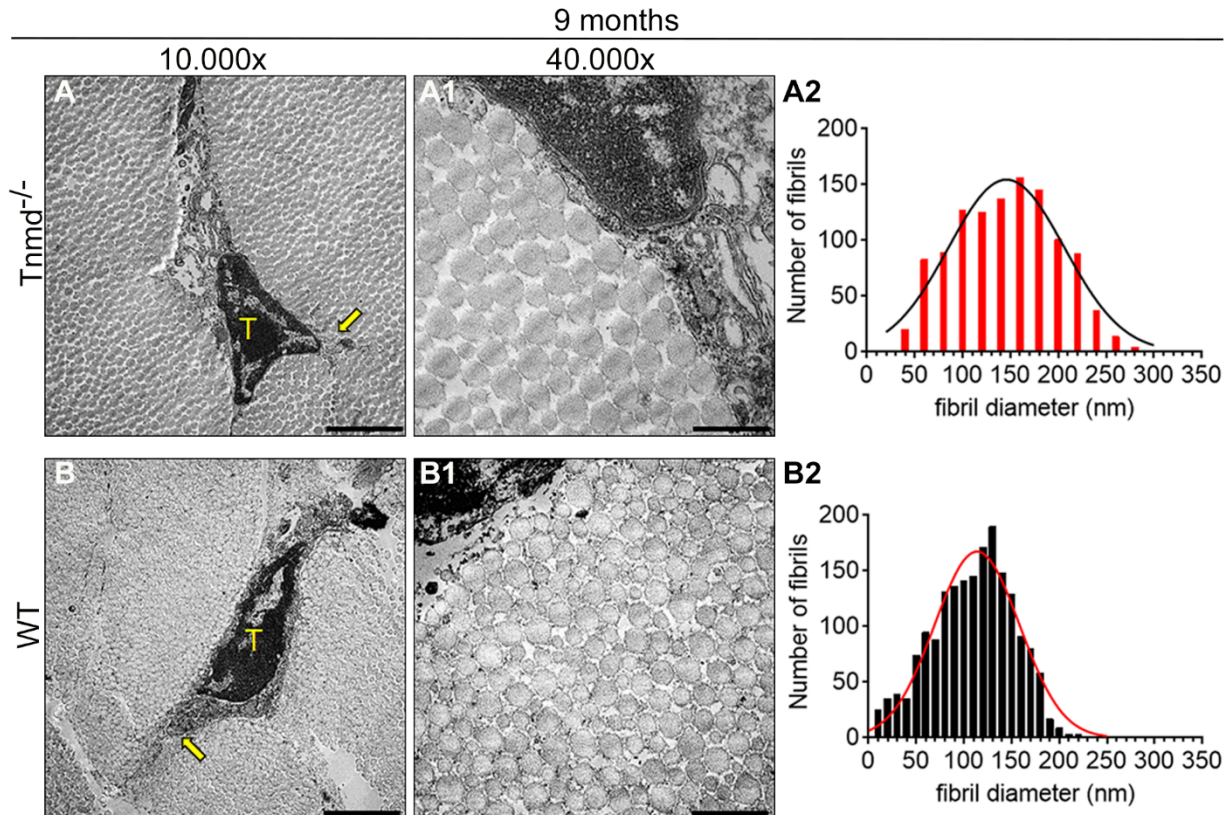


Fig. 30. TEM and collagen fibril diameter analysis of contralateral ATs in 9-month-old mice. (A-B) Representative 10000x and (A1-B1) 40000x magnification images of contralateral *Tnmd*^{-/-} and WT ATs. T=Tenocyte; yellow arrow=cell protrusions. Scale bars: 2 μ m (panels A-B); 500nm (panels A1-B1). (A2-B2) Histograms showing incidence of collagen fibril size. Figure was derived from Suppl. Fig. 4C-D2, Delgado Caceres *et al.*, 2021⁸⁹, which has been published under the gold open access model.

3.7 The ECM of *Tnmd*^{-/-} Achilles' tendons is distinguished by lower collagen fibril density concomitant with significantly thicker and atypically shaped collagen fibrils

We focused on the injury regions in the case of specimens analyzed 21- and 100 days post-operatively. “At day 21, representative TEM images of injured *Tnmd*^{-/-} and WT ATs revealed a general hypercellularity (also observed in H&E staining), decreased fibril size and density, broader gaps between cells and fibrils, and atypically shaped collagen fibrils (Fig. 31A-B2)”. Higher magnification images showed that in the WT group most of the fibrils were tightly organized and clustered in the range of 10-50nm diameters. In contrast, scattered and thicker collagen fibrils, reaching diameters of up to 340 nm, with irregular rough outlines were enriched in the *Tnmd*^{-/-} tendons (Fig. 31A3-B4)⁸⁹.

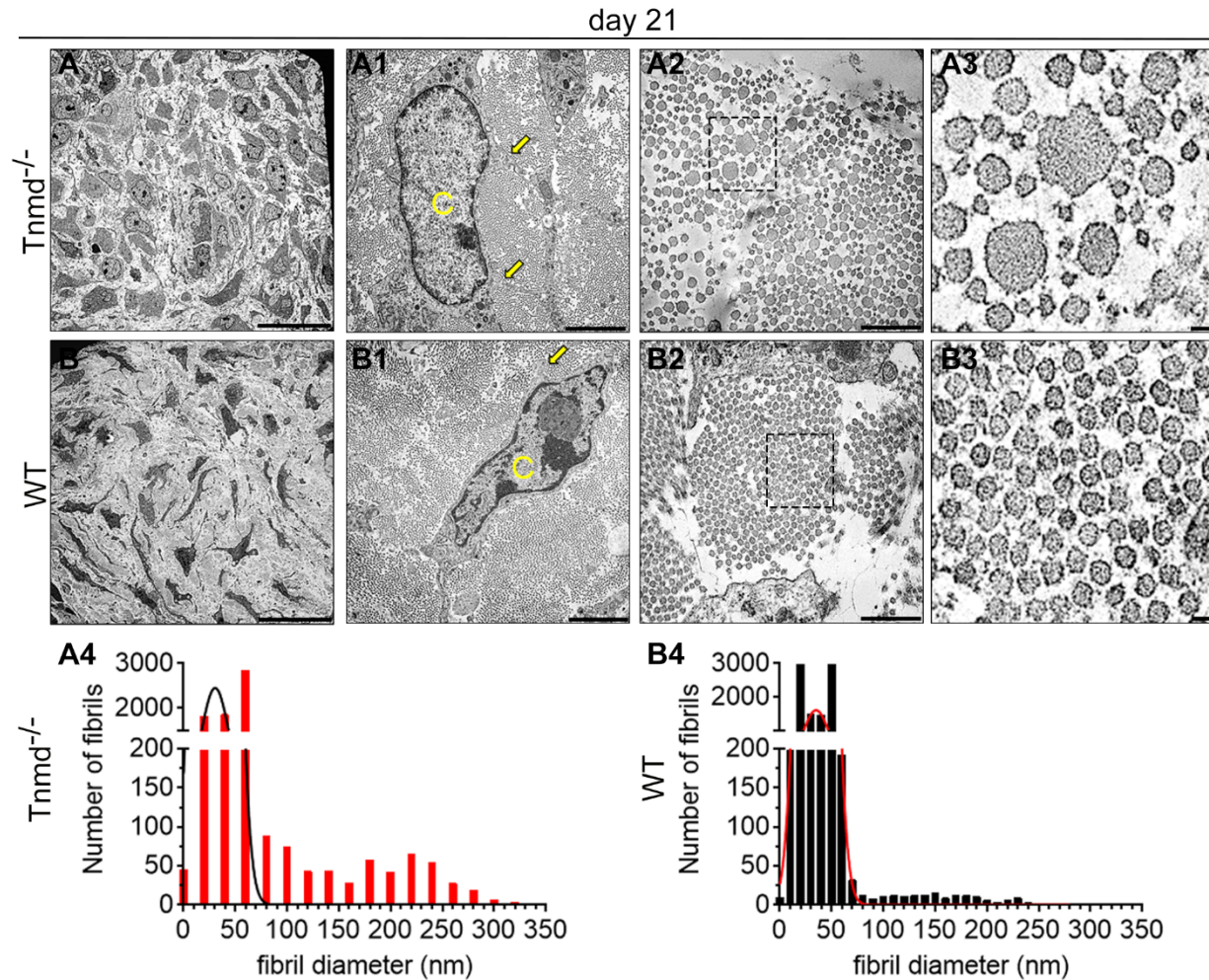


Fig. 31. TEM and collagen fibril diameter analysis of ATs at day 21 post-injury. (A-B) Representative 2000x, (A1-B1) 10000x and (A2-B3) 40000x magnification images of injured *Tnmd*^{-/-} and WT ATs at day 21 post-injury. C=cell; yellow arrow=cell protrusions. Scale bars: 20 μ m (panels A, B); 2 μ m (panels A1-B1); 500nm (panels A2-B3). (A4-B4) Histograms showing incidence of collagen fibril sizes. Figure was derived from Fig. 3A-B3 and E, Delgado Caceres *et al.*, 2021⁸⁹, which has been published under the gold open access model.

“When focused on the *Tnmd*^{-/-} and WT tendons at 100 days post-injury, we noticed the presence of mineral deposits (marked with yellow asterisks) within the ECM and osteocyte-like cells, a sign of HO (Fig. 32A-B1)”. Moreover, the pattern of collagen fibril shift towards significantly large sizes in *Tnmd*^{-/-} remained consistent in the injured setting at day 100 (Fig. 32A2-B3). While the largest collagen fibrils in the mutant tendons had a diameter of around 290 nm, the largest one found in the WT were of approx. 220 nm (Table 16, Fig. 32A4, and B4).

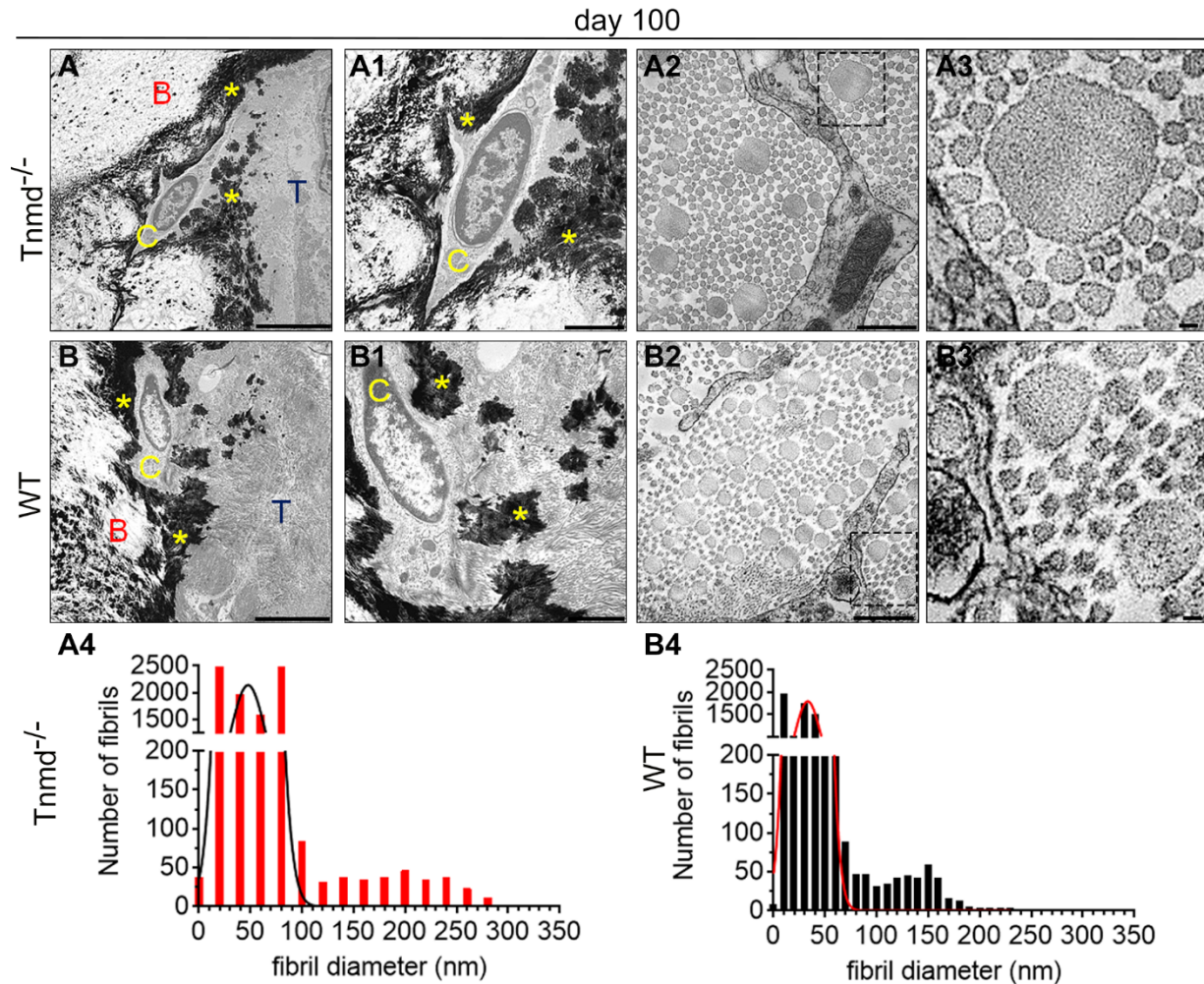


Fig. 32. TEM and collagen fibril diameter analysis of ATs at day 100 post-injury. (A-B) Representative 2000x, (A1-B1) 10000x and (A2-B3) 40000x magnification images of injured *Tnmd*^{-/-} and WT ATs at day 21 post-injury. C=cell; B=bone; yellow asterisks=mineralized zones. Scale bars: 5 μ m (panels A, B); 2 μ m (panels A1-B1); 500nm (panels A2-B3). (A4-B4) Histograms showing incidence of collagen fibril sizes. Figure was derived from Fig. 3C-D3 and E, Delgado Caceres *et al.*, 2021⁸⁹, which has been published under the gold open access model.

The overall quantification and the main results are summarized in Fig. 33A, B and in Table 16, respectively.

*“Taken together, the TEM imaging data reproducibly demonstrated the *Tnmd*^{-/-} tendons have naturally pathologically thicker collagen fibrils compared to WT tendons in both settings, intact and injured tendons, underpinning that *Tnmd* acts as a regulatory factor of collagen fibrillogenesis”.*

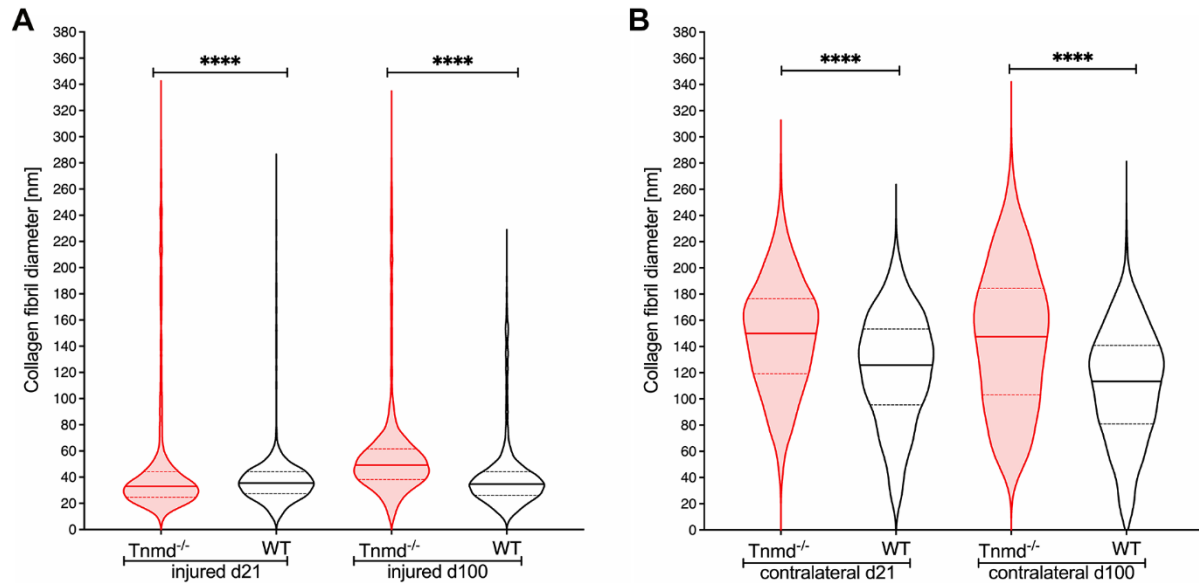


Fig. 33. Violin plot for collagen fibril diameter distribution. (A) Violin plot for injured ATs at day 21 and day 100. (B) Violin plot for contralateral *Tnmd*^{-/-} and WT ATs at the respective explantation time point. Median ± IQR, statistical significance was calculated by 2-tailed unpaired nonparametric Mann-Whitney test, **p*<0.05, ***p*<0.01, ****p*<0.001, *****p*<0.0001. Day 21, *n*=2 animals/genotype; day 100, *n*=2 animals/genotype. Figure was derived from Fig. 3F and Suppl. Fig. 4E, Delgado Caceres *et al.*, 2021⁸⁹, which has been published under the gold open access model.

Table 16. TEM fibril diameter quantification.

Statistic	Contralateral tendons day 21		Contralateral tendons day 100	
	<i>Tnmd</i> ^{-/-}	WT	<i>Tnmd</i> ^{-/-}	WT
Total number of quantified collagen fibrils	1488	1857	1127	1846
Minimum diameter [nm]	33.16	12.47	35.05	5.18
Median diameter [nm]	150.00	125.80	147.60	113.45
Maximum diameter [nm]	277.00	229.60	293.85	246.46
Mean value	148.30	122.30	145.83	109.90
Standard deviation (SD)	41.67	41.36	52.96	42.37
Standard error of the Mean (SEM)	1.08	0.96	1.58	0.99
Statistic	Injured tendons day 21		Injured tendons day 100	
	<i>Tnmd</i> ^{-/-}	WT	<i>Tnmd</i> ^{-/-}	WT
Total number of quantified collagen fibrils	4575	5088	4832	6021

Results

Minimum diameter [nm]	1.64	1.16	2.32	2.36
Median diameter [nm]	32.93	35.60	49.26	34.74
Maximum diameter [nm]	332.87	278.06	295	220.31
Mean value	48.28	39.19	57.54	40.72
Standard deviation (SD)	50.51	25.93	39.91	27.80
Standard error of the Mean (SEM)	0.75	0.36	0.57	0.36

Table was derived from Suppl. Table 2, Delgado Caceres *et al.*, 2021⁸⁹, which has been published under the gold open access model.

3.8 Loss of *Tnmd* leads to significantly inferior tendon healing and remodeling during late repair

To assess late tendon healing we adapted the scoring system from Lin *et al.*, 2017 and Stoll *et al.*, 2011^{160,169} (Table 14) and analyzed *Tnmd*^{-/-} and WT injured tendons 100 days post-injury. H&E staining revealed a different tendon tissue landscape and gross appearance compared to day 21, whereby the cartilage template has been replaced with prevalent bone-like tissue located proximally of the entheses (Fig. 34A-B1)⁸⁹. Moreover, histological scoring resulted in significantly inferior values in *Tnmd*^{-/-} compared to injured WT tendons (4.8 and 7.8 points, respectively; Fig. 34C). The most remarking differences leading to lower healing scores in the injured *Tnmd*^{-/-} tendons were regarding larger bone nodules containing trabecular space, poorer cell alignment in the fibrous regions of the tendon and looser ECM judged by faint Eosin staining⁸⁹.

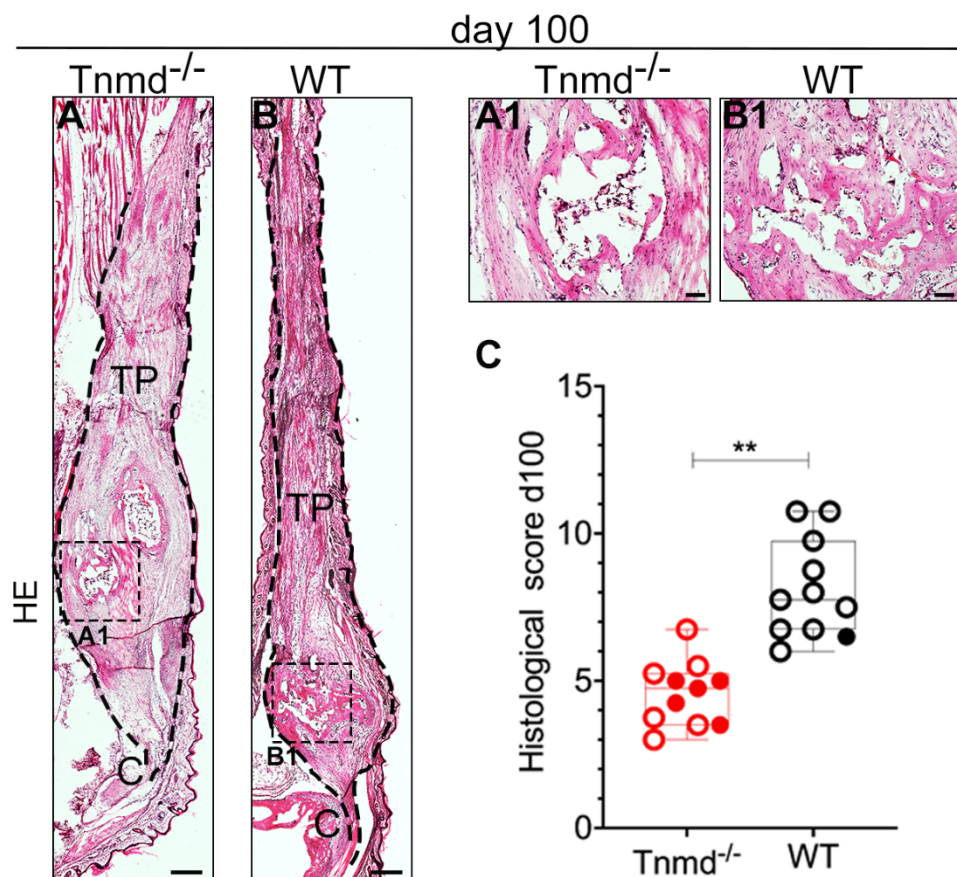


Fig. 34. Overall tissue morphology 100 days post-injury. (A-B) Representative mosaic, (A1-B1) higher magnification HE images and (C) histological scoring at day 100 post-injury. Black dotted lines frame ATs. C=calcaneus, TP=tendon proper. Scale bar: 200µm (panels A, B); 50µm (panels A1, B1). Histological scoring, n=11

Results

animals/genotype. Box plots show median \pm IQR. Empty dot represents female mouse; filled dot represents male mouse. Figure was derived from Fig. 4A-B, Delgado Caceres *et al.*, 2021⁸⁹, which has been published under the gold open access model.

“Furthermore, to exclude dystrophic calcification and validate the presence of osteoblasts and thus HO in the injured tendons, we performed immunofluorescence staining with the osteogenic marker osteopontin (OPN) (Fig. 35A-B1), which demonstrated broader OPN⁺ domain and higher protein levels in the *Tnmd*^{-/-} group. Interestingly, in the bone nodules, sparse double positive *ScxGFP*⁺/OPN⁺ cells were observable (Fig. 35A2-B2’’).

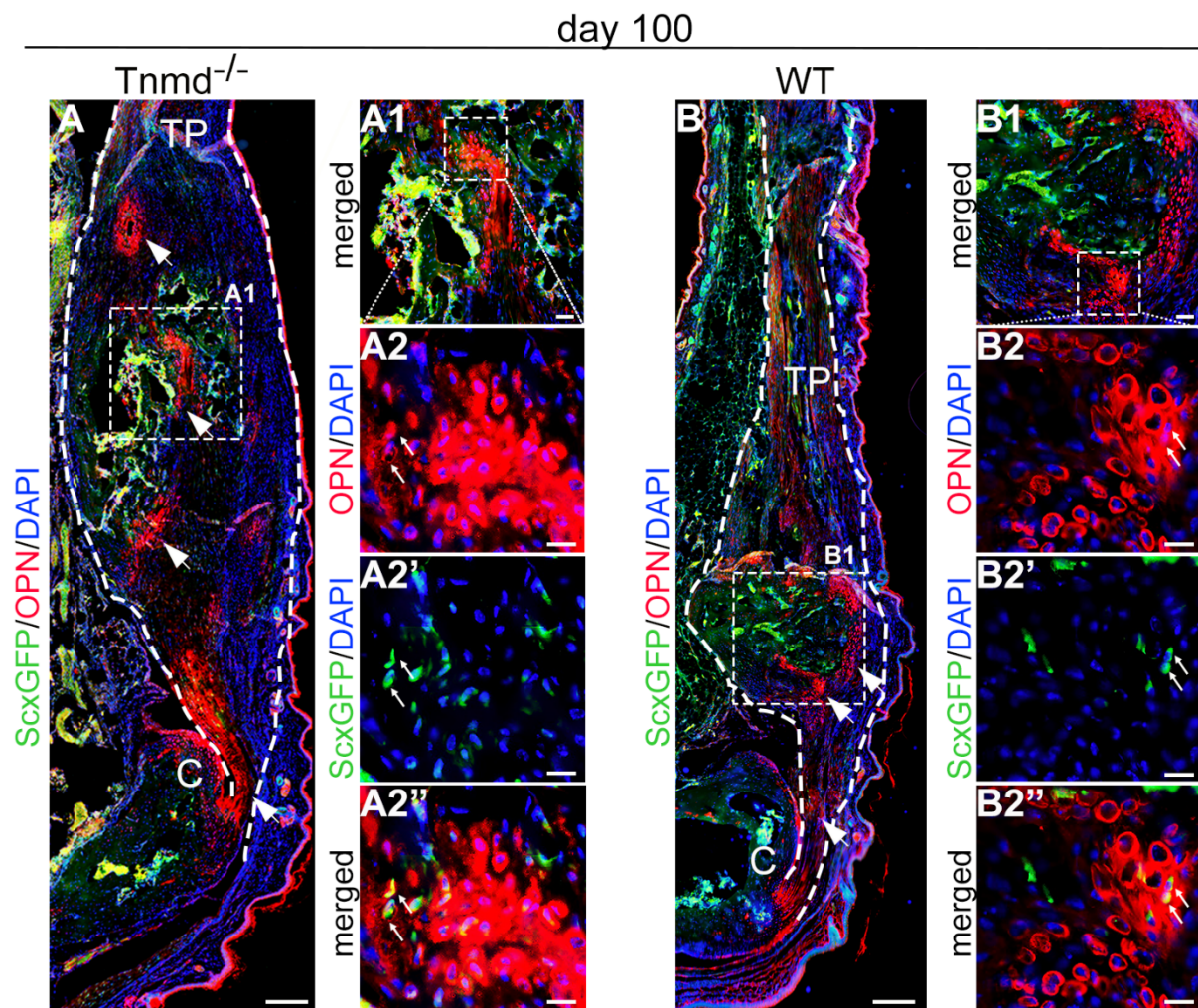


Fig. 35. Detection of osteogenic bone marker OPN. (A-B) Representative fluorescent images and (A1-B2’’) higher magnification images of Osteopontin (OPN)-staining of *Tnmd*^{-/-} *ScxGFP* and WT *ScxGFP* tendons. White dotted lines frame ATs; white arrows in A, B mark OPN⁺-stained regions. White arrows in A2-B2’’ mark double positive *ScxGFP*⁺/OPN⁺ cells. C=calcaneus, TP=tendon proper. Scale bar: 100 μ m (A, B panel); 50 μ m (A1, B1 panels); 20 μ m

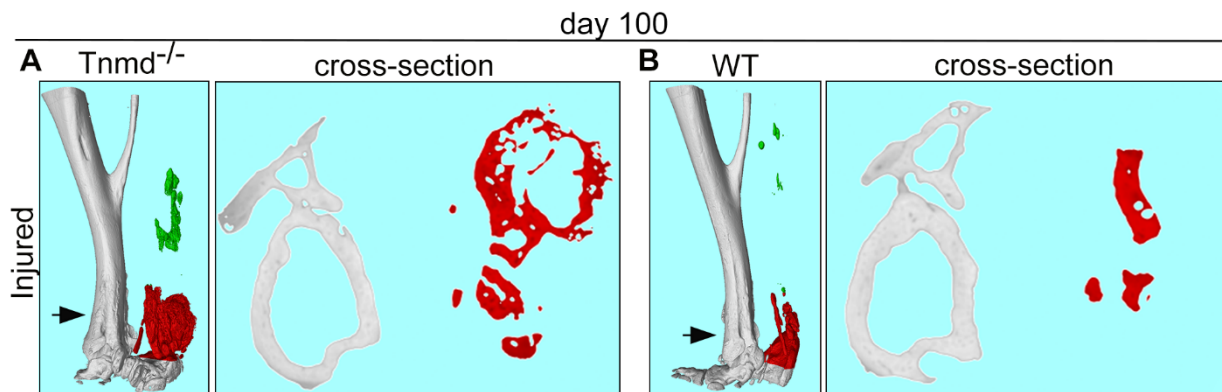
Results

(A2-B2'' panels). OPN staining was performed with $n=3/\text{genotype}$, each animal represented by three tissue sections. Figure was derived from Fig. 4C-D2'', Delgado Caceres *et al.*, 2021⁸⁹, which has been published under the gold open access model.

3.9 Lack of *Tnmd* results in significantly higher trauma-induced heterotopic ossification

“Next, to precisely quantify if HO was higher in injured *Tnmd*^{-/-} tendons, we performed micro-CT scanning with injured ATs 100 days post-injury. Longitudinal and cross-sectional representative images demonstrated a bipolar HO distribution in the tendon with the enthesis-adjacent site (marked in red) pervading the MTJ-adjacent (marked in green) site in terms of spreading magnitude (Fig. 36A, B)”. The quantitative analysis of HO volume at the enthesis, MTJ and in total did not reveal significant differences between the genotypes (Fig. 36C-E). Interestingly the measured HO surface at the enthesis site was significantly increased in *Tnmd*^{-/-} tendons compared to WT (42.4 mm² and 20.5 mm², respectively) (Fig. 36F). At the MTJ, the HO surfaces were comparable between genotypes (11.2 mm² in the *Tnmd*^{-/-} and 8.2 mm² in the WT) (Fig. 36G). Nevertheless, the total HO surface in injured *Tnmd*^{-/-} tendons remained 2-fold significantly higher than the WT (47.3 mm² and 27.8 mm², respectively) (Fig. 36H).

“Hence, these results showed that the absence of *Tnmd* causes overall worsening of the late stage of tendon repair process characterized by significantly augmented trauma-induced HO”.



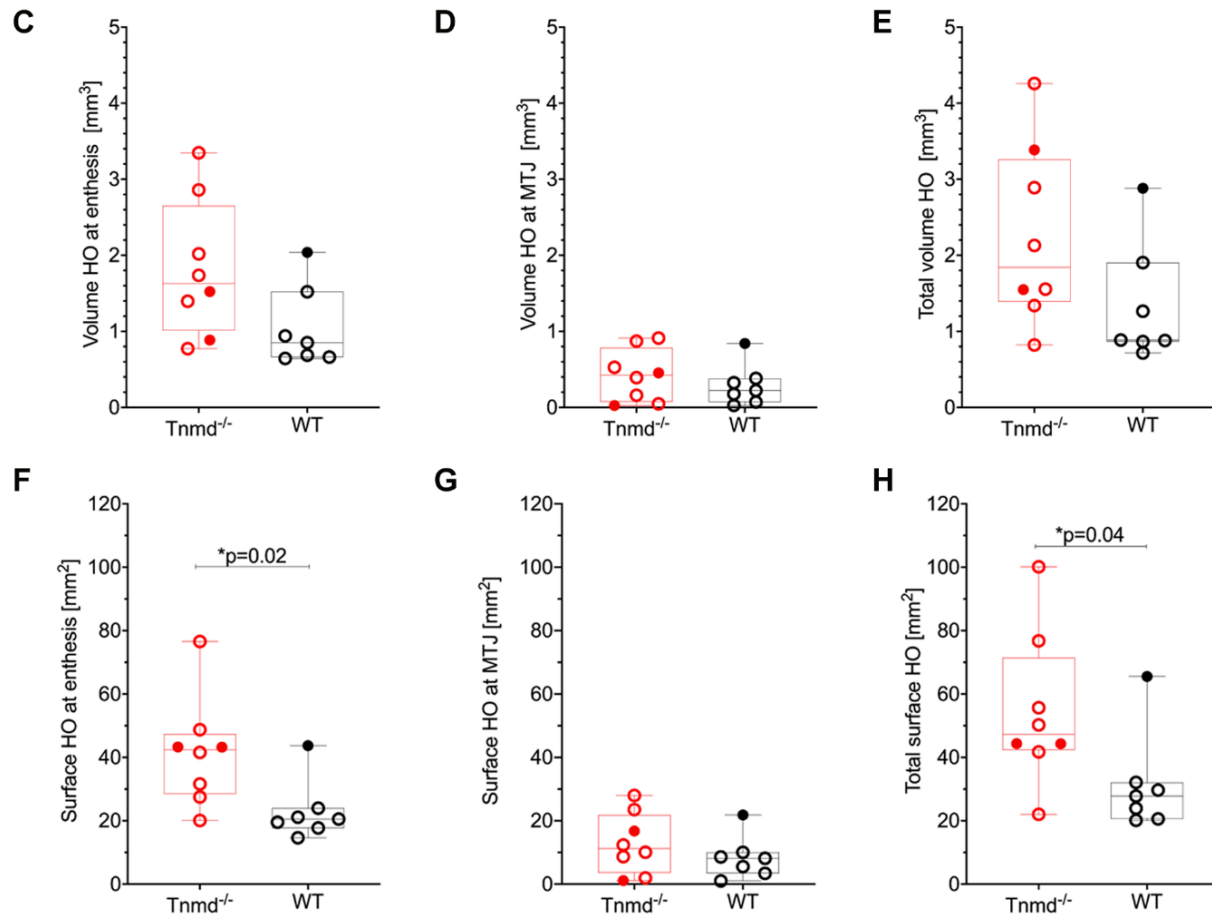
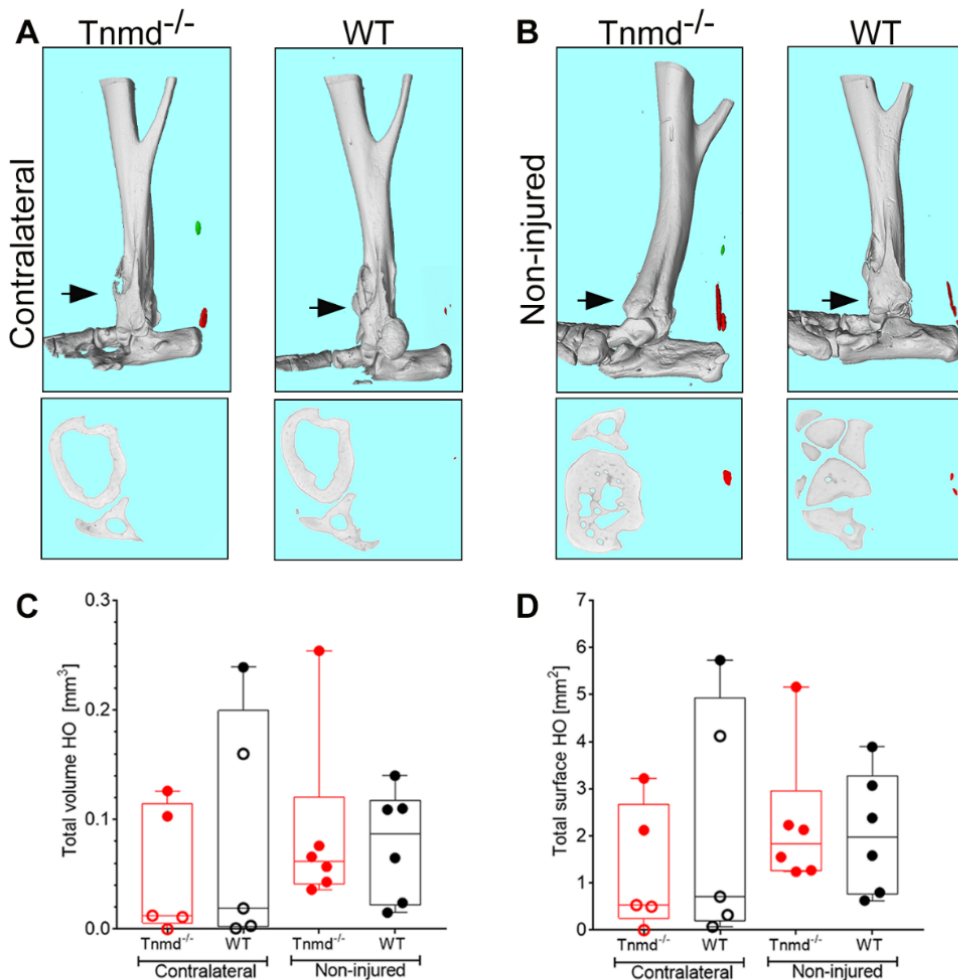


Fig. 36. Micro-CT quantification of injured ATs. (A-B) Longitudinal and cross-sectional representative μ CT scan of *Tnmd*^{-/-} and WT ATs at day 100 post-injury. Black arrows in A and B mark the regions from which the cross-sectional images below were derived. Quantification of (C-E) HO volume and (F-H) HO surface at the entheses, at the MTJ and in total HO, respectively in injured *Tnmd*^{-/-} and WT ATs. n=7-8 animals/genotype. Box plots show median \pm IQR. Statistical analysis was performed with unpaired non-parametric Mann-Whitney U test. Empty dot represents female mouse; filled dot represents male mouse. Figure was derived from Fig. 4E-I, Delgado Caceres *et al.*, 2021⁸⁹, which has been published under the gold open access model.

3.10 Contralateral and non-injured Achilles tendon present marginal age-related HO

Since trauma-induced HO was detected in *Tnmd*^{-/-} and WT ATs at day 100 post-injury, we further examined if contralateral tendons and non-injured tendons (from 9-months-old mice) presented HO as well. The rationale behind was to dismiss the possibility that HO formation was triggered alone by age and not by trauma. The longitudinal and cross-sectional representative μ CT scan images showed minor HO formation, which appeared to be slightly increased in *Tnmd*^{-/-} tendons (Fig. 37A, B). The respective total HO volume and surface quantification exposed comparable degree between the genotypes and between contralateral and non-injured tendons (Fig. 37C, D)⁸⁹.



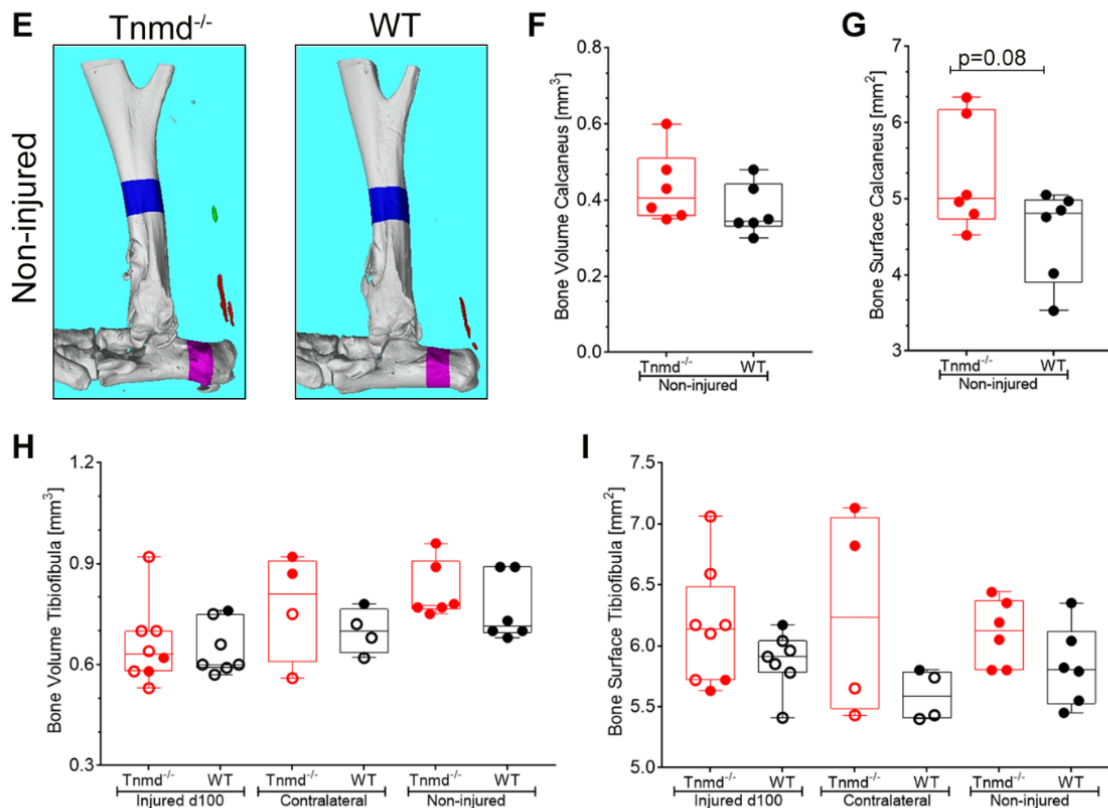
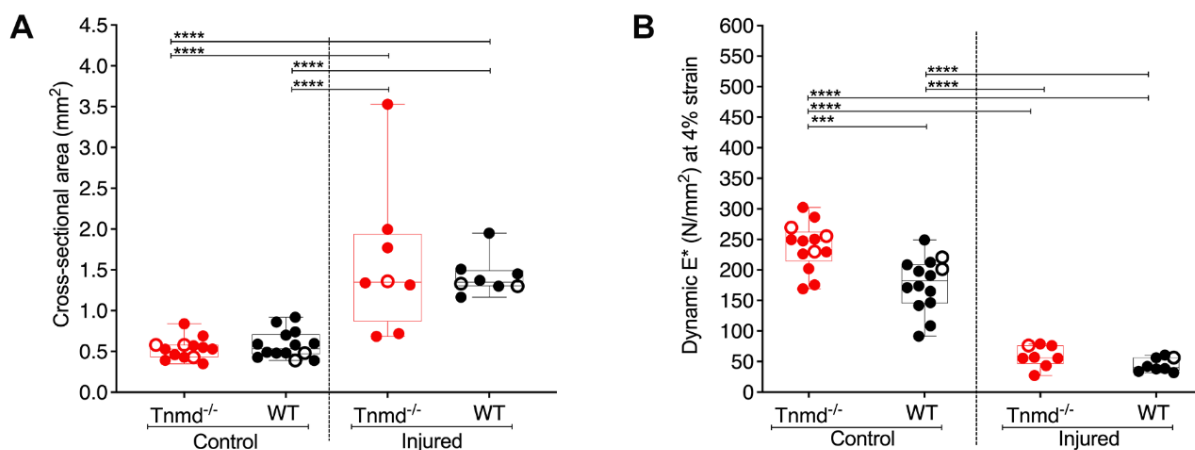


Fig. 37. Micro-CT quantification. (A, B) Representative μ CT scan of contralateral and non-injured *Tnmd*^{-/-} and WT ATs. Black arrows in A and B mark the regions from which the cross-sectional images below were derived. Quantification of (C) total HO volume and (D) surface in contralateral and non-injured tendons. (E) Representative μ CT scan of calcaneal and tibiofibular bones. Calcaneal bone volume (F) and surface (G) (magenta region quantified). Tibiofibular bone volume (H) and surface (I) (blue region quantified). n=4-8 animals/genotype. Box plots show median \pm IQR. Statistical analysis was performed with one-way ANOVA. Empty dot represents female mouse; filled dot represents male mouse. Figure was derived from Suppl. Fig. 5A-I, Delgado Caceres *et al.*, 2021⁸⁹, which has been published under the gold open access model.

Moreover, to rule out the possibility that *Tnmd*-deficiency affects bone quality, regional calcaneal and tibiofibular bone volume, and surface of specimens from the same groups were quantified and no significant differences were detected (Fig. 37E-I).

3.11 $Tnmd^{-/-}$ tendons are naturally stiffer and display significantly increased static and dynamic Elastic moduli; post injury, tendon viscoelastic properties are profoundly weakened in both genotypes

“We subjected non-injured contralateral control and injured $Tnmd^{-/-}$ and WT ATs to a viscoelastic biomechanical testing at day 100 post-injury (Fig. 14: testing apparatus and protocol). Cross-sectional tendon areas were measured and significantly larger values, indicative of tendon dilation, were obtained for the injured tendons compared to the controls, but no significant differences were detected between the genotypes (Fig. 38A). Next, we examined dynamic Elastic modulus, characteristic for the tissue resistance to be elastically deformed at 3 different strain levels (4%, 6% and 8%) by cyclic loading, and discovered for the first time, significantly higher dynamic E-modulus at each deformation level in control $Tnmd^{-/-}$ tendons compared to WTs. Moreover, an apparent linear rise in dynamic E-modulus with increasing strain rates was also observed (Fig. 38B-D). Upon injury, dynamic E-modulus decreased considerably compared to non-injured controls, (Fig. 38B-D). Furthermore, we evaluated the static E-modulus (calculated from the linear-elastic region of the load-to-failure curve) and yet again, the values in control $Tnmd^{-/-}$ tendons were significantly higher than in the WT. At day 100 post-injury, this parameter showed significant and comparable 2-fold decrease in both genotypes (Fig. 38E). Similar to the static E-modulus, control $Tnmd^{-/-}$ tendons exhibited a strong tendency ($p=0.0543$) to be stiffer than WT tendons, which is indicative of resistance to change in length upon load (Fig. 38F)”.



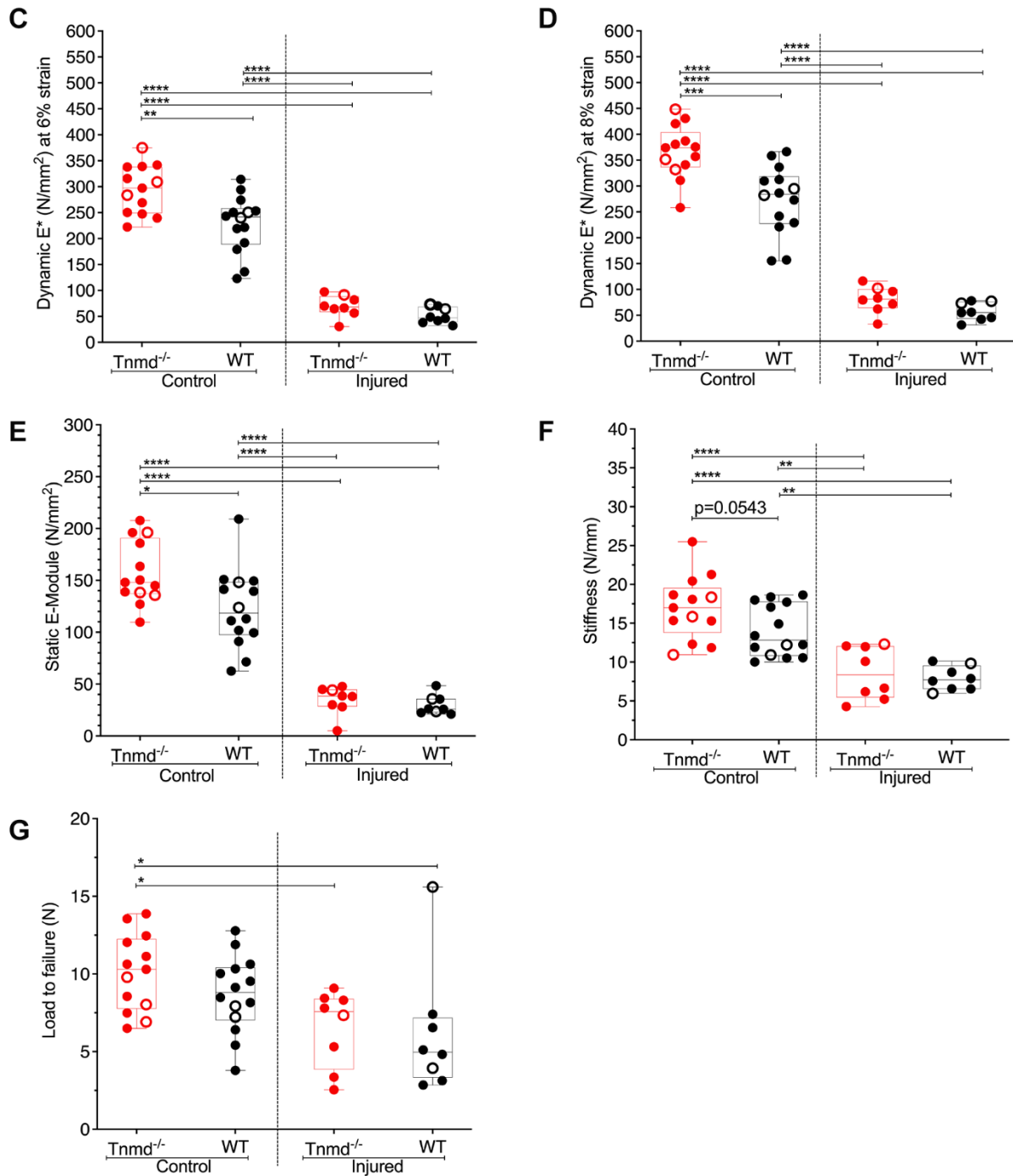


Fig. 38. Viscoelastic biomechanical testing of non-injured, control and injured ATs at day 100 post-injury. (A) Cross-sectional area of non-injured, control and injured ATs. Dynamic Elastic modulus in control and injured *Tnmd*^{-/-} and WT ATs at (B) 4%, (C) 6% and (D) 8% strain. (E) Static Elastic modulus and (F) stiffness of non-injured, control and injured ATs. (G) Load-to-failure tests. Box plots show median \pm IQR; statistical significance was performed with one-way ANOVA and Bonferroni post-hoc test. * $p < 0.05$, ** $p < 0.001$, *** $p < 0.001$, **** $p < 0.0001$. Empty dots represent female mouse; filled dot represent male mouse. Figure was derived from Fig. 5A-D and Suppl. Fig. 6G-H, Delgado Caceres *et al.*, 2021⁸⁹, which has been published under the gold open access model.

Results

“Irrespective of genotype, injury led to significant loss of tissue stiffness at day 100 post-injury that might relate to the observed trauma-induced tendon HO at this stage. Lastly, we measured the load required to produce tissue failure, and found a significant difference towards less load inducing failure in the injured groups, but our biomechanical system did not detect significant changes between the control groups (Fig. 38G).

Altogether, we demonstrated a profound decline in tendon viscoelastic properties at the late stage of AT healing of the *Tnmd*^{-/-} and WT groups; moreover, non-injured *Tnmd*-deficient tendons were stiffer and exhibited increased resistance to elastic deformation and reduced capacity to store muscle-generated energy”.

3.12 Tenomodulin-deficient mice run significantly less after injury

To test tissue functionality, we performed voluntary running tests with *Tnmd*^{-/-} and WT mice 100 days post-injury. Therefore, the total distance voluntarily ran was recorded and compared. After acclimatization, mice were left in experimental cage and allowed to voluntarily use the wheel (Fig. 15). Whilst injured *Tnmd*^{-/-} animals ran approx. 7 Km, their WT littermates ran 11.4 Km (Fig. 39). This data underpins *Tnmd* importance in tendon functionality, since *Tnmd*-deficient animals run significantly shorter distances 100 days post-injury.

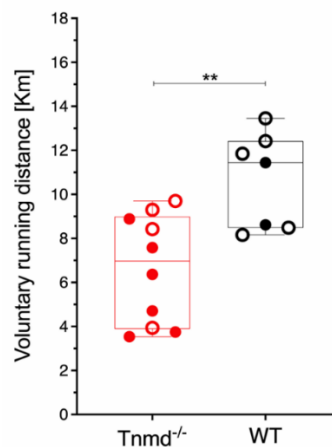


Fig. 39. Voluntary running test. Recorded running distance was performed with n=7-10 animals/genotype. Box plots show median \pm IQR; statistical significance was assessed with 2-tailed unpaired parametric Student's t-test, * $P < 0.05$, ** $p < 0.001$. Empty dots represent female mouse; filled dots represent male mouse. Figure was taken from Fig. 5F, Delgado Caceres *et al.*, 2021⁸⁹, which has been published under the gold open access model.

3.13 Pilot single cell RNA-Sequencing analysis reveals a significant transcriptomic shift between *Tnmd*^{-/-} ScxGFP⁺ and WT ScxGFP⁺ cells

“To fish out potential transcriptomic alterations driven by the absence of *Tnmd* in tendon lineage cells, we subjected *Tnmd*^{-/-} ScxGFP⁺ and WT ScxGFP⁺ cells, isolated from non-injured ATs to a pilot single cell RNA-sequencing (scRNA-seq) analysis. A total of 1278 significantly (adjusted *p*-value <0.05 and $|\log_2 Fc| > 1$) differentially expressed genes (DEGs) were identified between the genotypes by DESeq2-analysis. Volcano plot showing statistical significance (\log_{10} adjusted *p*-value / False Discovery Rate, FDR) versus magnitude of change (\log_2 Fold change, Fc) revealed that 749 DEGs were downregulated and 529 DEGs were upregulated in the *Tnmd*^{-/-} cells compared to the WTs (Fig. 40)”.

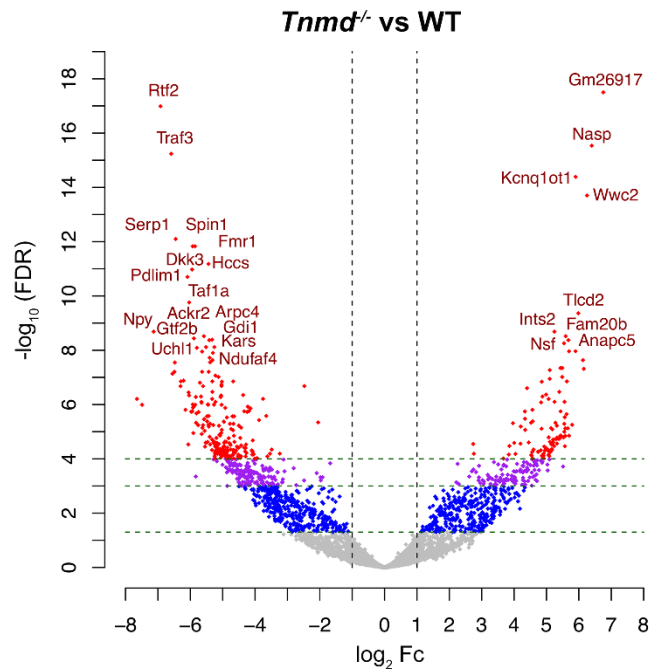


Fig. 40. ScRNA-Sequencing of *Tnmd*^{-/-} ScxGFP⁺ and WT ScxGFP⁺ cells isolated from non-injured ATs. Volcano plot shows $-\log_{10}$ FDR i.e. adjusted *p*-value and \log_2 FC expression values of all genes, each dot represents a gene. Significantly differentially expressed genes (DEGs) are highlighted in color other than grey. Vertical lines present the \log_2 FC threshold equaling 1 or -1; genes outside these lines are DEGs with at least 2-FC. The horizontal lines show $-\log_{10}$ FDR corresponding to FDR thresholds of 0.05, 0.001 and 0.0001 from the bottom respectively. Red, purple and blue dots represent the significant DEGs with 2-FC and $-\log_{10}$ FDR < 0.0001, $-\log_{10}$ FDR < 0.001 and $-\log_{10}$ FDR < 0.05 respectively. Grey dots are neither significant nor have expression above 2-FC. Figure was derived from Fig. 6A, Delgado Caceres *et al.*, 2021⁸⁹, which has been published under the gold open access model.

Results

“Moreover, the heat map (Fig. 41) of the top 100 significant DEGs (Table 17) pointed out gene targets such as *ninjurin-1* (*Ninj1*), *E2F-associated phosphoprotein* (*Eapp*), *reticulocalbin-3* (*Rcn3*), *serpin H1* (*Serpinh1*), *spinlin-1* (*Spin1*) and *secreted protein acidic and cysteine rich* (*Sparc*), to be significantly downregulated in the *Tnmd*^{-/-} group (Table 17). These genes are linked to regulatory mechanisms of cell adhesion, proliferation, apoptosis, and collagen synthesis. In contrast, *cyclin-D-binding Myb-like transcription factor 1* (*Dmtf1*), *E3 ubiquitin-protein ligase Rnfl167*, *glycosaminoglycan xylosylkinase* (*Fam20b*) and the *constitutive coactivator of PPAR-gamma-like protein 1* (*Fam120b*) were significantly upregulated in *Tnmd*^{-/-} cells (Fig. 41, Table 17). These genes play roles in negative regulation of cell cycle, senescence, proteoglycan expression and adipose cell differentiation”.

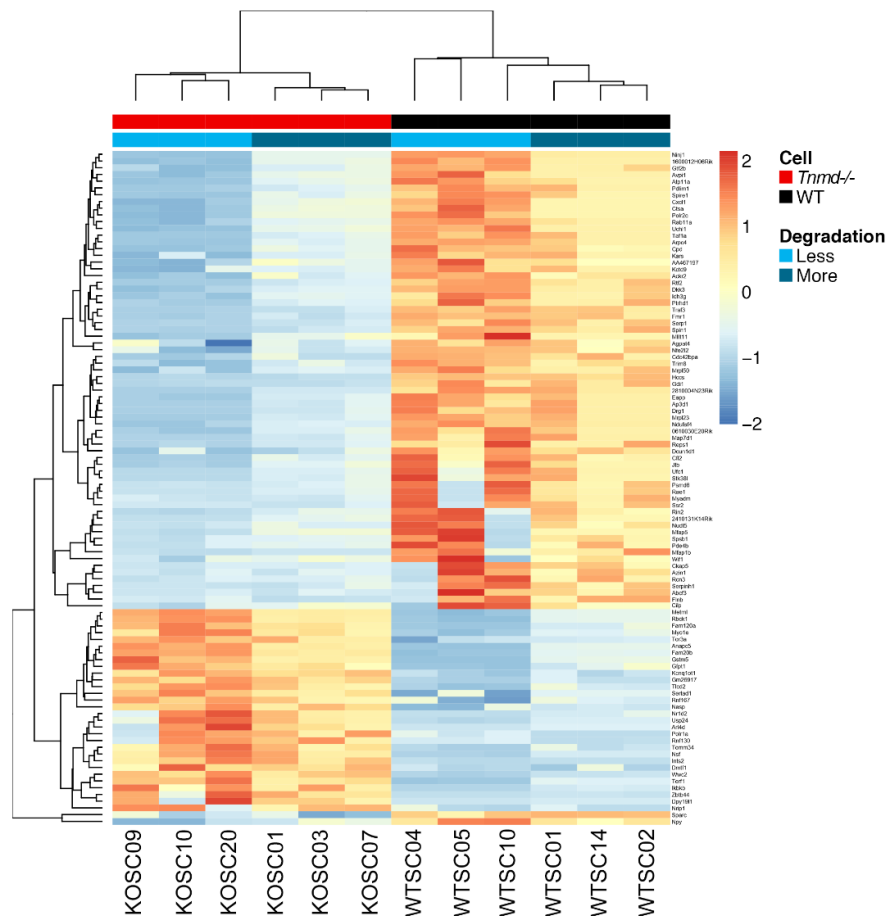


Fig. 41. Heat map with differently expressed genes. Heat map depicting the Log₂CPM expression value of selected top 100 significant DEGs. Top 100 genes with lowest adjusted p-values (q-values) are depicted. Genes are colored according to their Log₂CPM expression values. Clustering on the top is based on cell type and degradation level. Figure was derived from Fig. 6B, Delgado Caceres *et al.*, 2021⁸⁹, which has been published under the gold open access model.

Table 17. Top 100 differentially expressed genes based on adjusted p-values (q-values).

Upregulated genes in <i>Tnmd</i> ^{-/-}	Abrv.	Base Mean	log ₂ Fold change to WT	lfcSE	p-value	q-value	Logcpm <i>Tnmd</i> ^{-/-}	Logcpm WT
Gm26917	N/A	582.48	6.755	0.702	6.75E-22	3.16E-18	7.339	0.719
Nuclear autoantigenic sperm protein	Nasp	1910.93	6.399	0.709	1.86E-19	2.91E-16	8.882	2.350
Kcnq1 opposite strand/antisense transcript 1	Kcnq1ot1	541.44	5.899	0.681	4.36E-18	4.09E-15	7.297	1.437
WW and C2 domain containing 2	Wwc2	335.35	6.250	0.738	2.55E-17	1.99E-14	6.524	0.490
TLC domain-containing protein 2	Tlcd2	649.66	5.982	0.843	1.30E-12	4.34E-10	7.097	1.252
Integrator complex subunit 2	Ints2	131.53	5.245	0.765	7.05E-12	2.07E-09	5.104	0.167
Fam20b-Glycosaminoglycan Xylosylkinase	Fam20b	433.1	5.593	0.824	1.13E-11	3.03E-09	6.689	1.206
Anaphase promoting complex subunit 5	Anapc5	546.33	5.677	0.846	1.95E-11	4.25E-09	6.888	1.364
N-ethylmaleimide sensitive factor, vesicle fusing ATPase	Nsf	216.68	5.541	0.832	2.72E-11	5.54E-09	5.567	0.547
Glutathione S-transferase 5	Gstm5	721.90	5.897	0.902	6.26E-11	1.09E-08	6.829	1.486
Inhibitor of nuclear factor kappa B kinase subunit beta	Ikbkb	211.71	5.695	0.872	6.52E-11	1.09E-08	5.341	0.387
RNA polymerase I subunit A	Polr1a	228.17	6.126	0.958	1.63E-10	2.31E-08	5.113	0.014
Translocase of outer mitochondrial membrane 34	Tomm34	244.62	5.431	0.866	3.56E-10	4.52E-08	5.652	0.716
Myosin IE	Myo1e	389.92	5.488	0.875	3.57E-10	4.52E-08	6.247	1.215
Nuclear receptor subfamily 1 group D member 2	Nr1d2	351.18	6.153	0.983	3.92E-10	4.83E-08	5.325	0.630
Telomeric repeat binding factor 1	Terf1	213.76	5.103	0.818	4.48E-10	5.39E-08	5.688	0.826
Cyclin D binding myb like transcription factor 1	Dmtf1	207.25	5.486	0.896	9.36E-10	9.64E-08	5.381	0.364
Family with sequence similarity 120A	Fam120a	282.76	5.101	0.838	1.13E-09	1.13E-07	6.065	1.112
Ubiquitin specific peptidase 24	Usp24	227.39	5.628	0.932	1.56E-09	1.41E-07	5.107	0.526

Results

Upregulated genes in <i>Tnmd</i> ^{-/-}	Abrv.	Base Mean	log ₂ Fold change to WT	lfcSE	p-value	q-value	logcpm <i>Tnmd</i> ^{-/-}	logcpm WT
SERTA domain containing 1	Sertad1	796.94	4.854	0.805	1.66E-09	1.44E-07	7.523	2.554
Torsin family 3 member A	Tor3a	255.36	4.400	0.743	3.24E-09	2.49E-07	6.117	1.806
Glutamine-fructose-6-phosphatase transaminase 1	Gfpt1	490.71	5.396	0.920	4.54E-09	3.42E-07	6.576	1.254
Zinc finger and BTB domain containing 44	Zbtb44	103.00	4.988	0.858	5.99E-09	4.32E-07	4.321	0.063
Meteorin-like, glial cell differentiation regulator	Metrn1	279.00	4.876	0.844	7.58E-09	5.07E-07	6.034	1.277
Ring finger protein 130	Rnf130	89.19	5.064	0.883	9.93E-09	6.20E-07	4.032	-0.230
Nuclear receptor interacting protein 1	Nrip1	213.24	5.248	0.923	1.32E-08	7.95E-07	5.189	0.647
Dpy-19 like C-mannosyltransferase 1	Dpy19l1	156.28	5.557	0.978	1.32E-08	7.95E-07	4.280	0.094
RanBP-type and C3HC4-type zinc finger containing 1	Rbck1	252.59	4.835	0.853	1.44E-08	8.33E-07	5.872	1.162
Ring finger protein 167	Rnf167	711.52	4.564	0.825	3.21E-08	1.56E-06	7.388	2.576
ADP ribosylation factor-like GTPase 4D	Arl4d	170.51	5.436	0.989	3.82E-08	1.78E-06	4.340	0.3269

Downregulated genes in <i>Tnmd</i> ^{-/-} cells	Abrv.	Base Mean	log ₂ Fold change to WT	lfcSE	p-value	q-value	Logcpm. <i>Tnmd</i> ^{-/-}	Logcpm. WT
Replication termination factor 2	Rtf2	673.49	-6.921	0.734	4.39E-21	1.03E-17	0.927	7.412
TNF receptor associated factor 3	Traf3	372.32	-6.589	0.739	4.97E-19	5.82E-16	0.501	6.741
Stress associated endoplasmic reticulum protein 1	Serp1	338.11	-6.451	0.805	1.19E-15	7.95E-13	0.474	6.380
FMRP translational regulator 1	Fmr1	246.61	-5.854	0.740	2.77E-15	1.48E-12	0.532	6.186
Spindlin 1	Spin1	249.23	-5.926	0.750	2.84E-15	1.48E-12	0.525	6.153
Holocytochrome c synthase	Hcss	1417.19	-5.438	0.706	1.41E-14	6.60E-12	0.173	5.494

Results

Downregulated genes in <i>Tnmd</i> ^{-/-} cells	Abrv.	Base Mean	log ₂ Fold change to WT	lfcSE	p-value	q-value	Logcpm. <i>Tnmd</i> ^{-/-}	Logcpm. WT
Dickkopf WNT signaling pathway inhibitor 3	Dkk3	479.12	-5.947	0.780	2.49E-14	1.06E-11	1.268	6.900
PDZ and LIM domain 1	Pdlim1	502.44	-6.087	0.808	5.08E-14	1.98E-11	1.197	6.826
TATA-box binding protein associated factor, RNA polymerase I, A	Taf1a	388.03	-6.035	0.834	4.82E-13	1.74E-10	0.914	6.468
Neuropeptide Y	Npy	15199.1	-7.134	1.041	7.01E-12	2.07E-09	4.252	10.859
Actin related protein 2/3 complex, subunit 4	Arpc4	321.6	-5.580	0.822	1.16E-11	3.03E-09	1.008	6.301
Atypical chemokine receptor 2	Ackr2	1016.31	-5.889	0.873	1.48E-11	3.65E-09	1.616	7.681
Guanosine diphosphate dissociation inhibitor 1	Gdi1	147.05	-5.326	0.792	1.74E-11	4.08E-09	0.321	5.267
General transcription factor IIB	Gtf2b	364.41	-5.414	0.807	2.00E-11	4.25E-09	1.333	6.493
NADH ubiquinone oxidoreductase complex factor 4	Ndufaf4	196.56	-5.256	0.796	3.95E-11	7.64E-09	0.807	5.659
Lysyl-tRNA synthetase	Kars	453.79	-5.515	0.835	4.08E-11	7.64E-09	1.542	6.611
Ubiquitin carboxy-terminal hydrolase L1	Uchl1	688.99	-5.797	0.880	4.52E-11	8.15E-09	1.573	6.974
Peptidyl-tRNA hydrolase domain containing 1	Ptrhd1	286.82	-5.634	0.864	6.95E-11	1.12E-08	0.880	5.871
RAB11A, member RAS oncogene family	Rab11a	495.35	-5.301	0.816	8.04E-11	1.26E-08	1.767	6.834
Developmentally regulated GTP binding protein 1	Drg1	194.98	-5.405	0.840	1.25E-10	1.89E-08	0.547	5.491
E2F associated phosphoprotein	Eapp	211.21	-5.314	0.831	1.60E-10	2.31E-08	0.764	5.631
Adaptor-related protein complex 3, delta 1 subunit	Ap3d1	192.97	-5.388	0.847	2.01E-10	2.77E-08	0.535	5.446
Myeloid- associated differentiation maker	Myadm	342.73	-6.478	1.019	2.12E-10	2.84E-08	0.307	5.207
Proteasome prosome, macropain 26S	Psm6	334.28	-6.491	1.046	5.35E-10	6.22E-08	0.424	5.001

Results

subunit, non-ATPase 6								
Downregulated genes in <i>Tnmd</i> ^{-/-} cells	Abrv.	Base Mean	log ₂ Fold change to WT	lfcSE	p- value	q- value	Logcpm. <i>Tnmd</i> ^{-/-}	Logcpm. WT
Carboxypeptidase D	Cpd	425.61	-5.634	0.908	5.54E-10	6.22E-08	1.212	6.296
Isocitrate dehydrogenase 3 NAD ⁺ gamma	Idh3g	292.29	-5.434	0.876	5.58E-10	6.22E-08	1.076	5.872
SplA/ryanodine receptor domain and SOCS box containing 1	Spsb1	466.41	-6.551	1.061	6.74E-10	7.34E-08	0.795	5.110
Ninjurin 1	Ninj1	290.07	-5.225	0.850	8.01E-10	8.53E-08	1.132	6.076
Defective in cullin neddylation 1, domain containing 1	Dcun1d1	277.72	-5.128	0.838	9.46E-10	9.64E-08	1.191	6.073
Signal sequence receptor subunit 2	Ssr2	202.30	-6.208	1.024	1.36E-09	1.32E-07	-0.031	4.665
Cytoskeleton associated protein 5	Ckap5	318.08	-6.290	1.040	1.47E-09	1.40E-07	0.404	4.962
Spire type actin nucleation factor 1	Spire1	297.79	-5.320	0.880	1.53E-09	1.41E-07	1.063	5.978
Mitochondrial ribosomal protein L23	Mrpl23	111.66	-4.676	0.774	1.55E-09	1.41E-07	0.572	4.879
Potassium channel tetramerisation domain containing 9	Kctd9	374.88	-5.024	0.834	1.67E-09	1.44E-07	1.691	6.411
AA467197	N/A	1112.57	-5.702	0.949	1.84E-09	1.57E-07	2.059	7.057
MAP7 domain containing 1	Map7d1	127.59	-5.036	0.842	2.22E-09	1.86E-07	0.456	4.838
0610030E20Rik	N/A	194.28	-5.036	0.845	2.53E-09	2.08E-07	0.876	5.461
Secreted protein acidic and cysteine rich	Sparc	10319.9	-2.478	0.416	2.58E-09	2.09E-07	8.897	11.457
Cofilin 2	Cfl2	278.08	-5.606	0.942	2.65E-09	2.10E-07	0.817	5.490
Nudix, nucleoside diphosphate linked moiety X-type motif 5	Nudt5	372.47	-6.302	1.059	2.70E-09	2.11E-07	0.606	5.032
RalBP1 associated Eps domain containing protein	Reps1	170.30	-5.319	0.908	4.60E-09	3.42E-07	0.520	4.944
Ribonucleic acid export 1	Rae1	250.22	-6.052	1.034	4.89E-09	3.58E-07	0.356	4.729

Results

Downregulated genes in <i>Tnmd</i> ^{-/-} cells	Abrv.	Base Mean	log ₂ Fold change to WT	lfcSE	p-value	q-value	Logcpm. <i>Tnmd</i> ^{-/-}	Logcpm. WT
2810004N23Rik	N/A	79.29	-4.369	0.752	6.28E-09	4.45E-07	0.372	4.401
Reticulocalbin 3, EF-hand calcium binding domain	Rcn3	300.87	-6.036	1.040	6.56E-09	4.59E-07	0.710	4.863
1600012H06Rik	N/A	274.64	-5.048	0.871	6.79E-09	4.67E-07	1.218	5.907
Serpin family H member 1	Serpinh1	182.81	-5.669	0.981	7.53E-09	5.07E-07	0.275	4.681
Myeloid/lymphoid or mixed-lineage leukemia; translocated to, 11	Mllt11	654.86	-5.828	1.010	7.95E-09	5.25E-07	1.537	5.965
ATPase phospholipid transporting 11a	Atp11a	257.95	-5.062	0.878	8.14E-09	5.29E-07	1.144	5.760
Cathepsin a	Ctsa	568.05	-5.328	0.929	9.85E-09	6.20E-07	1.745	6.500
Nuclear factor, erythroid derived 2, like 2	Nfe2l2	702.01	-3.754	0.659	9.91E-09	6.20E-07	3.8301	7.600
Wnt inhibitory factor 1	Wif1	4558.33	-7.649	1.335	1.01E-08	6.21E-07	2.590	6.727
Arginine vasopressin-induced 1	Avp1l	341.57	-5.222	0.919	1.34E-08	7.96E-07	1.368	5.911
Serine/threonine kinase 38 like	Stk38l	195.88	-5.658	0.996	1.36E-08	7.96E-07	0.476	4.658
Ras und Rab interactor 2	Rin2	243.44	-5.653	0.999	1.51E-08	8.65E-07	0.682	4.902
Filamin beta	Flnb	134.58	-5.455	0.968	1.75E-08	9.90E-07	-0.080	4.399
Ubiquitin-fold modifier conjugating enzyme 1	Ufc1	182.59	-5.458	0.969	1.79E-08	9.90E-07	0.469	4.708
Phosphodiesterase 4B, cAMP specific	Pde4b	324.32	-5.922	1.052	1.80E-08	9.90E-07	0.893	4.812
RNA polymerase II polypeptide C	Polr2c	555.64	-5.268	0.936	1.85E-08	1.01E-06	1.714	6.480
C-X-C motif ligand 1	Cxcl1	521.29	-5.034	0.896	1.91E-08	1.02E-06	1.901	6.616
Cartilage intermediate layer protein	Cilp	4211.69	-7.490	1.333	1.94E-08	1.02E-06	2.500	6.781
Jumping translocation breakpoint	Jtb	255.29	-5.450	0.970	1.96E-08	1.02E-06	0.887	5.181
Antizyme inhibitor 1	Azin1	260.00	-5.848	1.042	1.97E-08	1.02E-06	0.530	4.682

Results

Downregulated genes in <i>Tnmd</i> ^{-/-} cells	Abrv.	Base Mean	log ₂ Fold change to WT	lfcSE	p-value	q-value	Logcpm. <i>Tnmd</i> ^{-/-}	Logcpm. WT
2410131K14Rik	N/A	246.97	-5.895	1.055	2.29E-08	1.18E-06	0.537	4.533
CDC42 binding protein kinase alpha	Cdc42bpa	118.23	-4.225	0.756	2.35E-08	1.20E-06	0.783	5.062
ATP binding cassette subfamily F member 3	Abcf3	196.55	-5.916	1.063	2.59E-08	1.30E-06	0.168	4.261
Microfibrillar-associated protein 1b	Mfap1b	104.72	-4.919	0.884	2.67E-08	1.33E-06	0.224	4.338
Tripartite motif-containing 8	Trim8	107.75	-4.143	0.746	2.81E-08	1.39E-06	0.960	4.880
Microfibrillar-associated protein 5	Mfap5	528.18	-6.150	1.112	3.23E-08	1.56E-06	1.152	4.822
1-Acylglycerol-3-phosphate O-acyltransferase 4	Agpat4	1128.05	-4.191	0.761	3.67E-08	1.76E-06	3.595	8.112
Mitochondrial ribosomal protein L50	Mrpl50	137.74	-4.335	0.788	3.74E-08	1.77E-06	1.046	5.119

Table was taken from Suppl. Table 3 from Delgado Caceres *et al.*, 2021⁸⁹, which has been published under the gold open access model.

Abbreviations (Abrv.): LfcSE, log fold change Standard Error; logcpm, mean value of log counts per million

3.13.1 Gene ontology analysis

“Gene ontology (GO) analysis of only the significantly DEGs showed enrichment of gene clusters under biological process (BP), molecular function (MF) and cellular component (CC). For BP, the top 10 enriched terms included “signaling”, “cell surface receptor signaling pathway”, “cell adhesion”, “cell communication” and “circulatory system development” (Fig. 42A). For MF (Fig. 42B), “protein domain specific binding”, “phosphotransferase activity” and “purine and adenyl nucleotide binding” scored in the top 10 enriched terms. For CC, terms related to “cell periphery”, “plasma membrane bounded cell projection” and “anchoring and cell junction” were among the top 10 enriched terms (Fig. 42C)”.

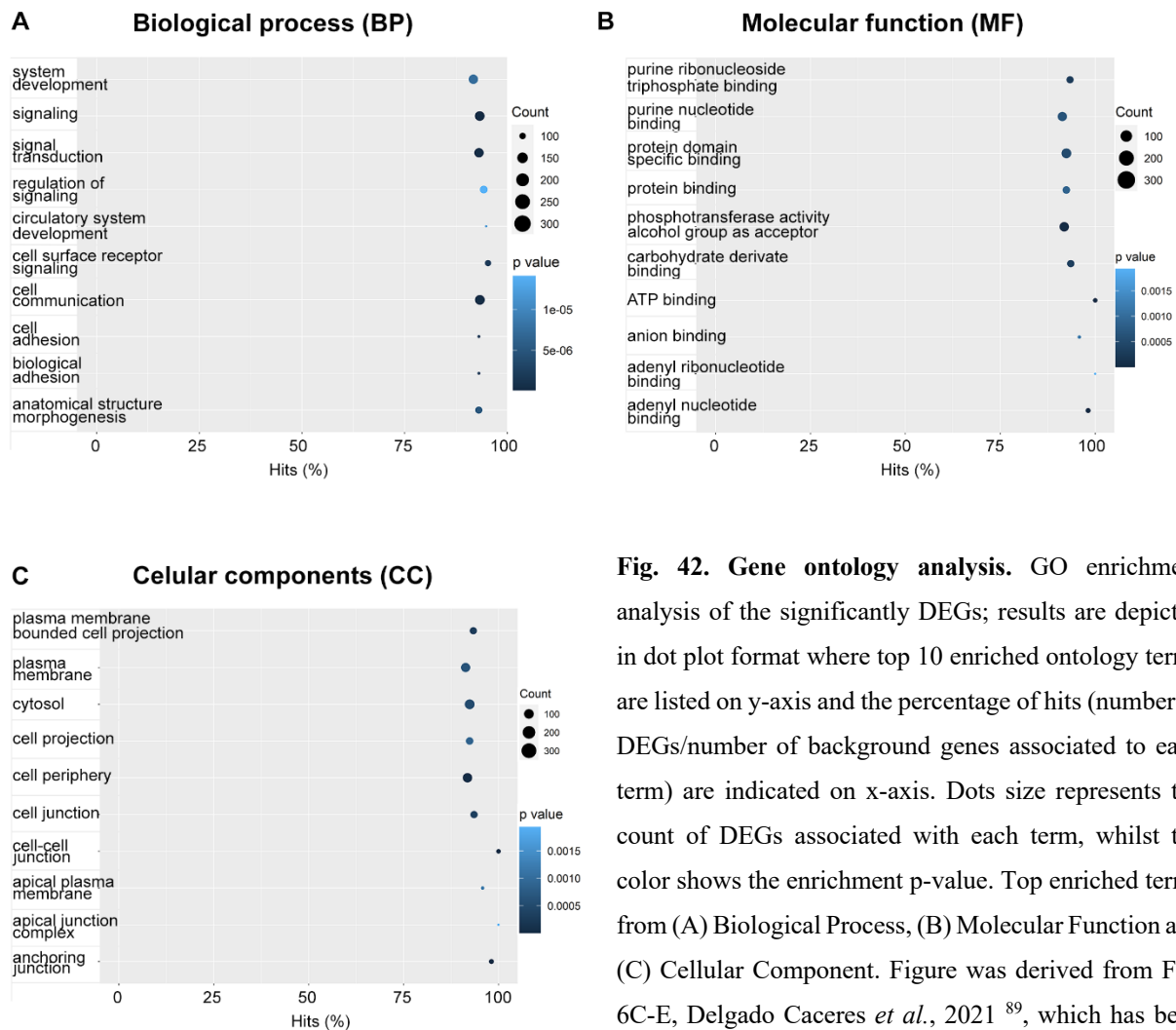


Fig. 42. Gene ontology analysis. GO enrichment analysis of the significantly DEGs; results are depicted in dot plot format where top 10 enriched ontology terms are listed on y-axis and the percentage of hits (number of DEGs/number of background genes associated to each term) are indicated on x-axis. Dots size represents the count of DEGs associated with each term, whilst the color shows the enrichment p-value. Top enriched terms from (A) Biological Process, (B) Molecular Function and (C) Cellular Component. Figure was derived from Fig. 6C-E, Delgado Caceres *et al.*, 2021⁸⁹, which has been published under the gold open access model.

3.13.2 Signaling pathway analysis suggest a *Tnmd* involvement in Hippo and Wnt-signaling cascades

“When subjecting all DEGs to Kyoto Encyclopedia of Genes and Genomes (KEGG) signaling pathway analysis, hits on “Hippo and Wnt-signaling cascades”, “metabolic and insulin signaling pathways”, and “chemokine and receptor signaling pathways” were uncovered (Fig. 43).

In sum, this very novel scRNA-seq data demonstrates that loss of *Tnmd* results in profound gene expression changes in tendon lineage cells from the non-injured setting. It also suggests unprecedented signaling pathways involving indirectly or directly *Tnmd* and strongly urges for follow-up analyses on tendon lineage cells from the injured setting”.

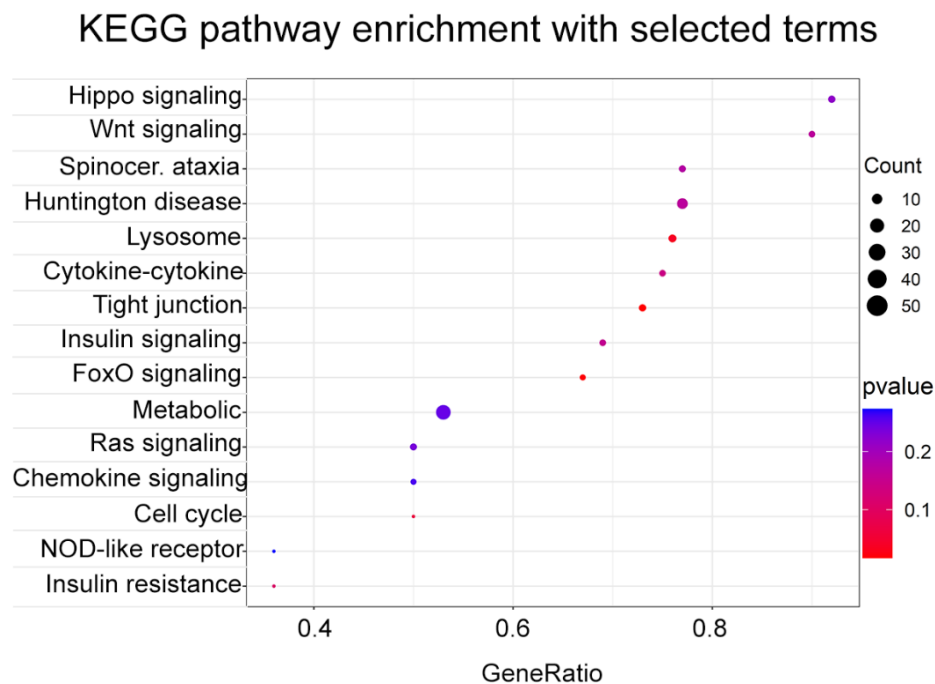


Fig. 43. KEGG signaling pathway. Kyoto Encyclopedia of Genes and Genomes signaling analysis of the significant DEGs in dot plot format; y-axis shows top 15 enriched pathways; x-axis indicates gene ratio (number of DEGs/number of background genes associated to each term). Dots size is based on the number of DEGs that were associated with each term, whilst the color shows the p-value of enrichment. Figure was derived from Fig. 6F, Delgado Caceres *et al.*, 2021⁸⁹, which has been published under the gold open access model.

4. DISCUSSION

I would like to state clearly that parts of the discussion have already been published in Delgado Caceres M, Angerpointner K, Galler M, Lin D, Michel PA, Brochhausen C, Lu X, Varadarajan AR, Warfsmann J, Stange R, Alt V, Pfeifer CG, Docheva D. Tenomodulin knockout mice exhibit worse late healing outcomes with augmented trauma-induced heterotopic ossification of Achilles tendon. *Cell Death & Disease* (2021) ⁸⁹.

“Heterotopic ossification results from the abnormal healing process that involves ectopic bone formation in response to tendon tissue trauma ¹⁹⁵. Upon tendon injury, local tissue destruction and inflammation activates the recruitment of macrophages, followed by the stimulation and proliferation of fibroblastic cells forming a temporary scar ¹²². Cells of mesenchymal origin differentiate into chondro-, and osteogenic cells instead of tenoblasts/tenocytes ¹¹⁹, thereby resulting in tendon HO with strong adverse effects to the tendon structure, strength and function ¹²². Despite the clinical relevance of trauma-induced tendon HO ^{126,127}, the evolution of cell populations regulating the healing outcome, as well as the molecular mechanisms of HO have not been fully elucidated”. Recently, Mead TJ *et al.*, 2018 suggested that the combined functions of ADAMTS7 and ADAMTS12 (A disintegrin and metalloproteinase with thrombospondin motifs-7 and 12) deliver an intrinsic tendon-specific protective mechanism against HO by degrading components of the ECM, by regulating inflammation and binding to TGF- β , as well as by inhibition of BMP signaling pathways, which are associated with HO ^{196,197}.

*“In this study we focused on *Tnmd* gene by subjecting *Tnmd*^{-/-} and control animals to surgically induced complete Achilles tenotomy and evaluated the repair at early, day 8 and later, day 21 proliferative and day 100 remodeling stages. We hypothesized *Tnmd* to be a protective factor of trauma-induced HO in tendon based on the following notions: i) loss of *Tnmd* results in augmented fibrovascular scar tissue in the early phase of tendon repair process ¹⁶⁰; ii) *Tnmd*-deficiency is associated with aging-related mineralization of the chordae tendineae cordis (tendon structures in the heart) ¹⁵⁸; and iii) double knockout of *Tnmd* and its homologous gene chondromodulin I (*Chm1*) leads to premature intervertebral disc degeneration characterized by ectopic appearance of hypertrophic chondrocytes and osteoblasts ¹⁵⁹”*.

4.1 The interplay between extrinsic and intrinsic tissue repair in the context of *Tnmd*

“Our results demonstrated that the absence of *Tnmd* alters the interplay throughout the healing process between intrinsic *ScxGFP*⁺ tendon lineage cells and the extrinsic α SMA-expressing myofibroblastic cells. By cell lineage tracing we detected 8 days post-injury only minor numbers of *ScxGFP*⁺ cells being located directly in the scar lesions, which is consistent with other studies^{116,198}. During the later repair stages, the presence of *ScxGFP*⁺ cells increased in the sutured and end-to-end reconstructed ATs, although their numbers were consistently and significantly less in *Tnmd*^{-/-} than WT scars. *Tnmd* might directly influence the tendon lineage cells, since it has been shown to regulate tendon cell density and proliferation in vivo and in vitro^{33,34}, as well as when ablated to cause augmented senescent and apoptotic cell scores in tendon stem/progenitor cell culture and injured tendon tissue^{33,34,160}. BrdU analysis confirmed the significantly lower number of proliferative cells in the *Tnmd*^{-/-} group. Interestingly, we detected significantly more α SMA⁺ cells in day 8 *Tnmd*^{-/-} scars. In healthy tendons, a population of α SMA⁺ cells is primarily contained in the epitenon sheath¹⁹⁹. In an injured setting (first two weeks upon injury), these cells become active, are recruited and dominate fibrotic scar formation^{116,200}. We postulate that the significant influx of α SMA⁺ cells in *Tnmd*^{-/-} scars is related to the enhanced vascularization of the ruptured mutant tendons that we previously reported¹⁶⁰. Dymant et al., 2014 suggested, by using a triple transgenic α SMACre-ERT2Ai9-*ScxGFP* mice in a patella injury model, that α SMA⁺ cells from the tendon sheaths not only populate and contribute to the defect bridging, but can also be differentiated towards *ScxGFP*⁺ cells⁷⁰. Similarly, in our model, we could also detect some *ScxGFP*⁺ cells to be positively stained for α SMA at the three different time points post injury. Moreover, an α SMA⁺ sub-population located in the calcaneal periosteum has been reported to have an increased predisposition to differentiate towards bone^{201–204}, suggesting a great myofibroblastic cells plasticity”.

In sum, our lineage tracing results underpin a novel regulatory function of *Tnmd* in the tendon healing process, namely supporting tendon-lineage *Scx*⁺ cell proliferation, whilst obstructing α SMA⁺ cell overexpansion.

4.2 *Tnmd* role during the reparative proliferative stage of healing

We consider the second time point chosen for analysis (21 days post-injury) to represent the reparative proliferative phase of healing. At this stage, we observed overall increased cellularity in the injury site in both genotypes and moreover, we detected chondrocyte-like cells surrounded by COLII ECM within the fibroblastic scars indicating cartilaginous formation, and such designated areas tended to be larger in the *Tnmd*-deficient group. *“The chondrocyte origin is still disputable and is well possible that several cell types are able to differentiate into this lineage, including Scx-expressing subpopulations such as Scx⁺CD105⁻, Scx⁺ α SMA⁺, Scx⁺S100a4⁺, Scx⁺Sox9⁺ and Cathepsin-K⁺ cells^{74,83,100,205–207}”*. Hence, it will be of great relevance in follow-up studies to evaluate specifically whether the existence and abundance of these discrete subpopulations it has been altered upon *Tnmd* loss.

As reviewed by Kraft *et al.*, 2016 and Meyers *et al.*, 2019 the innate and adaptive immune responses have been directly implicated as having a negative impact in healing by inducing ectopic bone formation^{121,195}. *“Macrophages are a very diverse cell entity with a crucial task in stimulating and resolving inflammation, therefore assisting and regulating the ongoing process of tissue repair⁸⁸. We have already shown that *Tnmd*^{-/-} scars at day 8 contain significantly higher number of F4/80⁺ macrophages and the inflammatory M1 subtype (CD68⁺/CD80⁺) contrary to the WT scars that were richer in the resolving M2 macrophages (CD163⁺)¹⁶⁰. This phenomenon was persistent also at day 21 post-injury, suggesting that *Tnmd* absence can result in a chronic inflammation in the injured tendons. A study by Sorkin *et al.*, 2020 mechanistically revealed in burn tenotomy that invading macrophages can initiate tendon HO by producing transforming growth factor beta-1 (TGF- β 1), thus stimulating mesenchymal progenitors to chondrogenically differentiate¹¹⁹. In a previous study focused on the early stage of tendon repair, we detected significantly increased Tgf- β 1 mRNA levels in tendon tissue extracts from *Tnmd*^{-/-} group¹⁶⁰. The molecular mechanisms involved in the crosstalk between distinct cell populations during trauma-induced tendon HO still remains to be fully unravelled. To this end, our data provides the first evidences that *Tnmd* is an important molecular factor involved in the cellular interplay behind the complex tendon HO process”*.

Our results regarding scar tissue composition and qRT-PCR can be interpreted as *Tnmd*^{-/-} and WT study groups having uneven healing baselines. First, the significant downregulation of the transcription factor *Mkx* in the *Tnmd*^{-/-} group provided a further important hint, namely, that HO

formation might occur. Suzuki et al. showed using CRISPR/Cas9 precise gene editing technique in a rat model that *Mkx*-targeting led to HO formation through failed tenogenesis²⁰⁸.

Second, the majority of ECM and collagen fibril regulator genes were significantly downregulated in the mutant tendons, suggesting delayed healing speed and impaired remodeling. *Tgm2* act as cross-linker and has been studied in the context of connective tissue formation, stabilisation and aging^{209,210}. Small leucine-rich repeat proteoglycans (SLRPs) *Bgn* and *Fmod* are a class of regulatory molecules involved in collagen fibrillogenesis²¹¹ and play an important role maintaining fibril structure, fiber alignment and therefore, improving tendon biomechanical functions^{212–214}. Moreover, it has been reported that biglycan/fibromodulin double-deficient mice exhibit impaired gait and develop spontaneous hindlimbs HO²¹⁵. Altogether, the detected downregulation of the above-mentioned genes in injured *Tnmd*-deficient tendons might result in detrimental and impaired tendon mechanical functionality.

4.3 Changes in Achilles tendon's ultrastructure, biomechanics and functionality upon injury and *Tnmd*-deficiency

Extracellular matrix changes in tendons, whether as result of traumatic lesions or genetic disorders, have a negative impact in tissue's integrity, biomechanical properties and lastly, in functionality^{51,216–218}. Moreover, the relation between collagen fibril morphology, size distribution and corresponding mechanical properties has been investigated using several models^{219–221}. “*We followed the repair process up to day 100 after injury, and we monitored mRNA expression levels via qRT-PCR, ECM fibrillar composition by TEM, HO spreading by μ CT and biomechanical properties by viscoelastic testing. Our TEM data revealed a very consistent ECM phenotypic feature specific to the loss of *Tnmd*^{33,35}, namely a significant increase of COL fibril diameters coupled with aberrant fibril morphology, which we observed in both, non-injured contralateral and injured (day 21 and 100) tendons. TEM imaging also demonstrated at the ultrastructural level mineral deposits and osteocyte-like cells in both genotypes at day 100 post-trauma, but μ CT imaging clarified a significantly higher total and enthelial HO in *Tnmd*^{-/-} tendons compared to WT*”. HO has been described to be a common feature in AT injury models with and without surgical reconstruction^{197,222–224}. Interestingly, our μ CT quantitative analysis detected only higher HO surface but no differences concerning HO volume. Brownley *et al.*, 2015 characterized the structural properties and differences between regular bone (tibia) and tenotomy-induced HO and

demonstrated that the latter had significantly lower density but higher porosity and therefore, the measurements resulted in only HO surface increment²²⁵. In our case, a plausible explanation might be related to the accuracy and resolution of the μ CT device that was used, since it was a material and not a medical device. Hence, important parameters such as tissue mineral density (TMD) and porosity could not be measured.

“Biomechanical analysis showed that even 100 days post-injury, the tendons in both groups suffered significant negative changes in their viscoelastic properties compared to non-injured tendons. We detected significant differences in injured tendons between both groups only in the dynamic E-modulus at 8% strain, which might be related to the sensitivity of the biomechanical testing system when HO-compromised tendons were measured. However, we discovered in non-injured controls as well as in the contralateral legs of injured animals that the absence of Tnmd results in a significant increase in static and dynamic E-moduli, representing a stronger resistance to elastic deformation and thus stiffening of the ATs. These novel findings correlate with the pathological thickening of COL fibrils^{33,35} and increase in their nano-stiffness³⁵ as well as dysregulated expression of COL cross-linking and small leucine-rich proteoglycan genes in Tnmd-deficient tendons¹⁶⁰. Cross-linker proteins, such as lysyl oxidase²²⁶ and proteoglycans modulate collagen I fibrillogenesis and have a significant impact in tendon tensile strength and viscoelastic properties^{171,227-229}. Biomechanical alteration in the tendon tissue, serving as a spring in the locomotive apparatus can result in deficient storage and transmission of the muscle-generated energy, hence reduced tendon functionality”.

De Bono *et al.*, 2006 and Goh and Ladiges, 2015 reported that mice endurance fitness depends on strain genetic background and age; while 4-months-old C57BL/6 mice run in average 15 km/day (during active dark cycle) 12-month old animals run approx. 12 km^{230,231}. We have already shown that Tnmd is required for optimal running performance, by performing force endurance tests; Tnmd^{-/-} mice ran significantly less, experienced fatigue and developed secondary myopathy³⁵.

“In this study, we subjected at day 100 post-injury, Tnmd^{-/-} animals to voluntary running tests and found that yet again this group undertakes significantly shorter distances compared to their WT littermates. We propose that this behaviour is the combined result of the significant stiffening of the contralateral ATs and significant HO of the injured ones”.

4.4 Transcriptomics shifts due to *Tnmd* absence

Current mechanistic understanding of tendon repair is limited, and little is known about transcriptome profile changes that occur throughout healing since only few studies have been conducted to address this issue. De Micheli *et al.*, 2020 developed recently a single-cell transcriptomic atlas that recognizes the vast heterogeneity in tendon's cellular composition⁸¹.

Apart from tissue-resident macrophages, endothelial cells, pericytes and sensory neurons, De Micheli *et al.*, 2020 identified three previously undescribed populations of tendon fibroblast, whose role in tendon homeostasis and/or injury is yet to be defined. The particularity of these three cell subsets was their categorization based on the moderate-to-high expression of *Colla1*, and the additional expression of *Col22a1*, or co-expression of *Scx* and/or *Sox9*⁸¹. Moreover, Harvey *et al.*, 2019 reported using scRNA-Seq. that a tubulin polymerization-promoting protein family member 3- and platelet-derived growth factor receptor alpha (*Tppp3⁺Pdgfra⁺*)-expressing tendon stem cell population isolated from the paratenon has the potential to contribute to regeneration⁷³. Yin *et al.*, 2016 showed that a *nestin⁺* stem/progenitor cell population has strong tenogenic potential and participates in endogenous tendon injury repair⁷⁵.

Our scRNA-Seq. data obtained from cells isolated from non-injured ATs clearly identifies an altered expression pattern between *Tnmd^{-/-}* and WT cells. By taking advantage of the *ScxGFP* reporter mouse we ensured that the *GFP⁺* cells isolated and analyzed for scRNA-seq. belong to the tenogenic lineage. “*This pilot analysis revealed clear genotype differences and suggested that loss of Tnmd results in dysregulated gene expression associated with cell adhesion, proliferation, senescence and collagen synthesis, the latter based on the significant downregulation of Rcn3 and Serpinh1^{232,233}*”. Park *et al.* 2021 postulated recently that *Rcn3* is involved in postnatal tendon development and is a pivotal collagen fibrillogenesis regulator, since the *Rcn3*-deficient mice exhibited decreased tendon thickness, abnormal tendon cell maturation, decreased mechanical properties and smaller collagen fibril distribution²²⁵.

“*GO analysis offered very intriguing enrichment of gene clusters in biological process, molecular function and cellular component. Among the enriched clusters, frequently referenced genes belong to the bone morphogenic protein (BMP) and BMP receptor family, which are worthwhile for follow-up detailed investigations. Moreover, KEGG signalling pathway analysis identified significant terms including the Hippo-signalling pathway, connected to the transcriptional co-activator complex YAP/TAZ that plays key roles in organ size control, tissue homeostasis and*

Discussion

regeneration. Remarkably, elevated BMP and Hippo-dependent pathway have been strongly allied with HO of mesenchymal progenitors ²³⁴. Another significant KEGG term was the Wnt-pathway, which is in line with *in vitro* studies reporting that Wnt/ β -catenin signalling can mediate Scx-independent expression of *Tnmd* in tendon- and bone marrow-derived mesenchymal stem cells ^{235,236}. KEGG analysis also referenced metabolic and insulin pathways, which is in agreement with several genetic, clinical and experimental studies that have linked *Tnmd* to metabolic syndrome, diabetes and obesity (reviewed by Dex et al., 2016 ⁸⁰). Altogether, the scRNA-seq approach can support the identification of putative *Tnmd*-dependent cascades and elucidation of *Tnmd* mode-of-action. By employing scRNA-seq on tendon lineage cells isolated from distinct stages of the repair process, this approach can also contribute to a better understanding on the longitudinally dysregulated molecular events behind the inferior tendon healing in *Tnmd*-deficient animals”.

Altogether, the results presented in this thesis indicate that *Tnmd* is responsible for a variety of functions during tendon healing. Yet, follow-up studies should involve *Tnmd*-overexpression mouse model to demonstrate if higher levels of *Tnmd* lead to improved repair or even prevent completely the development of undesired ossification of injured tendons; thus, delivering further prove that it is a suitable gene candidate for the development of a therapeutic drug.

5. CONCLUSIONS

In this study, the main goal was to compare and identify the differences in the healing process between *Tnmd*^{-/-} and WT mice after a surgically-induced AT rupture. Taken together (graphical synopsis, Fig. 44) our study demonstrates for the first time that:

1. Loss of *Tnmd* leads to long-term inferior tendon healing outcome, initially observed during the early inflammatory stage, and characterized by an imbalance between tendon-lineage ScxGFP⁺ and myofibroblastic α SMA⁺ cells, hence resulting in the formation of a fibrotic scar tissue.
2. The persistent inflammatory macrophage profile in injured *Tnmd*^{-/-} ATs, characterized by increased number of M1 polarized and the reduction of M2 polarized macrophages, and the emergence of robust cartilaginous template results in inferior healing process.
3. Lack of *Tnmd* results in the significant downregulation of tendon-related transcription factors, ECM genes and collagen fibril regulators during the reparative proliferative stage of healing. Moreover, the absence of *Tnmd* leads to the dysregulation of the same investigated genes during the late remodeling healing.
4. Ultrastructural analysis of non-injured, as well as injured *Tnmd*^{-/-} ATs confirmed that mutant tendons are pathologically thicker and the collagen fibrils atypically shaped, thus, suggesting that *Tnmd* is a collagen fibril regulator.
5. *Tnmd*-deficiency does not affect bone quality but leads to the formation of significant intertendinous heterotopic ossification after injury.
6. Loss of *Tnmd* compromises tendon viscoelastic properties and reduces running capacity at the remodelling stage, providing important evidence about *Tnmd*'s protective and attenuating role against trauma-induced HO formation.

Conclusions

7. The absence of *Tnmd* in tendon lineage cells creates a significant transcriptional shift, mostly characterized by the downregulation of genes involved in cell adhesion, proliferation, apoptosis and collagen synthesis.

“Based on the above-mentioned, we consider that *Tnmd* is a suitable gene candidate for the generation of novel dual function therapeutic drugs – accelerating repair and protecting against undesired ossification of injured tendons”.

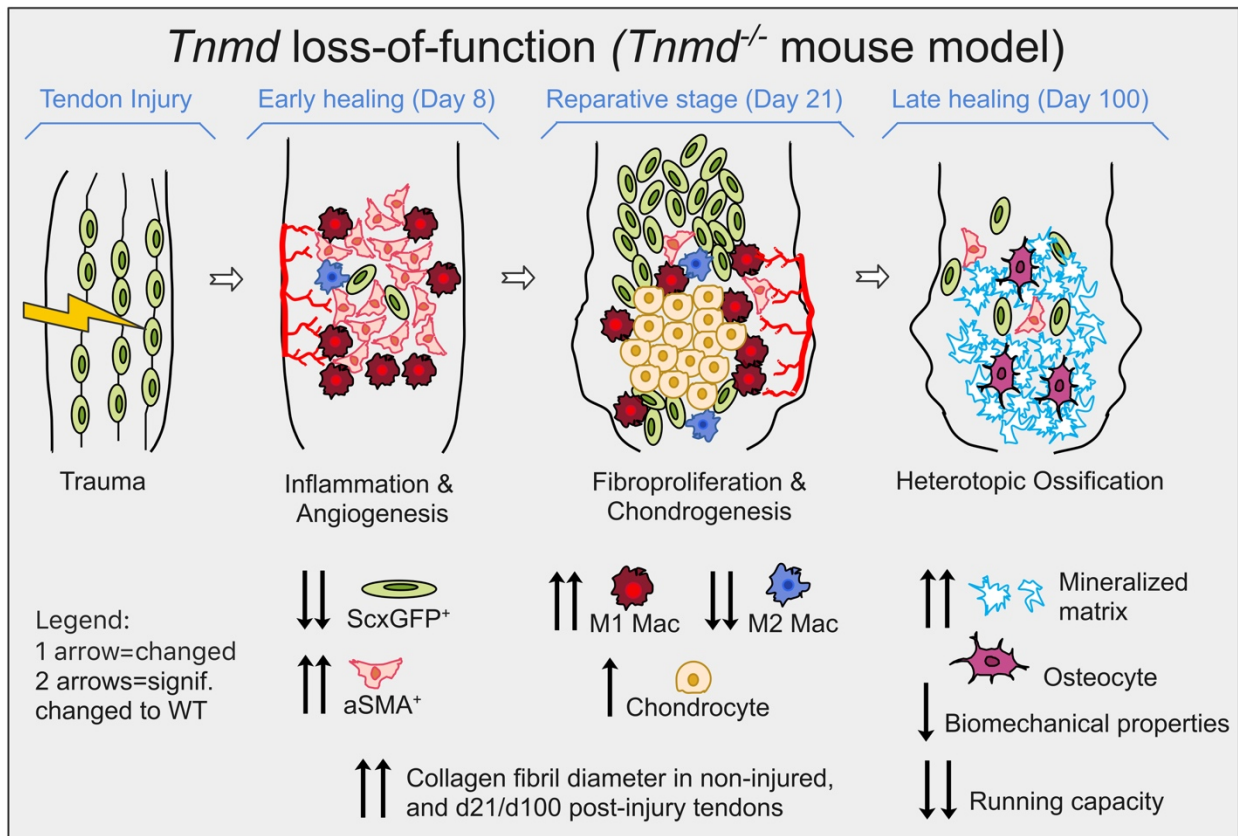


Fig. 44. Graphical synopsis of phenotypic changes in *Tnmd*^{-/-} mice over the time course upon injury⁸⁹

6. OUTLOOK

The results obtained in this extensive study have arisen further questions, which should be addressed in follow-up studies:

For an instance, atomic force microscopy (AFM) and second harmonic generation microscopy (SHG) techniques should be implemented using day 21 and day 100 injured samples from *Tnmd*^{-/-} and WT ATs to analyze more in depth the collagen fibril nanostructure, alignment, and reorganization after injury; thus, delivering further important cues regarding *Tnmd*'s role in collagen fibrillogenesis.

After the description for the first time of the transcriptomic “status quo” in tendon-specific cells isolated from non-injured *Tnmd*^{-/-} and WT ATs, the identification of genes that are differentially expressed throughout the healing process (inflammation, proliferation, and remodeling) should be targeted using scRNA-Seq. To this end, single cells from injured tendons at day 8, day 21 and day 100 post-injury have been already isolated, the RNA processed and stored. In a follow-up investigation these samples will be analyzed.

Moreover, concrete gene targets should be validated. We plan protein-protein interaction assays such as co-immunoprecipitation and pull-down assays to be carried out. This research might lead to the identification of *Tnmd* binding partners and hence, deliver insights in its molecular mechanism of action.

Finally, it would be of great importance for future projects to address the investigation of *Tnmd* expression pattern in diseased human tendons, with special emphasis in ossified tendons.

7. BIBLIOGRAPHY

1. O'Brien, M. Functional anatomy and physiology of tendons. *Clinics in sports medicine* 11, 505–520 (1992).
2. O'Brien, M. The anatomy of the Achilles tendon. *Foot and ankle clinics* 10, 225–238; 10.1016/j.fcl.2005.01.011 (2005).
3. Bryan Dixon, J. Gastrocnemius vs. soleus strain: how to differentiate and deal with calf muscle injuries. *Current reviews in musculoskeletal medicine* 2, 74–77; 10.1007/s12178-009-9045-8 (2009).
4. Valdivia, M., Vega-Macaya, F. & Olguín, P. Mechanical Control of Myotendinous Junction Formation and Tendon Differentiation during Development. *Frontiers in cell and developmental biology* 5; 10.3389/fcell.2017.00026 (2017).
5. Schweitzer, R., Zelzer, E. & Volk, T. Connecting muscles to tendons: tendons and musculoskeletal development in flies and vertebrates. *Development (Cambridge, England)* 137, 2807–2817; 10.1242/dev.047498 (2010).
6. Subramanian, A. & Schilling, T. F. Tendon development and musculoskeletal assembly: emerging roles for the extracellular matrix. *Development (Cambridge, England)* 142, 4191–4204; 10.1242/dev.114777 (2015).
7. Wu, F., Nerlich, M. & Docheva, D. Tendon injuries: Basic science and new repair proposals. *EFORT open reviews* 2, 332–342; 10.1302/2058-5241.2.160075 (2017).
8. Schwartz, A. G., Lipner, J. H., Pasteris, J. D., Genin, G. M. & Thomopoulos, S. Muscle loading is necessary for the formation of a functional tendon enthesis. *Bone* 55, 44–51; 10.1016/j.bone.2013.03.010 (2013).
9. Benjamin, M., Kaiser, E. & Milz, S. Structure-function relationships in tendons: a review. *Journal of anatomy* 212, 211–228; 10.1111/j.1469-7580.2008.00864.x (2008).
10. Komi, P. V., Fukashiro, S. & Järvinen, M. Biomechanical loading of Achilles tendon during normal locomotion. *Clinics in sports medicine* 11, 521–531 (1992).
11. Mazzone, M. F. & McCue, T. Common conditions of the achilles tendon. *American family physician* 65, 1805–1810 (2002).
12. Pennisi, E. Tending tender tendons. *Science (New York, N.Y.)* 295, 1011; 10.1126/science.295.5557.1011 (2002).
13. Maffulli, N. Rupture of the Achilles tendon. *The Journal of bone and joint surgery. American volume* 81, 1019–1036; 10.2106/00004623-199907000-00017 (1999).
14. Sheth, U. *et al.* The epidemiology and trends in management of acute Achilles tendon ruptures in Ontario, Canada: a population-based study of 27 607 patients. *The bone & joint journal* 99-B, 78–86; 10.1302/0301-620X.99B1.BJJ-2016-0434.R1 (2017).

15. Huttunen, T. T., Kannus, P., Rolf, C., Felländer-Tsai, L. & Mattila, V. M. Acute achilles tendon ruptures: incidence of injury and surgery in Sweden between 2001 and 2012. *The American journal of sports medicine* 42, 2419–2423; 10.1177/0363546514540599 (2014).
16. Suchak, A. A., Bostick, G., Reid, D., Blitz, S. & Jomha, N. The incidence of Achilles tendon ruptures in Edmonton, Canada. *Foot & ankle international* 26, 932–936; 10.1177/107110070502601106 (2005).
17. Leppilahti, J., Puranen, J. & Orava, S. Incidence of Achilles tendon rupture. *Acta orthopaedica Scandinavica* 67, 277–279; 10.3109/17453679608994688 (1996).
18. Lemme, N. J., Li, N. Y., DeFroda, S. F., Kleiner, J. & Owens, B. D. Epidemiology of Achilles Tendon Ruptures in the United States: Athletic and Nonathletic Injuries From 2012 to 2016. *Orthopaedic journal of sports medicine* 6, 2325967118808238; 10.1177/2325967118808238 (2018).
19. Chan, J. J. *et al.* Epidemiology of Achilles tendon injuries in collegiate level athletes in the United States. *International orthopaedics* 44, 585–594; 10.1007/s00264-019-04471-2 (2020).
20. Markus Müller (ed.). *Chirurgie für Studium und Praxis*. 11th ed. (Medizinische Vlg.- u. Inform.-Dienste, Breisach, 2014/15).
21. Hertel, G., Götz, J., Grifka, J. & Willers, J. Achillessehnenruptur: Aktuelle Standards in Diagnostik und Therapie. *Der Orthopäde* 45, 709–720; 10.1007/s00132-016-3287-0 (2016).
22. Delgado Caceres, M., Pfeifer, C. G. & Docheva, D. Understanding Tendons: Lessons from Transgenic Mouse Models. *Stem cells and development* 27, 1161–1174; 10.1089/scd.2018.0121 (2018).
23. Brent, A. E., Braun, T. & Tabin, C. J. Genetic analysis of interactions between the somitic muscle, cartilage and tendon cell lineages during mouse development. *Development (Cambridge, England)* 132, 515–528; 10.1242/dev.01605 (2005).
24. Cserjesi, P. *et al.* Scleraxis: a basic helix-loop-helix protein that prefigures skeletal formation during mouse embryogenesis. *Development (Cambridge, England)* 121, 1099–1110 (1995).
25. Schweitzer, R. *et al.* Analysis of the tendon cell fate using Scleraxis, a specific marker for tendons and ligaments. *Development (Cambridge, England)* 128, 3855–3866 (2001).
26. Brent, A. E., Schweitzer, R. & Tabin, C. J. A somitic compartment of tendon progenitors. *Cell* 113, 235–248; 10.1016/s0092-8674(03)00268-x (2003).
27. Brent, A. E. & Tabin, C. J. Developmental regulation of somite derivatives: muscle, cartilage and tendon. *Current opinion in genetics & development* 12, 548–557; 10.1016/s0959-437x(02)00339-8 (2002).
28. Dubrulle, J. & Pourquie, O. Welcome to syndetome: a new somitic compartment. *Developmental cell* 4, 611–612; 10.1016/s1534-5807(03)00133-3 (2003).
29. Tozer, S. & Duprez, D. Tendon and ligament: development, repair and disease. *Birth defects research. Part C, Embryo today: reviews* 75, 226–236; 10.1002/bdrc.20049 (2005).

30. Murchison, N. D. *et al.* Regulation of tendon differentiation by scleraxis distinguishes force-transmitting tendons from muscle-anchoring tendons. *Development (Cambridge, England)* 134, 2697–2708; 10.1242/dev.001933 (2007).
31. Brent, A. E. & Tabin, C. J. FGF acts directly on the somitic tendon progenitors through the Ets transcription factors Pea3 and Erm to regulate scleraxis expression. *Development (Cambridge, England)* 131, 3885–3896; 10.1242/dev.01275 (2004).
32. Liu, H. *et al.* Crucial transcription factors in tendon development and differentiation: their potential for tendon regeneration. *Cell and tissue research* 356, 287–298; 10.1007/s00441-014-1834-8 (2014).
33. Docheva, D., Hunziker, E. B., Fässler, R. & Brandau, O. Tenomodulin is necessary for tenocyte proliferation and tendon maturation. *Molecular and cellular biology* 25, 699–705; 10.1128/MCB.25.2.699-705.2005 (2005).
34. Alberton, P. *et al.* Loss of tenomodulin results in reduced self-renewal and augmented senescence of tendon stem/progenitor cells. *Stem cells and development* 24, 597–609; 10.1089/scd.2014.0314 (2015).
35. Dex, S. *et al.* Tenomodulin is required for Tendon Endurance Running and Collagen I Fibril Adaptation to Mechanical Load. *EBioMedicine* 20, 240–254; 10.1016/j.ebiom.2017.05.003 (2017).
36. Chevallier, A., Kieny, M. & Mauger, A. Limb-somite relationship: origin of the limb musculature. *Journal of embryology and experimental morphology* 41, 245–258 (1977).
37. Edom-Vovard, F. & Duprez, D. Signals regulating tendon formation during chick embryonic development. *Developmental dynamics: an official publication of the American Association of Anatomists* 229, 449–457; 10.1002/dvdy.10481 (2004).
38. Kuo, C. K., Petersen, B. C. & Tuan, R. S. Spatiotemporal protein distribution of TGF-betas, their receptors, and extracellular matrix molecules during embryonic tendon development. *Developmental dynamics: an official publication of the American Association of Anatomists* 237, 1477–1489; 10.1002/dvdy.21547 (2008).
39. Pryce, B. A., Brent, A. E., Murchison, N. D., Tabin, C. J. & Schweitzer, R. Generation of transgenic tendon reporters, ScxGFP and ScxAP, using regulatory elements of the scleraxis gene. *Developmental dynamics: an official publication of the American Association of Anatomists* 236, 1677–1682; 10.1002/dvdy.21179 (2007).
40. Hasson, P. "Soft" tissue patterning: muscles and tendons of the limb take their form. *Developmental dynamics: an official publication of the American Association of Anatomists* 240, 1100–1107; 10.1002/dvdy.22608 (2011).
41. Havis, E. *et al.* Transcriptomic analysis of mouse limb tendon cells during development. *Development (Cambridge, England)* 141, 3683–3696; 10.1242/dev.108654 (2014).
42. Dünker, N. & Kriegelstein, K. Tgfbeta2 *-/-* Tgfbeta3 *-/-* double knockout mice display severe midline fusion defects and early embryonic lethality. *Anatomy and embryology* 206, 73–83; 10.1007/s00429-002-0273-6 (2002).
43. Maeda, T. *et al.* Conversion of mechanical force into TGF- β -mediated biochemical signals. *Current biology: CB* 21, 933–941; 10.1016/j.cub.2011.04.007 (2011).

44. Xu, P. X., Cheng, J., Epstein, J. A. & Maas, R. L. Mouse Eya genes are expressed during limb tendon development and encode a transcriptional activation function. *Proceedings of the National Academy of Sciences of the United States of America* 94, 11974–11979; 10.1073/pnas.94.22.11974 (1997).
45. Bonnin, M.-A. *et al.* Six1 is not involved in limb tendon development, but is expressed in limb connective tissue under Shh regulation. *Mechanisms of development* 122, 573–585; 10.1016/j.mod.2004.11.005 (2005).
46. Liu, H. *et al.* Whole transcriptome expression profiling of mouse limb tendon development by using RNA-seq. *Journal of orthopaedic research: official publication of the Orthopaedic Research Society* 33, 840–848; 10.1002/jor.22886 (2015).
47. Nourissat, G., Berenbaum, F. & Duprez, D. Tendon injury: from biology to tendon repair. *Nature reviews. Rheumatology* 11, 223–233; 10.1038/nrrheum.2015.26 (2015).
48. Wu, M. *et al.* Essential roles for early growth response transcription factor Egr-1 in tissue fibrosis and wound healing. *The American journal of pathology* 175, 1041–1055; 10.2353/ajpath.2009.090241 (2009).
49. Guerquin, M.-J. *et al.* Transcription factor EGR1 directs tendon differentiation and promotes tendon repair. *The Journal of clinical investigation* 123, 3564–3576; 10.1172/JCI67521 (2013).
50. Lejard, V. *et al.* EGR1 and EGR2 involvement in vertebrate tendon differentiation. *The Journal of biological chemistry* 286, 5855–5867; 10.1074/jbc.M110.153106 (2011).
51. Screen, H. R. C., Berk, D. E., Kadler, K. E., Ramirez, F. & Young, M. F. Tendon functional extracellular matrix. *Journal of orthopaedic research: official publication of the Orthopaedic Research Society* 33, 793–799; 10.1002/jor.22818 (2015).
52. KER, R. Mechanics of tendon, from an engineering perspective. *International Journal of Fatigue* 29, 1001–1009; 10.1016/j.ijfatigue.2006.09.020 (2007).
53. Shepherd, J. H. *et al.* Functionally distinct tendon fascicles exhibit different creep and stress relaxation behaviour. *Proceedings of the Institution of Mechanical Engineers. Part H, Journal of engineering in medicine* 228, 49–59; 10.1177/0954411913509977 (2014).
54. Godinho, M. S. C., Thorpe, C. T., Greenwald, S. E. & Screen, H. R. C. Elastin is localised to the Interfascicular Matrix of Energy Storing Tendons and Becomes Increasingly Disorganised with Ageing. *Scientific reports* 7, 9713; 10.1038/s41598-017-09995-4 (2017).
55. Kjaer, M. Role of extracellular matrix in adaptation of tendon and skeletal muscle to mechanical loading. *Physiological reviews* 84, 649–698; 10.1152/physrev.00031.2003 (2004).
56. Thorpe, C. T., Birch, H. L., Clegg, P. D. & Screen, H. R. C. The role of the non-collagenous matrix in tendon function. *International journal of experimental pathology* 94, 248–259; 10.1111/iep.12027 (2013).
57. Banos, C. C., Thomas, A. H. & Kuo, C. K. Collagen fibrillogenesis in tendon development: current models and regulation of fibril assembly. *Birth defects research. Part C, Embryo today: reviews* 84, 228–244; 10.1002/bdrc.20130 (2008).
58. Kannus, P. Structure of the tendon connective tissue. *Scandinavian journal of medicine & science in sports* 10, 312–320; 10.1034/j.1600-0838.2000.010006312.x (2000).

59. Starborg, T., Lu, Y., Kadler, K. E. & Holmes, D. F. Electron microscopy of collagen fibril structure in vitro and in vivo including three-dimensional reconstruction. *Methods in cell biology* 88, 319–345; 10.1016/S0091-679X(08)00417-2 (2008).
60. Kjaer, M. *et al.* From mechanical loading to collagen synthesis, structural changes and function in human tendon. *Scandinavian journal of medicine & science in sports* 19, 500–510; 10.1111/j.1600-0838.2009.00986.x (2009).
61. Lui, P. P. Y. Stem cell technology for tendon regeneration: current status, challenges, and future research directions. *Stem cells and cloning: advances and applications* 8, 163–174; 10.2147/SCCAA.S60832 (2015).
62. Voleti, P. B., Buckley, M. R. & Soslowsky, L. J. Tendon healing: repair and regeneration. *Annual review of biomedical engineering* 14, 47–71; 10.1146/annurev-bioeng-071811-150122 (2012).
63. Docheva, D., Müller, S. A., Majewski, M. & Evans, C. H. Biologics for tendon repair. *Advanced drug delivery reviews* 84, 222–239; 10.1016/j.addr.2014.11.015 (2015).
64. Thorpe, C. T., Udeze, C. P., Birch, H. L., Clegg, P. D. & Screen, H. R. C. Specialization of tendon mechanical properties results from interfascicular differences. *Journal of the Royal Society, Interface* 9, 3108–3117; 10.1098/rsif.2012.0362 (2012).
65. Bi, Y. *et al.* Identification of tendon stem/progenitor cells and the role of the extracellular matrix in their niche. *Nature medicine* 13, 1219–1227; 10.1038/nm1630 (2007).
66. Walia, B. & Huang, A. H. Tendon stem progenitor cells: Understanding the biology to inform therapeutic strategies for tendon repair. *Journal of orthopaedic research: official publication of the Orthopaedic Research Society* 37, 1270–1280; 10.1002/jor.24156 (2019).
67. Huang, Z. *et al.* Tendon Stem/Progenitor Cell Subpopulations and Their Implications in Tendon Biology. *Frontiers in cell and developmental biology* 9, 631272; 10.3389/fcell.2021.631272 (2021).
68. Gumucio, J. P., Schonk, M. M., Kharaz, Y. A., Comerford, E. & Mendias, C. L. Scleraxis is required for the growth of adult tendons in response to mechanical loading. *JCI insight* 5; 10.1172/jci.insight.138295. (2020).
69. Xu, W. *et al.* Perivascular-derived stem cells with neural crest characteristics are involved in tendon repair. *Stem cells and development* 24, 857–868; 10.1089/scd.2014.0036 (2015).
70. Dymant, N. A. *et al.* Lineage tracing of resident tendon progenitor cells during growth and natural healing. *PloS one* 9, e96113; 10.1371/journal.pone.0096113 (2014).
71. Wang, Y. *et al.* Osteocalcin expressing cells from tendon sheaths in mice contribute to tendon repair by activating Hedgehog signaling. *eLife* 6; 10.7554/eLife.30474 (2017).
72. Staverosky, J. A., Pryce, B. A., Watson, S. S. & Schweitzer, R. Tubulin polymerization-promoting protein family member 3, Tppp3, is a specific marker of the differentiating tendon sheath and synovial joints. *Developmental dynamics: an official publication of the American Association of Anatomists* 238, 685–692; 10.1002/dvdy.21865 (2009).
73. Harvey, T., Flamenco, S. & Fan, C.-M. A Tppp3+Pdgfra+ tendon stem cell population contributes to regeneration and reveals a shared role for PDGF signalling in regeneration and fibrosis. *Nature cell biology* 21, 1490–1503; 10.1038/s41556-019-0417-z (2019).

74. Feng, H. *et al.* Tendon-derived cathepsin K-expressing progenitor cells activate Hedgehog signaling to drive heterotopic ossification. *The Journal of clinical investigation* 130, 6354–6365; 10.1172/JCI132518. (2020).
75. Yin, Z. *et al.* Single-cell analysis reveals a nestin⁺ tendon stem/progenitor cell population with strong tenogenic potentiality. *Science advances* 2, e1600874; 10.1126/sciadv.1600874 (2016).
76. Sakabe, T. *et al.* Transcription factor scleraxis vitally contributes to progenitor lineage direction in wound healing of adult tendon in mice. *The Journal of biological chemistry* 293, 5766–5780; 10.1074/jbc.RA118.001987 (2018).
77. Doral, M. N. *et al.* Functional anatomy of the Achilles tendon. *Knee surgery, sports traumatology, arthroscopy: official journal of the ESSKA* 18, 638–643; 10.1007/s00167-010-1083-7 (2010).
78. Liu, W. *et al.* The atypical homeodomain transcription factor Mohawk controls tendon morphogenesis. *Molecular and cellular biology* 30, 4797–4807; 10.1128/MCB.00207-10 (2010).
79. Frolova, E. G. *et al.* Control of organization and function of muscle and tendon by thrombospondin-4. *Matrix biology: journal of the International Society for Matrix Biology* 37, 35–48; 10.1016/j.matbio.2014.02.003 (2014).
80. Dex, S., Lin, D., Shukunami, C. & Docheva, D. Tenogenic modulating insider factor. Systematic assessment on the functions of tenomodulin gene. *Gene* 587, 1–17; 10.1016/j.gene.2016.04.051 (2016).
81. Micheli, A. J. de *et al.* Single-cell transcriptomic analysis identifies extensive heterogeneity in the cellular composition of mouse Achilles tendons. *American journal of physiology. Cell physiology* 319, C885–C894; 10.1152/ajpcell.00372.2020 (2020).
82. Benjamin, M., Qin, S. & Ralphs, J. R. Fibrocartilage associated with human tendons and their pulleys. *Journal of anatomy* 187 (Pt 3), 625–633 (1995).
83. Sugimoto, Y. *et al.* Scx⁺/Sox9⁺ progenitors contribute to the establishment of the junction between cartilage and tendon/ligament. *Development (Cambridge, England)* 140, 2280–2288; 10.1242/dev.096354 (2013).
84. Dymant, N. A. *et al.* Gdf5 progenitors give rise to fibrocartilage cells that mineralize via hedgehog signaling to form the zonal enthesis. *Developmental biology* 405, 96–107; 10.1016/j.ydbio.2015.06.020 (2015).
85. Ideo, K. *et al.* Role of Scx⁺/Sox9⁺ cells as potential progenitor cells for postnatal supraspinatus enthesis formation and healing after injury in mice. *PloS one* 15, e0242286; 10.1371/journal.pone.0242286 (2020).
86. Lehner, C. *et al.* Tenophages: a novel macrophage-like tendon cell population expressing CX3CL1 and CX3CR1. *Disease models & mechanisms* 12; 10.1242/dmm.041384 (2019).
87. Kendal, A. R. *et al.* Multi-omic single cell analysis resolves novel stromal cell populations in healthy and diseased human tendon. *Scientific reports* 10, 13939; 10.1038/s41598-020-70786-5 (2020).

88. Thomopoulos, S., Parks, W. C., Rifkin, D. B. & Derwin, K. A. Mechanisms of tendon injury and repair. *Journal of orthopaedic research: official publication of the Orthopaedic Research Society* 33, 832–839; 10.1002/jor.22806. (2015).
89. Delgado Caceres, M. *et al.* Tenomodulin knockout mice exhibit worse late healing outcomes with augmented trauma-induced heterotopic ossification of Achilles tendon. *Cell death & disease* 12, 1049; 10.1038/s41419-021-04298-z (2021).
90. Agarwal, S., Sorkin, M. & Levi, B. Heterotopic Ossification and Hypertrophic Scars. *Clinics in plastic surgery* 44, 749–755; 10.1016/j.cps.2017.05.006 (2017).
91. O'Brien, E. J. O., Frank, C. B., Shrive, N. G., Hallgrímsson, B. & Hart, D. A. Heterotopic mineralization (ossification or calcification) in tendinopathy or following surgical tendon trauma. *International journal of experimental pathology* 93, 319–331; 10.1111/j.1365-2613.2012.00829.x (2012).
92. Schneider, M., Angele, P., Järvinen, T. A. H. & Docheva, D. Rescue plan for Achilles: Therapeutics steering the fate and functions of stem cells in tendon wound healing. *Advanced drug delivery reviews* 129, 352–375; 10.1016/j.addr.2017.12.016 (2018).
93. Lin, T. W. T. W., Cardenas, L. & Soslowky, L. J. L. J. Biomechanics of tendon injury and repair. *Journal of biomechanics* 37, 865–877; 10.1016/j.jbiomech.2003.11.005 (2004).
94. Chen, C. H. *et al.* Tendon healing in vivo: gene expression and production of multiple growth factors in early tendon healing period. *The Journal of hand surgery* 33, 1834–1842; 10.1016/j.jhssa.2008.07.003 (2008).
95. Oryan, A. & Moshiri, A. Recombinant fibroblast growth protein enhances healing ability of experimentally induced tendon injury in vivo. *Journal of tissue engineering and regenerative medicine* 8, 421–431; 10.1002/term.1534 (2014).
96. Lee, C. H. *et al.* Harnessing endogenous stem/progenitor cells for tendon regeneration. *The Journal of clinical investigation* 125, 2690–2701; 10.1172/JCI81589 (2015).
97. Tempfer, H. & Traweger, A. Tendon Vasculature in Health and Disease. *Frontiers in physiology* 6, 330; 10.3389/fphys.2015.00330 (2015).
98. Kaux, J.-F. *et al.* Vascular Endothelial Growth Factor-111 (VEGF-111) and tendon healing: preliminary results in a rat model of tendon injury. *Muscles, Ligaments and Tendons Journal* 4, 24–28 (2014).
99. Najafbeygi, A. *et al.* Effect of Basic Fibroblast Growth Factor on Achilles Tendon Healing in Rabbit. *World Journal of Plastic Surgery* 6, 26–32 (2017).
100. Ackerman, J. E., Best, K. T., O'Keefe, R. J. & Loiselle, A. E. Deletion of EP4 in S100a4-lineage cells reduces scar tissue formation during early but not later stages of tendon healing. *Scientific reports* 7, 8658; 10.1038/s41598-017-09407-7 (2017).
101. Chazaud, B. Macrophages: supportive cells for tissue repair and regeneration. *Immunobiology* 219, 172–178; 10.1016/j.imbio.2013.09.001 (2014).
102. Xu, Z.-J. *et al.* The M2 macrophage marker CD206: a novel prognostic indicator for acute myeloid leukemia. *Oncoimmunology* 9; 10.1080/2162402X.2019.1683347 (2019).

103. Sugg, K. B., Lubardic, J., Gumucio, J. P. & Mendias, C. L. Changes in macrophage phenotype and induction of epithelial-to-mesenchymal transition genes following acute Achilles tenotomy and repair. *Journal of orthopaedic research: official publication of the Orthopaedic Research Society* 32, 944–951; 10.1002/jor.22624 (2014).
104. Lichtnekert, J., Kawakami, T., Parks, W. C. & Duffield, J. S. Changes in macrophage phenotype as the immune response evolves. *Current opinion in pharmacology* 13, 555–564; 10.1016/j.coph.2013.05.013 (2013).
105. Chhabra, A. *et al.* GDF-5 deficiency in mice delays Achilles tendon healing. *Journal of orthopaedic research: official publication of the Orthopaedic Research Society* 21, 826–835; 10.1016/S0736-0266(03)00049-4 (2003).
106. Eriksen, H. A., Pajala, A., Leppilahti, J. & Risteli, J. Increased content of type III collagen at the rupture site of human Achilles tendon. *Journal of orthopaedic research: official publication of the Orthopaedic Research Society* 20, 1352–1357; 10.1016/S0736-0266(02)00064-5 (2002).
107. Hansen, M. *et al.* Local administration of insulin-like growth factor-I (IGF-I) stimulates tendon collagen synthesis in humans. *Scandinavian journal of medicine & science in sports* 23, 614–619; 10.1111/j.1600-0838.2011.01431.x (2013).
108. Freedman, B. R., Sarver, J. J., Buckley, M. R., Voleti, P. B. & Soslowky, L. J. Biomechanical and structural response of healing Achilles tendon to fatigue loading following acute injury. *Journal of biomechanics* 47, 2028–2034; 10.1016/j.jbiomech.2013.10.054 (2014).
109. Eming, S. A., Martin, P. & Tomic-Canic, M. Wound repair and regeneration: mechanisms, signaling, and translation. *Science translational medicine* 6, 265sr6; 10.1126/scitranslmed.3009337 (2014).
110. Ackermann, P. W. *et al.* Neuronal pathways in tendon healing and tendinopathy--update. *Frontiers in bioscience (Landmark edition)* 19, 1251–1278; 10.2741/4280 (2014).
111. Snedeker, J. G. & Foolen, J. Tendon injury and repair - A perspective on the basic mechanisms of tendon disease and future clinical therapy. *Acta biomaterialia* 63, 18–36; 10.1016/j.actbio.2017.08.032 (2017).
112. Stauber, T. *et al.* Extrinsic Macrophages Protect While Tendon Progenitors Degrade: Insights from a Tissue Engineered Model of Tendon Compartmental Crosstalk. *Advanced healthcare materials* 10, e2100741; 10.1002/adhm.202100741 (2021).
113. Ackermann, P. W., Salo, P. & Hart, D. A. Tendon Innervation. *Advances in experimental medicine and biology* 920, 35–51; 10.1007/978-3-319-33943-6_4 (2016).
114. Wang, J. H.-C. Mechanobiology of tendon. *Journal of biomechanics* 39, 1563–1582; 10.1016/j.jbiomech.2005.05.011 (2006).
115. Chisari, E., Rehak, L., Khan, W. S. & Maffulli, N. The role of the immune system in tendon healing: a systematic review. *British medical bulletin* 133, 49–64; 10.1093/bmb/ldz040 (2020).
116. Howell, K. *et al.* Novel Model of Tendon Regeneration Reveals Distinct Cell Mechanisms Underlying Regenerative and Fibrotic Tendon Healing. *Scientific reports* 7, 45238; 10.1038/srep45238 (2017).

117. Best, K. T. & Loisel, A. E. Scleraxis lineage cells contribute to organized bridging tissue during tendon healing and identify a subpopulation of resident tendon cells. *FASEB journal: official publication of the Federation of American Societies for Experimental Biology* 33, 8578–8587; 10.1096/fj.201900130RR (2019).
118. Dymant, N. A. *et al.* The paratenon contributes to scleraxis-expressing cells during patellar tendon healing. *PloS one* 8, e59944; 10.1371/journal.pone.0059944 (2013).
119. Sorkin, M. *et al.* Regulation of heterotopic ossification by monocytes in a mouse model of aberrant wound healing. *Nature communications* 11, 722; 10.1038/s41467-019-14172-4 (2020).
120. Xu, R., Hu, J., Zhou, X. & Yang, Y. Heterotopic ossification: Mechanistic insights and clinical challenges. *Bone* 109, 134–142; 10.1016/j.bone.2017.08.025 (2018).
121. Meyers, C. *et al.* Heterotopic Ossification: A Comprehensive Review. *JBMR plus* 3, e10172; 10.1002/jbm4.10172 (2019).
122. Shimono, K., Uchibe, K., Kuboki, T. & Iwamoto, M. The pathophysiology of heterotopic ossification: Current treatment considerations in dentistry. *The Japanese dental science review* 50, 1–8; 10.1016/j.jdsr.2013.07.003 (2014).
123. Zhang, Q., Zhou, D., Wang, H. & Tan, J. Heterotopic ossification of tendon and ligament. *Journal of cellular and molecular medicine* 24, 5428–5437; 10.1111/jcmm.15240 (2020).
124. Lees-Shepard, J. B. & Goldhamer, D. J. Stem cells and heterotopic ossification: Lessons from animal models. *Bone* 109, 178–186; 10.1016/j.bone.2018.01.029 (2018).
125. Shore, E. M. *et al.* A recurrent mutation in the BMP type I receptor ACVR1 causes inherited and sporadic fibrodysplasia ossificans progressiva. *Nature genetics* 38, 525–527; 10.1038/ng1783 (2006).
126. Ateshrang, A., Gratzner, C. & Weise, K. Incidence and effect of calcifications after open-augmented Achilles tendon repair. *Archives of orthopaedic and trauma surgery* 128, 1087–1092; 10.1007/s00402-007-0441-5 (2008).
127. Kraus, R. *et al.* Frequency and effects of intratendinous and peritendinous calcifications after open Achilles tendon repair. *Foot & ankle international* 25, 827–832; 10.1177/107110070402501113 (2004).
128. Pagani, C. A. *et al.* Novel Lineage-Tracing System to Identify Site-Specific Ectopic Bone Precursor Cells. *Stem cell reports* 16, 626–640; 10.1016/j.stemcr.2021.01.011 (2021).
129. Pineault, K. M., Song, J. Y., Kozloff, K. M., Lucas, D. & Wellik, D. M. Hox11 expressing regional skeletal stem cells are progenitors for osteoblasts, chondrocytes and adipocytes throughout life. *Nature communications* 10, 3168; 10.1038/s41467-019-11100-4 (2019).
130. Chalmers, J., Gray, D. H. & Rush, J. OBSERVATIONS ON THE INDUCTION OF BONE IN SOFT TISSUES. *The Journal of Bone and Joint Surgery. British volume* 57-B, 36–45; 10.1302/0301-620X.57B1.36 (1975).
131. Marusić, A., Katavić, V., Grcević, D. & Lukić, I. K. Genetic variability of new bone induction in mice. *Bone* 25, 25–32; 10.1016/s8756-3282(99)00095-2 (1999).

132. Freedman, B. R. *et al.* Dynamic Loading and Tendon Healing Affect Multiscale Tendon Properties and ECM Stress Transmission. *Scientific reports* 8, 10854; 10.1038/s41598-018-29060-y (2018).
133. Eisenstein, N., Stapley, S. & Grover, L. Post-Traumatic Heterotopic Ossification: An Old Problem in Need of New Solutions. *Journal of orthopaedic research: official publication of the Orthopaedic Research Society* 36, 1061–1068; 10.1002/jor.23808 (2018).
134. Convente, M. R., Wang, H., Pignolo, R. J., Kaplan, F. S. & Shore, E. M. The immunological contribution to heterotopic ossification disorders. *Current osteoporosis reports* 13, 116–124; 10.1007/s11914-015-0258-z (2015).
135. Yu, P. B. *et al.* BMP type I receptor inhibition reduces heterotopic corrected ossification. *Nature medicine* 14, 1363–1369; 10.1038/nm.1888 (2008).
136. Mohedas, A. H. *et al.* Development of an ALK2-biased BMP type I receptor kinase inhibitor. *ACS chemical biology* 8, 1291–1302; 10.1021/cb300655w (2013).
137. Regard, J. B. *et al.* Activation of Hedgehog signaling by loss of GNAS causes heterotopic ossification. *Nature medicine* 19, 1505–1512; 10.1038/nm.3314 (2013).
138. Agarwal, S. *et al.* Inhibition of Hif1 α prevents both trauma-induced and genetic heterotopic ossification. *Proceedings of the National Academy of Sciences of the United States of America* 113, E338-47; 10.1073/pnas.1515397113 (2016).
139. Chakkalakal, S. A. *et al.* Palovarotene Inhibits Heterotopic Ossification and Maintains Limb Mobility and Growth in Mice With the Human ACVR1(R206H) Fibrodysplasia Ossificans Progressiva (FOP) Mutation. *Journal of bone and mineral research: the official journal of the American Society for Bone and Mineral Research* 31, 1666–1675; 10.1002/jbmr.2820 (2016).
140. Pavey, G. J. *et al.* Targeted stimulation of retinoic acid receptor- γ mitigates the formation of heterotopic ossification in an established blast-related traumatic injury model. *Bone* 90, 159–167; 10.1016/j.bone.2016.06.014 (2016).
141. Bojsen-Møller, J. & Magnusson, S. P. Heterogeneous Loading of the Human Achilles tendon In Vivo. *Exercise and sport sciences reviews* 43, 190–197; 10.1249/JES.0000000000000062 (2015).
142. Gains, C. C. *et al.* Force Transmission between the Gastrocnemius and Soleus Sub-Tendons of the Achilles tendon in Rat. *Frontiers in bioengineering and biotechnology* 8, 700; 10.3389/fbioe.2020.00700 (2020).
143. Edama, M. *et al.* The twisted structure of the human Achilles tendon. *Scandinavian journal of medicine & science in sports* 25, e497-503; 10.1111/sms.12342 (2015).
144. Arndt, A., Bengtsson, A.-S., Peolsson, M., Thorstensson, A. & Movin, T. Non-uniform displacement within the Achilles tendon during passive ankle joint motion. *Knee surgery, sports traumatology, arthroscopy: official journal of the ESSKA* 20, 1868–1874; 10.1007/s00167-011-1801-9 (2012).
145. Lee, A. H. & Elliott, D. M. Comparative multi-scale hierarchical structure of the tail, plantaris, and Achilles tendons in the rat. *Journal of anatomy* 234, 252–262; 10.1111/joa.12913 (2019).

146. Pardes, A. M. *et al.* Aging leads to inferior Achilles tendon mechanics and altered ankle function in rodents. *Journal of biomechanics* 60, 30–38; 10.1016/j.jbiomech.2017.06.008 (2017).
147. Freedman, B. R. *et al.* Tendon healing affects the multiscale mechanical, structural and compositional response of tendon to quasi-static tensile loading. *Journal of the Royal Society, Interface* 15; 10.1098/rsif.2017.0880 (2018).
148. Freedman, B. R. *et al.* Mechanical, histological, and functional properties remain inferior in conservatively treated Achilles tendons in rodents: Long term evaluation. *Journal of biomechanics* 56, 55–60; 10.1016/j.jbiomech.2017.02.030 (2017).
149. Freedman, B. R. *et al.* The (dys)functional extracellular matrix. *Biochimica et biophysica acta* 1853, 3153–3164; 10.1016/j.bbamcr.2015.04.015 (2015).
150. Freedman, B. R., Zuskov, A., Sarver, J. J., Buckley, M. R. & Soslowsky, L. J. Evaluating changes in tendon crimp with fatigue loading as an ex vivo structural assessment of tendon damage. *Journal of orthopaedic research: official publication of the Orthopaedic Research Society* 33, 904–910; 10.1002/jor.22875 (2015).
151. Zuskov, A. *et al.* Tendon Biomechanics and Crimp Properties Following Fatigue Loading Are Influenced by Tendon Type and Age in Mice. *Journal of orthopaedic research: official publication of the Orthopaedic Research Society* 38, 36–42; 10.1002/jor.24407 (2020).
152. Woo, S. L. *et al.* Injury and repair of ligaments and tendons. *Annual review of biomedical engineering* 2, 83–118; 10.1146/annurev.bioeng.2.1.83 (2000).
153. Robi, K., Jakob, N., Matevz, K. & Matjaz, V. The Physiology of Sports Injuries and Repair Processes. In *Current Issues in Sports and Exercise Medicine*, edited by M. Hamlin (InTech2013).
154. Brandau, O., Meindl, A., Fässler, R. & Aszódi, A. A novel gene, tendin, is strongly expressed in tendons and ligaments and shows high homology with chondromodulin-I. *Developmental dynamics: an official publication of the American Association of Anatomists* 221, 72–80; 10.1002/dvdy.1126 (2001).
155. Shukunami, C., Oshima, Y. & Hiraki, Y. Molecular cloning of tenomodulin, a novel chondromodulin-I related gene. *Biochemical and biophysical research communications* 280, 1323–1327; 10.1006/bbrc.2001.4271 (2001).
156. Oshima, Y. *et al.* Anti-angiogenic action of the C-terminal domain of tenomodulin that shares homology with chondromodulin-I. *Journal of cell science* 117, 2731–2744; 10.1242/jcs.01112 (2004).
157. Shukunami, C., Yoshimoto, Y., Takimoto, A., Yamashita, H. & Hiraki, Y. Molecular characterization and function of tenomodulin, a marker of tendons and ligaments that integrate musculoskeletal components. *The Japanese dental science review* 52, 84–92; 10.1016/j.jdsr.2016.04.003 (2016).
158. Kimura, N. *et al.* Local tenomodulin absence, angiogenesis, and matrix metalloproteinase activation are associated with the rupture of the chordae tendineae cordis. *Circulation* 118, 1737–1747; 10.1161/CIRCULATIONAHA.108.780031. (2008).

159. Lin, D. *et al.* Loss of tenomodulin expression is a risk factor for age-related intervertebral disc degeneration. *Aging cell*, e13091; 10.1111/accel.13091 (2020).
160. Lin, D. *et al.* Tenomodulin is essential for prevention of adipocyte accumulation and fibrovascular scar formation during early tendon healing. *Cell death & disease* 8, e3116; 10.1038/cddis.2017.510 (2017).
161. Yin, H. *et al.* Tenomodulin regulates matrix remodeling of mouse tendon stem/progenitor cells in an ex vivo collagen I gel model. *Biochemical and biophysical research communications* 512, 691–697; 10.1016/j.bbrc.2019.03.063 (2019).
162. Komiyama, Y. *et al.* Tenomodulin expression in the periodontal ligament enhances cellular adhesion. *PLoS one* 8, e60203; 10.1371/journal.pone.0060203 (2013).
163. Oshima, Y. *et al.* Expression and localization of tenomodulin, a transmembrane type chondromodulin-I-related angiogenesis inhibitor, in mouse eyes. *Investigative ophthalmology & visual science* 44, 1814–1823; 10.1167/iovs.02-0664 (2003).
164. Palmes, D. *et al.* Achilles tendon healing: long-term biomechanical effects of postoperative mobilization and immobilization in a new mouse model. *Journal of orthopaedic research: official publication of the Orthopaedic Research Society* 20, 939–946; 10.1016/S0736-0266(02)00032-3 (2002).
165. Reiprich, S. *et al.* Adhesive Properties of the Hyaluronan Pericellular Coat in Hyaluronan Synthases Overexpressing Mesenchymal Stem Cells. *International journal of molecular sciences* 21; 10.3390/ijms21113827 (2020).
166. Somerville, J. M., Aspden, R. M., Armour, K. E., Armour, K. J. & Reid, D. M. Growth of C57BL/6 mice and the material and mechanical properties of cortical bone from the tibia. *Calcified tissue international* 74, 469–475; 10.1007/s00223-003-0101-x (2004).
167. Fischer, A. H., Jacobson, K. A., Rose, J. & Zeller, R. Hematoxylin and eosin staining of tissue and cell sections. *CSH protocols* 2008, pdb.prot4986; 10.1101/pdb.prot4986 (2008).
168. Lillie, R. D., Tracy, R. E., Pizzolato, P., Donaldson, P. T. & Reynolds, C. Differential staining of collagen types in paraffin sections: a color change in degraded forms. *Virchows Archiv. A, Pathological anatomy and histology* 386, 153–159; 10.1007/BF00427227 (1980).
169. Stoll, C. *et al.* Healing parameters in a rabbit partial tendon defect following tenocyte/biomaterial implantation. *Biomaterials* 32, 4806–4815; 10.1016/j.biomaterials.2011.03.026 (2011).
170. Best, T. M. *et al.* Achilles tendon healing: a correlation between functional and mechanical performance in the rat. *Journal of orthopaedic research: official publication of the Orthopaedic Research Society* 11, 897–906; 10.1002/jor.1100110617 (1993).
171. Dourte, L. M. *et al.* Influence of decorin on the mechanical, compositional, and structural properties of the mouse patellar tendon. *Journal of biomechanical engineering* 134, 31005; 10.1115/1.4006200 (2012).
172. Hochstrat, E. *et al.* Cryopreservation of tendon tissue using dimethyl sulfoxide combines conserved cell vitality with maintained biomechanical features. *PLoS one* 14, e0215595; 10.1371/journal.pone.0215595 (2019).

173. Picelli, S. *et al.* Full-length RNA-seq from single cells using Smart-seq2. *Nature protocols* 9, 171–181; 10.1038/nprot.2014.006 (2014).
174. JGI DataScience. BBtools software suite 2019. Available at <https://jgi.doe.gov/data-and-tools/bbtools>.
175. Chu, J. *et al.* BioBloom tools: fast, accurate and memory-efficient host species sequence screening using bloom filters. *Bioinformatics (Oxford, England)* 30, 3402–3404; 10.1093/bioinformatics/btu558 (2014).
176. Babraham Bioinformatics 2019. FastQC. Available at <https://www.bioinformatics.babraham.ac.uk/projects/fastqc>.
177. Ewels, P., Magnusson, M., Lundin, S. & Källér, M. MultiQC: summarize analysis results for multiple tools and samples in a single report. *Bioinformatics (Oxford, England)* 32, 3047–3048; 10.1093/bioinformatics/btw354 (2016).
178. Dobin, A. *et al.* STAR: ultrafast universal RNA-seq aligner. *Bioinformatics (Oxford, England)* 29, 15–21; 10.1093/bioinformatics/bts635 (2013).
179. Liao, Y., Smyth, G. K. & Shi, W. The Subread aligner: fast, accurate and scalable read mapping by seed-and-vote. *Nucleic acids research* 41, e108; 10.1093/nar/gkt214 (2013).
180. Deng, C., Daley, T. & Smith, A. D. Applications of species accumulation curves in large-scale biological data analysis. *Quantitative biology (Beijing, China)* 3, 135–144; 10.1007/s40484-015-0049-7 (2015).
181. Okonechnikov, K., Conesa, A. & García-Alcalde, F. Qualimap 2: advanced multi-sample quality control for high-throughput sequencing data. *Bioinformatics (Oxford, England)* 32, 292–294; 10.1093/bioinformatics/btv566 (2016).
182. McCarthy, D. J., Campbell, K. R., Lun, A. T. L. & Wills, Q. F. *scater: pre-processing, quality control, normalisation and visualisation of single-cell RNA-seq data in R* (2016).
183. Leek, J. T., Johnson, W. E., Parker, H. S., Jaffe, A. E. & Storey, J. D. The sva package for removing batch effects and other unwanted variation in high-throughput experiments. *Bioinformatics (Oxford, England)* 28, 882–883; 10.1093/bioinformatics/bts034 (2012).
184. Johnson, W. E., Li, C. & Rabinovic, A. Adjusting batch effects in microarray expression data using empirical Bayes methods. *Biostatistics (Oxford, England)* 8, 118–127; 10.1093/biostatistics/kxj037 (2007).
185. Robinson, M. D., McCarthy, D. J. & Smyth, G. K. edgeR: a Bioconductor package for differential expression analysis of digital gene expression data. *Bioinformatics (Oxford, England)* 26, 139–140; 10.1093/bioinformatics/btp616 (2010).
186. Love, M. I., Huber, W. & Anders, S. Moderated estimation of fold change and dispersion for RNA-seq data with DESeq2. *Genome biology* 15, 550; 10.1186/s13059-014-0550-8 (2014).
187. Ashburner, M. *et al.* Gene ontology: tool for the unification of biology. The Gene Ontology Consortium. *Nature genetics* 25, 25–29; 10.1038/75556 (2000).
188. Kanehisa, M., Goto, S., Furumichi, M., Tanabe, M. & Hirakawa, M. KEGG for representation and analysis of molecular networks involving diseases and drugs. *Nucleic acids research* 38, D355–60; 10.1093/nar/gkp896. (2010).

189. R Core Team 2021. R: A Language and Environment for Statistical Computing. R Foundation for Statistical Computing. Vienna, Austria. Available at www.r-project.org/.
190. Young, M. D., Wakefield, M. J., Smyth, G. K. & Oshlack, A. Gene ontology analysis for RNA-seq: accounting for selection bias. *Genome biology* 11, R14; 10.1186/gb-2010-11-2-r14 (2010).
191. Yu, G., Wang, L.-G., Han, Y. & He, Q.-Y. clusterProfiler: an R package for comparing biological themes among gene clusters. *Omics: a journal of integrative biology* 16, 284–287; 10.1089/omi.2011.0118 (2012).
192. Hadley Wickham. *ggplot2: Elegant Graphics for Data Analysis* (Springer-Verlag New York, 2016).
193. Dymont, N. A. & Galloway, J. L. Regenerative biology of tendon: mechanisms for renewal and repair. *Current molecular biology reports* 1, 124–131; 10.1007/s40610-015-0021-3 (2015).
194. Gross, G. & Hoffmann, A. Therapeutic strategies for tendon healing based on novel biomaterials, factors and cells. *Pathobiology: journal of immunopathology, molecular and cellular biology* 80, 203–210; 10.1159/000347059 (2013).
195. Kraft, C. T. *et al.* Trauma-induced heterotopic bone formation and the role of the immune system: A review. *The journal of trauma and acute care surgery* 80, 156–165; 10.1097/TA.0000000000000883. (2016).
196. Mead, T. J. *et al.* The metalloproteinase-proteoglycans ADAMTS7 and ADAMTS12 provide an innate, tendon-specific protective mechanism against heterotopic ossification. *JCI insight* 3; 10.1172/jci.insight.92941 (2018).
197. Zhang, K. *et al.* Tendon mineralization is progressive and associated with deterioration of tendon biomechanical properties, and requires BMP-Smad signaling in the mouse Achilles tendon injury model. *Matrix biology: journal of the International Society for Matrix Biology* 52-54, 315–324; 10.1016/j.matbio.2016.01.015 (2016).
198. Loisel, A. E. *et al.* Remodeling of murine intrasynovial tendon adhesions following injury: MMP and neotendon gene expression. *Journal of orthopaedic research: official publication of the Orthopaedic Research Society* 27, 833–840; 10.1002/jor.20769 (2009).
199. Cadby, J. A., Buehler, E., Godbout, C., van Weeren, P. R. & Snedeker, J. G. Differences between the cell populations from the peritenon and the tendon core with regard to their potential implication in tendon repair. *PloS one* 9, e92474; 10.1371/journal.pone.0092474 (2014).
200. Yoshida, R. *et al.* Murine supraspinatus tendon injury model to identify the cellular origins of rotator cuff healing. *Connective tissue research* 57, 507–515; 10.1080/03008207.2016.1189910 (2016).
201. Grcevic, D. *et al.* In vivo fate mapping identifies mesenchymal progenitor cells. *Stem cells (Dayton, Ohio)* 30, 187–196; 10.1002/stem.780 (2012).
202. Kalajzic, Z. *et al.* Use of an alpha-smooth muscle actin GFP reporter to identify an osteoprogenitor population. *Bone* 43, 501–510; 10.1016/j.bone.2008.04.023 (2008).

203. Moser, H. L. *et al.* Genetic lineage tracing of targeted cell populations during enthesis healing. *Journal of orthopaedic research: official publication of the Orthopaedic Research Society* 36, 3275–3284; 10.1002/jor.24122 (2018).
204. Gracey, E. *et al.* Tendon and ligament mechanical loading in the pathogenesis of inflammatory arthritis. *Nature reviews. Rheumatology* 16, 193–207; 10.1038/s41584-019-0364-x (2020).
205. Asai, S. *et al.* Tendon progenitor cells in injured tendons have strong chondrogenic potential: the CD105-negative subpopulation induces chondrogenic degeneration. *Stem cells (Dayton, Ohio)* 32, 3266–3277; 10.1002/stem.1847 (2014).
206. Agarwal, S. *et al.* Scleraxis-Lineage Cells Contribute to Ectopic Bone Formation in Muscle and Tendon. *Stem cells (Dayton, Ohio)* 35, 705–710; 10.1002/stem.2515 (2017).
207. Dey, D. *et al.* Two tissue-resident progenitor lineages drive distinct phenotypes of heterotopic ossification. *Science translational medicine* 8, 366ra163; 10.1126/scitranslmed.aaf1090 (2016).
208. Suzuki, H. *et al.* Gene targeting of the transcription factor Mohawk in rats causes heterotopic ossification of Achilles tendon via failed tenogenesis. *Proceedings of the National Academy of Sciences of the United States of America* 113, 7840–7845; 10.1073/pnas.1522054113 (2016).
209. Bains, W. Transglutaminase 2 and EGGL, the protein cross-link formed by transglutaminase 2, as therapeutic targets for disabilities of old age. *Rejuvenation research* 16, 495–517; 10.1089/rej.2013.1452 (2013).
210. Oliva, F. *et al.* Transglutaminases expression in human supraspinatus tendon ruptures and in mouse tendons. *Biochemical and biophysical research communications* 379, 887–891; 10.1016/j.bbrc.2008.12.188 (2009).
211. Chen, S. & Birk, D. E. The regulatory roles of small leucine-rich proteoglycans in extracellular matrix assembly. *The FEBS journal* 280, 2120–2137; 10.1111/febs.12136 (2013).
212. Pechanec, M. Y., Boyd, T. N., Baar, K. & Mienaltowski, M. J. Adding exogenous biglycan or decorin improves tendon formation for equine peritenon and tendon proper cells in vitro. *BMC musculoskeletal disorders* 21, 627; 10.1186/s12891-020-03650-2 (2020).
213. Delalande, A. *et al.* Enhanced Achilles tendon healing by fibromodulin gene transfer. *Nanomedicine: nanotechnology, biology, and medicine* 11, 1735–1744; 10.1016/j.nano.2015.05.004 (2015).
214. Robinson, K. A. *et al.* Decorin and biglycan are necessary for maintaining collagen fibril structure, fiber realignment, and mechanical properties of mature tendons. *Matrix biology: journal of the International Society for Matrix Biology* 64, 81–93; 10.1016/j.matbio.2017.08.004 (2017).
215. Ameye, L. *et al.* Abnormal collagen fibrils in tendons of biglycan/fibromodulin-deficient mice lead to gait impairment, ectopic ossification, and osteoarthritis. *FASEB journal: official publication of the Federation of American Societies for Experimental Biology* 16, 673–680; 10.1096/fj.01-0848com (2002).

216. Ezura, Y., Chakravarti, S., Oldberg, A., Chervoneva, I. & Birk, D. E. Differential expression of lumican and fibromodulin regulate collagen fibrillogenesis in developing mouse tendons. *The Journal of cell biology* 151, 779–788; 10.1083/jcb.151.4.779 (2000).
217. Pingel, J. *et al.* 3-D ultrastructure and collagen composition of healthy and overloaded human tendon: evidence of tenocyte and matrix buckling. *Journal of anatomy* 224, 548–555; 10.1111/joa.12164 (2014).
218. Sun, M. *et al.* Collagen XI regulates the acquisition of collagen fibril structure, organization and functional properties in tendon. *Matrix biology: journal of the International Society for Matrix Biology* 94, 77–94; 10.1016/j.matbio.2020.09.001 (2020).
219. Franchi, M., Trirè, A., Quaranta, M., Orsini, E. & Ottani, V. Collagen structure of tendon relates to function. *TheScientificWorldJournal* 7, 404–420; 10.1100/tsw.2007.92 (2007).
220. Mikic, B., Schalet, B. J., Clark, R. T., Gaschen, V. & Hunziker, E. B. GDF-5 deficiency in mice alters the ultrastructure, mechanical properties and composition of the Achilles tendon. *Journal of orthopaedic research: official publication of the Orthopaedic Research Society* 19, 365–371; 10.1016/S0736-0266(00)90018-4 (2001).
221. Rigozzi, S., Müller, R. & Snedeker, J. G. Collagen fibril morphology and mechanical properties of the Achilles tendon in two inbred mouse strains. *Journal of anatomy* 216, 724–731; 10.1111/j.1469-7580.2010.01225.x (2010).
222. Michel, P. A. *et al.* Microsurgical reconstruction affects the outcome in a translational mouse model for Achilles tendon healing. *Journal of orthopaedic translation* 24, 1–11; 10.1016/j.jot.2020.04.003 (2020).
223. O'Brien, E. J. O. *et al.* Tendon mineralization is accelerated bilaterally and creep of contralateral tendons is increased after unilateral needle injury of murine achilles tendons. *Journal of orthopaedic research: official publication of the Orthopaedic Research Society* 31, 1520–1528; 10.1002/jor.22404 (2013).
224. Tuzmen, C., Verdelis, K., Weiss, L. & Campbell, P. Crosstalk between substance P and calcitonin gene-related peptide during heterotopic ossification in murine Achilles tendon. *Journal of orthopaedic research: official publication of the Orthopaedic Research Society* 36, 1444–1455; 10.1002/jor.23833 (2018).
225. Brownley, R. C. *et al.* Characterization of Heterotopic Ossification Using Radiographic Imaging: Evidence for a Paradigm Shift. *PloS one* 10, e0141432; 10.1371/journal.pone.0141432 (2015).
226. Herchenhan, A. *et al.* Lysyl Oxidase Activity Is Required for Ordered Collagen Fibrillogenesis by Tendon Cells. *The Journal of biological chemistry* 290, 16440–16450; 10.1074/jbc.M115.641670 (2015).
227. Dourte, L. M. *et al.* Mechanical, compositional, and structural properties of the mouse patellar tendon with changes in biglycan gene expression. *Journal of orthopaedic research: official publication of the Orthopaedic Research Society* 31, 1430–1437; 10.1002/jor.22372 (2013).
228. Dunkman, A. A. *et al.* The injury response of aged tendons in the absence of biglycan and decorin. *Matrix biology: journal of the International Society for Matrix Biology* 35, 232–238; 10.1016/j.matbio.2013.10.008 (2014).

Bibliography

229. Gordon, J. A. *et al.* Achilles tendons from decorin- and biglycan-null mouse models have inferior mechanical and structural properties predicted by an image-based empirical damage model. *Journal of biomechanics* 48, 2110–2115; 10.1016/j.jbiomech.2015.02.058 (2015).
230. Bono, J. P. de, Adlam, D., Paterson, D. J. & Channon, K. M. Novel quantitative phenotypes of exercise training in mouse models. *American journal of physiology. Regulatory, integrative and comparative physiology* 290, R926-34; 10.1152/ajpregu.00694.2005 (2006).
231. Goh, J. & Ladiges, W. Voluntary Wheel Running in Mice. *Current protocols in mouse biology* 5, 283–290; 10.1002/9780470942390.mo140295 (2015).
232. Park, N. R. *et al.* *Reticulocalbin 3 is Involved in Postnatal Tendon Development by Regulating Collagen Fibrillogenesis and Cellular Maturation* (2020).
233. Ito, S. & Nagata, K. Biology of Hsp47 (Serpin H1), a collagen-specific molecular chaperone. *Seminars in cell & developmental biology* 62, 142–151; 10.1016/j.semcdb.2016.11.005 (2017).
234. Stanley, A., Heo, S.-J., Mauck, R. L., Mourkioti, F. & Shore, E. M. Elevated BMP and Mechanical Signaling Through YAP1/RhoA Poises FOP Mesenchymal Progenitors for Osteogenesis. *Journal of bone and mineral research: the official journal of the American Society for Bone and Mineral Research* 34, 1894–1909; 10.1002/jbmr.3760 (2019).
235. Kishimoto, Y. *et al.* Wnt/ β -catenin signaling suppresses expressions of Scx, Mlx, and Tnmd in tendon-derived cells. *PloS one* 12, e0182051; 10.1371/journal.pone.0182051 (2017).
236. Miyabara, S., Yuda, Y., Kasashima, Y., Kuwano, A. & Arai, K. Regulation of Tenomodulin Expression Via Wnt/ β -catenin Signaling in Equine Bone Marrow-derived Mesenchymal Stem Cells. *Journal of equine science* 25, 7–13; 10.1294/jes.25.7 (2014).

8. ATTACHMENT

8.1 List of abbreviations

ADAMTS	A disintegrin and metalloproteinase with thrombospondin motifs
bFGF	Basic fibroblast growth factor
BMP	Bone morphogenetic protein
CD	Cluster of differentiation
CD68	Macrophage Antigen CD68, Macrosialin
CD80	T-lymphocyte activation antigen CD80
CD105	Endoglin, homodimeric transmembrane protein
CD146	Melanoma cell adhesion molecule (MCAM)
CD163	Scavenger receptor cysteine-rich type 1 protein M130
CD206	Mannose Receptor C-Type 1
Comp	Cartilage oligo matrix protein
DAPI	4,6-diamidino-2-phenylindole
DMEM	Dulbecco's minimal essential medium
DNA	Deoxyribonucleic acid
dNTP	Deoxyribonucleotide triphosphate
ECM	Extracellular matrix
EDTA	Ethylenediaminetetraacetic acid
Eya	Eyes absent Transcriptional Coactivator and Phosphatase
FBS	Fetal bovine serum
GAPDH	Glyceraldehyde 3-phosphate dehydrogenase
GDF	Growth/differentiation factor
H&E	Haematoxylin & eosin
IGF	Insulin-like growth factor
IL	Interleukin
km	Kilometer
mRNA	Messenger RNA
MSC	Mesenchymal stromal cells or mesenchymal stem cells

MTJ	Myotendinous junction
ON	Over night
OTJ	Osteotendinous junction
PBS	Phosphate buffered saline
PDGFR	Platelet-derived growth factor receptor
Pen/Strep	Penicillin/streptomycin
PGE2	Prostaglandin E2
RNA	Ribonucleic acid
RT	Room temperature
RT-PCR	Reverse transcriptase polymerase chain reaction
SLRP	Small leucine-rich proteoglycan
Scx	Scleraxis
TGF- β	Transforming growth factor- β
Tnmd	Tenomodulin
TSPC	Tendon stem/progenitor cell
VEGF	Vascular endothelial growth factor

8.2 Figures

Fig. 1. Anatomy of the Achilles tendon

Fig. 2. Tendon hierarchical architecture and TSPCs subpopulation

Fig. 3. Schematic illustration of the stages of tendon repair

Fig. 4. Tendon's intrinsic and extrinsic compartments

Fig. 5. HO formation process

Fig. 6. Schematic representation of tensile load applied on collagen fibril, and load/elongation, and stress/strain curves

Fig. 7. Tenomodulin gene and protein structure

Fig. 8. Roles of Tenomodulin in early healing

Fig. 9. Breeding scheme shows Mendelian ratio of genotypes

Fig. 10. Gel electrophoresis showing genotyping results

Fig. 11. Experimental design

- Fig. 12. Surgical procedure
- Fig. 13. Region of interest (ROI) used for μ CT quantification
- Fig. 14. Testing apparatus and viscoelastic testing protocol
- Fig. 15. Voluntary running test
- Fig. 16. Incidence of ScxGFP⁺ and α SMA⁺ cell populations during tendon healing at day 8 post-injury
- Fig. 17. Incidence of ScxGFP⁺ and α SMA⁺ cell populations during tendon healing at day 21
- Fig. 18. Incidence of ScxGFP⁺ and α SMA⁺ cell populations during tendon healing at day 100
- Fig. 19. Comparison of AT repair between *Tnmd*^{-/-} and WT mice at day 21 post-injury
- Fig. 20. Comparison of cartilage-like tissue formation and COLII deposition in *Tnmd*^{-/-} and WT ATs at day 21 post-injury
- Fig. 21. Detection of nerves in *Tnmd*^{-/-} and WT ATs at day 21 post-injury
- Fig. 22. Analysis of blood vessels in *Tnmd*^{-/-} and WT ATs at day 21 post-injury
- Fig. 23. Detection of pericytes at day 21 post-injury
- Fig. 24. Collagen maturation and fibril alignment in *Tnmd*^{-/-} and WT ATs at day 21 post-injury
- Fig. 25. Detection and quantification of BrdU⁺ cells in *Tnmd*^{-/-} and WT ATs at day 21 post-injury
- Fig. 26. Analysis of M1 macrophages in *Tnmd*^{-/-} and WT ATs at day 21 post-injury
- Fig. 27. Analysis of M2 macrophages in *Tnmd*^{-/-} and WT ATs at day 21 post-injury
- Fig. 28. Gene expression analyses at day 21 and 100 post-injury
- Fig. 29. TEM and collagen fibril diameter analysis of ATs at day 21 post-injury
- Fig. 30. TEM and collagen fibril diameter analysis of ATs at day 100 post-injury
- Fig. 31. TEM and collagen fibril diameter analysis of contralateral ATs in 6-month-old mice
- Fig. 32. TEM and collagen fibril diameter analysis of contralateral ATs in 9-month-old mice
- Fig. 33. Violin plot for collagen fibril diameter distribution
- Fig. 34. Overall tissue morphology 100 days post-injury
- Fig. 35. Detection of osteogenic bone marker OPN
- Fig. 36. Micro-CT quantification of injured ATs
- Fig. 37. Micro-CT quantification
- Fig. 38. Viscoelastic biomechanical testing of non-injured, control and injured ATs at day 100 post-injury
- Fig. 39. Voluntary running test

Fig. 40. ScRNA-Sequencing of *Tnmd*^{-/-} *ScxGFP*⁺ and WT *ScxGFP*⁺ cells isolated from non-injured ATs

Fig. 41. Heat map with differently expressed genes

Fig. 42. Gene ontology analysis

Fig. 43. KEGG signaling pathway

Fig. 44. Graphical synopsis of phenotypic changes in *Tnmd*^{-/-} mice over the time course upon injury

8.3 Tables

Table 1. Summary of *Tnmd* functions

Table 2. List of transgenic mice

Table 3. List of used cells

Table 4. List of media and supplements

Table 5. List of chemicals

Table 6. List of buffers

Table 7. List of used kits

Table 8. List of primers used

Table 9. Primary and secondary antibodies used

Table 10. List of disposables

Table 11. List of used instruments

Table 12. List of software used

Table 13. PCR reaction mix and program for *Tnmd* and GFP genotyping

Table 14. Histological scoring system, 21- and 100-days post-injury

Table 15. List of genes analyzed by quantitative PCR using custom-designed PCR plates

Table 16. TEM fibril diameter quantification

Table 17. Top 100 differentially expressed genes based on adjusted p-values (q-values)

ACKNOWLEDGMENTS

First, I wish to express my deepest gratitude to my supervisor Prof. Dr. Denitsa Docheva for supporting me during the entire period of my doctoral study. I really appreciate the PhD topic you have offered, and that you have always provided me with new ideas and input to the project. During the PhD study, you gave me the opportunity to collaborate with other scientists from around the world, for which I am grateful. Thank you, Denitsa for helping me to grow as a scientist and as a person.

I would like to give a special thanks to Prof. Dr. Christian Pfeifer, Prof. Dr. Dr. Volker Alt, and Prof. Dr. Michael Nerlich from the Department of Trauma Surgery for their continuous support. I also wish to show my gratitude to my PhD mentors from the BIOMEDIGS graduate school - Prof. Dr. Susanne Grässel and Prof. Dr. Christoph Brochhausen-Delius for their advices and the critical discussions.

Moreover, I would like to thank my colleagues with whom I collaborated and without whom I would not have been able to complete this research. Thanks to Dr. Katharina Angerpointner, Dr. Michael Galler, Dr. Zexing Yan and all co-authors in the published papers. Thanks to Daniela Drenkard, Ruth Schewior, Theresia Stich and Swetlana Stryshkova for sharing their laboratory experience and for always being willing to help me.

Very special thanks go to all colleagues from the Laboratory of Experimental Trauma Surgery and the Center of Medical Biotechnology (ZMB) for the positive and constructive atmosphere.

I am grateful for the financial support obtained by Prof. Docheva through research grants from the German Research Foundation (DO1414/3-1), the EU Twinning Grant Achilles (Nr. 810850), and the EU Bavarian–Czech Republic Cross-Border Cooperation (Nr. 201 and 349).

I wish to express my gratitude to my friends for their continuous support and encouragement during the last years. Special thanks to Julian, Philine, Melissa and Dustin.

Most importantly, I would like to finish with the acknowledgments to my family for the support they have shown me over the years. You have been amazing!

9. SELBSTSTÄNDIGKEITSERKLÄRUNG

“Ich, Manuel Delgado Cáceres, geboren am 03.10.1988 in Arequipa, Peru, erkläre hiermit, dass ich die vorliegende Arbeit ohne unzulässige Hilfe Dritter und ohne Benutzung anderer als der angegebenen Hilfsmittel angefertigt habe.

Die aus anderen Quellen direkt oder indirekt übernommenen Daten und Konzepte sind unter Angabe der Quelle gekennzeichnet. Insbesondere habe ich nicht die entgeltliche Hilfe von Vermittlungs- bzw. Beratungsdiensten (Promotionsberater oder andere Personen) in Anspruch genommen.

Die Arbeit wurde bisher weder im In- noch im Ausland in gleicher oder ähnlicher Form einer anderen Prüfungsbehörde vorgelegt.

Ort, Datum

Eigenhändige Unterschrift des Promovenden

CURRICULUM VITAE

MANUEL DELGADO CÁCERES



Westendstr. 1, 80339 Munich



+49 (0)174-7091292



manueldelgadocaceres@hotmail.com



www.linkedin.com/in/manudelgadoc/

PROFESSIONAL SUMMARY

Ph.D. candidate in Biomedical & Life Sciences, and Master's degree in Molecular and applied biotechnology. Solid track in musculoskeletal research and immunology, and altogether, 5+ years of experience in basic research.

EDUCATION

PHD AT UNIVERSITY HOSPITAL REGENSBURG

REGENSBURG, GERMANY

Laboratory of Experimental Trauma Surgery | PhD Student

SEPT.2016-NOV. 2021

- Co-designed, validated and optimized an in vivo animal model to study the role of the Tenomodulin gene in tendon healing, which resulted in 1 publication in peer-reviewed journals.
- Collaborated in 3 projects associated to regenerative and orthopedic medicine with researchers from Europe, Asia and America, which have resulted to date in 3 publications in peer-reviewed journals.

MSC RWTH-AACHEN UNIVERSITY

AACHEN, GERMANY

Institute for Biomedical Engineering and Cell Biology | M.Sc. Student

APR.2015-AUG.2016

- Generated a conditional immortalized hematopoietic stem cell line to explore differentiation commitment and arrest. CRISPR/Cas genome editing tool was employed to study the involvement of transcription factor IRF8 in cancer. Results were summarized in a master's thesis and were published.

PROFESSIONAL EXPERIENCE

MEDPACE GERMANY GMBH

MUNICH, GERMANY

Regulatory Submissions Coordinator

JAN.2022-CURRENT JOB POSITION

- Distribute, track, review, and approve individual site trial master file (TMF) essential documentation at project start
- Provide advice and guidance to internal and external team members to ensure compliance with applicable regulations and requirements
- Review pertinent regulations and guides to develop proactive solutions to clinical trial submissions issues and challenges

RWTH AACHEN UNIVERSITY HOSPITAL

AACHEN, GERMANY

Research Assistant | Institute of Molecular Cardiovascular Research

NOV.2014-MAY 2015

- Detected and assessed atherosclerotic lesions in an animal model using immunohistochemistry and immunofluorescence techniques.

Internship | Urology Department

OCT.2012-JUL.2013

- Evaluated the therapeutic potential of mesenchymal stromal cells against prostate cancer using 3D cell culture models. Results were summarized in a bachelor's thesis.

TESA LABTEC GMBH

LANGENFELD, GERMANY

Pre-study internship & Student Assistant

JUL.-AUG.2009 & FEB.2011-APR.2012

- Supported the Development & Quality Control teams with chemical and physical raw materials and active ingredients testing (finished medical products) using standard techniques such as UV-Spectrometry, HPLC, and drug release tests.
- Processed and analyzed pharmaceutical products following European Pharmacopoeia.

PUBLICATIONS

- Xu H, Look T, (...), **Delgado Caceres M**, (...), Zenke M. CRISPR/Cas9 editing in conditionally immortalized HoxB8 cells for studying gene regulation in mouse dendritic cells. *Eur J Immunol*. 2021 Nov 26. (4-Year IF: 4.147)
- **Delgado Caceres M**, Angerpointner K, (...), Docheva D. Tenomodulin knockout mice exhibit worse late healing outcomes with augmented trauma-induced heterotopic ossification of Achilles tendon. *Cell Death Dis*. 2021 Nov 5;12(11):1049. (5-Year IF: 8.713)
- Di Pauli von Treuheim T, (...), **Delgado Caceres M**, (...), Iatridis JC. Tenomodulin and Chondromodulin-1 are both required to maintain biomechanical function and prevent intervertebral disc degeneration. *Cartilage*. 2021 Sep 4:19476035211029696 (5-Year IF: 4.634)
- Lin D, Alberton P, **Delgado Caceres M**, (...), Docheva D. Loss of tenomodulin expression is a risk factor for age-related intervertebral disc degeneration. *Aging Cell*. 2020 Mar;19(3):e13091. (4-Year IF: 8.515)
- Yin H, **Delgado Caceres M**, (...), Docheva D. Tenomodulin regulates matrix remodeling of mouse tendon stem/progenitor cells in an ex vivo collagen I gel model. *Biochem Biophys Res Commun*. 2019 May 14;512(4):691-697. (5-Year IF: 3.381)
- **Delgado Caceres M**, Pfeifer CG, Docheva D. Understanding Tendons: Lessons from transgenic mouse models. *Stem Cells Dev*. 2018 Sep 1;27(17):1161-1174. (4-Year IF: 3.471)
- Lin D, Alberton P, **Delgado Caceres M**, (...), Docheva D. Tenomodulin is essential for prevention of adipocyte accumulation and fibrovascular scar formation during early tendon healing. *Cell Death Dis*. 2017 Oct 12;8(10):e3116. (5-Year IF: 8.713)

LANGUAGES

German and English (highly proficient in spoken and written); Spanish (native speaker)

HONORS & AWARDS

- ON/EORS Education Grant for virtual EORS conference attendance AUG.2020
- Best short oral presentation award (2nd ACHILLES Conference, Braga, Portugal) NOV.2019
- Degree Completion Grant (DAAD & Doktor Carl-Arthur-Pastor-Stiftung) SEPT.2015

QUALIFICATIONS & SKILLS

- FELASA B, project manager and biological safety officer (BBS) certification.
- Cellular & molecular biology techniques: Cell isolation and culture, DNA-, RNA-Isolation, qRT-PCR, ELISA, Immunohisto-, immunocytochemistry, CRISPR/Cas genome editing tool.

OTHER INTERESTING INFORMATION

- Spokesperson Biomedical International Graduate School, University Regensburg